CHARLES UNIVERSITY

FIRST FACULTY OF MEDICINE

DOCTORAL THESIS

Prague 2023 **MUDr. Lukáš Farhád Mirchi**

Charles University

First Faculty of Medicine

Study program: Molecular and Cellular Biology, Genetics and Virology

MUDr. Lukáš Farhád Mirchi

GENETIC FACTORS RESPONSIBLE FOR DEVELOPMENT OF METABOLIC SYNDROME

Genetické faktory podílející se na vzniku metabolického syndromu

Institute of Biology and Medical Genetics, First Faculty of Medicine, Charles University and General University Hospital in Prague

Doctoral thesis

Supervisor: doc. MUDr. František Liška, Ph.D.

Prague 2023

Prohlášení:

Prohlašuji, že jsem závěrečnou práci zpracoval samostatně a že jsem řádně uvedl a citoval všechny použité prameny a literaturu. Současně prohlašuji, že práce nebyla využita k získání jiného nebo stejného titulu.

Souhlasím s trvalým uložením elektronické verze mé práce v databázi systému meziuniverzitního projektu Theses.cz za účelem soustavné kontroly podobnosti kvalifikačních prací.

V Praze, 23.6.2023

MUDr. Lukáš Farhád Mirchi

1. Identifikační záznam

MIRCHI, Lukáš Farhád. Genetic factors responsible for development of metabolic syndrome. [Genetické faktory podílející se na vzniku metabolického syndromu]. Praha, 2023, 162 stran, 26 stran příloh. Disertační práce. Univerzita Karlova, 1. lékařská fakulta, Ústav biologie a lékařské genetiky 1. LF UK a VFN v Praze. Vedoucí práce doc. MUDr. František Liška, Ph.D.

2. Acknowledgement

I hereby wish to express my uttermost gratitude to my supervisor associate professor František Liška for his bottomless patience, insightful thoughts and excellent leadership throughout the course. My thanks goes to Prof. Ondřej Šeda and Kristýna Procyková, MD for their valuable comments and professional help. My gratitude belongs to Michaela Janků and Blanka Chylíková for their technical support. Last but not least I cannont thank enough my brother and my parents for their aid and patience. Without the above mentioned colleagues this work would not have been possible.

This work was supported by grants no. 244215 and no. 36317 from the Grant Agency of the Charles University, SVV 260367/2017 from the Charles University and by Ministry of Health, Czech Republic – conceptual development of research organization 64165, General University Hospital in Prague, Czech Republic.

3. Table of contents

4. Abbreviations

20-HETE Hydroxyeicosatetraenoic acid

Acsm3 Acyl-CoA-synthetase for medium-chain member 3

Akt Protein kinase B

AngII angiotensin II

ANOVA Analysis of variance

AOX1 Aldehyde oxidase

Apo B Apolipoprotein B

AT2 Angiotensin II receptor type 2

ATP Adenosine-5'-triphosphate

ATPIII Adult Treatment Panel III

AUC Area under curve

BC Backcross

BILs Backcross inbred lines

BMI Body mass index

BN Brown Norway

Bp Base pair

BTB/POZ Broad-Complex, Tramtrack and Bric a brac/poxvirus domain

CD36 Cluster of differentiation 36

CM Chylomicrons

CRISPR- Clustered regularly interspaced short palindromic repeats

cRNA Complementary RNA

CSSLs Chromosome segment substitution lines

Ct cycle threshold

CVDs Cardiovascular diseases

CYP450 Cytochrome P450

DAG Diacylglycerol

DAVID – Database for Annotation, Visualization and Integrated Discovery

DEG Differentially expressed genes

DNA Deoxyribonucleic acid

dNTP Deoxynucleotide triphosphates

DOC2A – double C2 domain alpha

DRD2 – dopamine receptor D2

DTT Dithiothreitol

Drd2 Dopamine receptor D2

EcoRI Endonuclease enzyme isolated from species E. coli

EDTA Ethylenediaminetetraacetic acid

EGIR European Group for the study of Insulin Resistance

ELISA Enzyme-linked immuno-sorbent assay

ENO1 Alpha-enolase 1

eQTL Expression quantitative trait locus

ET-1 Endothelin 1

F1 First filial generation

F2 Second filial generation

FA fatty acid

$FADH_2$ Flavin adenine dinucleotide (hydroquinone form)

FFA Free fatty acids

FoxO Forkhead box O

G-CSF granulocyte colony stimulating factor

GAPDH Glyceraldehyde-3-phosphate dehydrogenase

GCA Grancalcin

GIP Gastric inhibitory polypeptide

GLP-1 Glucagon-like peptide-1

GM-CSF Granulocyte-macrophage colony-stimulating factor

GRO/KC Human growth-regulated oncogene/Keratinocyte chemoattractant

GWAS Genome-wide association studies

HCD Higher-energy C-trap dissociation

HDAC3 Histone deacetylase 3

HDL High density lipoprotein

HEK 293 Human embryonic kidney

HepG2 Human cervical hepatocellular carcinoma

HFD High fat diet

HindIII Restriction enzyme isolated from Haemophilus influenzae

HPLC High-performance liquid chromatography

HSD Honestly significant difference (Tukey´s post hoc HSD test)

IFG Impaired fasting glucose

IFN-γ Interferon gamma

IGT Impaired glucose tolerance

IGV Integrated Genome Viewer

IKK-b Inhibitor of kappa kinase beta

IRS-1 Insulin receptor substrate 1

IRS-2 Insulin receptor substrate 2

IL-10 Interleukin 10

IL-12p70 Interleukin 12p70

IL-13 Interleukin 13

IL-17 Interleukin 17

IL-18 Interleukin 18

IL-1α Interleukin 1α

IL-1β Interleukin 1β

IL-2 Interleukin 2

IL-4 Interleukin 4

IL-5 Interleukin 5

Il-6 Interleukin 6

IL-7 Interleukin 7

IL-8 Interleukin 8

*i*NKT Invariant natural killer T cells

IR Insulin resistance

Htr3a 5-hydroxytryptamine (serotonin) receptor 3A

JNK-1 c-Jun-N-terminal kinase

KCNA5 Potassium voltage-gated channel, shaker-related subfamily, member 5

KRLB Kinase regulatory loop binding

LB Luria broth

LC/MS Liquid chromatography-mass spectrometry

LDL Low density lipoprotein

Lep Leptin encoding gene

LINE Long interspersed nuclear element

LINE-L1Rn – Long Interspersed Nuclear Element of *Rattus norvegicus* origin

LMOD2 Leiomodin 2

lncRNA Long noncoding ribonucleic acid

MAPK Mitogen-activated protein kinases

MCP-1 Monocyte Chemoattractant Protein-1

M-CSF Macrophage colony-stimulating factor

MetS Metabolic syndrome

MgCl2 Magnesium chloride

MIP-1α Macrophage inflammatory protein

MIP-3α Macrophage Inflammatory Protein 3α

MMP12 Matrix metalloproteinase 12

mRNA Messenger ribonucleic acid

MS/MS Tandem mass spectrometry

mTORC Mammalian target of rapamycin complex

NaCl Natrium chloride

NADH Nicotinamide adenine dinucleotide + hydrogen

NCoR Nuclear hormone receptor co-repressor

NCP:ATPIII National Cholesterol Education Adult Treatment Panel III

NIL Near isogenic lines

nLC-MS/MS Nano-liquid chromatography mass spectrometry

NOX4 NADPH oxidase

Nr4a1 Nuclear receptor subfamily 4 group A member 3

Nur77/Nr4a1 Nuclear receptor subfamily 4 group A member 1

OGTT Oral glucose tolerance test

OD Optical density

PAI-1 Plasminogen activator inhibitor-1

PBS – Phosphate Buffered Saline

PD/Cub Polydactylous rat strain, Charles university breed

PD5 SHR.PD-chr.8 minimal congenic strain

Per1 Period circadian clock 1, period circadian regulator

PH Pleckstrin homology

PI3K/Akt Phosphoinositide 3-kinase/Protein kinase B

PKC Protein kinase C

Plzf promyelocytic zinc finger, identical to Zbtb16

PPAR peroxisome proliferator-activated receptor

PVDF Polyvinylidene difluoride membrane

qPCR Quantitative polymerase chain reaction

QTL Quantitative trait locus

RAA Renin-angiotensin-aldosterone axis

RANTES Regulated on Activation, Normal T Cell Expressed and Secreted

Ras Rat sarcoma virus

RAS Renin - angiotensin - aldosterone pathway

RFLP Restriction fragment length polymorphisms

RGDID Rat genome database identification number

RIL Recombinant inbred lines

RLU Relative luminescence units

RNA Ribonucleic acid

ROS Reactive oxygen species

rRNA Ribosomal ribonucleic acid

RT-PCR Reverse transcription polymerase chain reaction

SalI Restriction enzyme from Streptomyces albus G

SCD1 Scd1 stearoyl-Coenzyme A desaturase 1

SCFA Short chain fatty acid

SDC Sodium deoxycholate

SDS-PAGE Sodium dodecyl-sulfate polyacrylamide gel electrophoresis

SEM Standard error of the mean

SH2 Src homology-2

SHR Spontaneously Hypertensive Rat

siRNA Small interference ribonucleic acid

SLC17A2 – solute carrier family 17 member 2

SMRT Silencing mediator for retinoic acid receptor and thyroid-hormone receptor

SNF Similarity network fusion

snoRNA Small nucleolar ribonucleic acid

SNP Single nucleotide polymorphism

snRNA Small nuclear ribonucleic acid

ssDNA Single strand DNA

SREBP Sterol regulatory element binding protein

SRF Serum response factor

STD Standard diet

T2DM Type 2 Diabetes

TAC Transcriptome Analysis Console

TAG Triacylglycerol

TALEN Transcription activator-like effector nucleases

TCEP Tris-2-carboxyethyl phosphine

TdT Terminal deoxynukleotidyltransferase

TEAB Triethylammonium bicarbonate

TFA trifluoroacetic acid

TG Triacylglycerols

TLR2 Toll-like receptor 2

TLR4 Toll-like receptor 4

Tmprss5 Transmembrane serine protease 5

TNF-α tumor necrosis factor alpha

TRL Triacylglycerol rich proteins

tRNA Transfer ribonucleic acid

TSC Tuberous sclerosis complex

Usp28 Ubiquitin-specific protease 28

VEGF Vascular endothelial growth factor

VLDL Very low density lipoprotein

WB Western blot

WC Waist circumference

WHO World Health Organization

Zbtb16 Zinc finger and BTB domain-containing protein 16, identical to Plzf

ZF Zinc finger domain

ZFNs Zinc-finger nucleases

Zw10 Zeste-white

5. Abstrakt

Metabolický syndrom je celosvětově vysoce prevalentní onemocnění charakterizované přítomností alespoň tří z následujících znaků: abdominální obezity, hypertenze, diabetu mellitu, vyšší hladiny LDL cholesterolu či snížené hladiny HDL cholesterolu. Metabolický syndrom je komplexní onemocnění, při kterém je fenotyp daného jedince determinován výslednicí interakce genomu a faktorů prostředí. Bohužel se v současné době metabolický syndrom díky své nezastavitelně rostoucí incidenci jeví jako celosvětová neinfekční pandemie představující významnou socioekonomickou zátěž. Pochopení genetického pozadí metabolického syndromu za pomocí geneticky definovaných savčích modelů představuje jednu ze strategií ke zlepšení možností boje s MetS a jeho zdravotnámi následky.

Cíl této dizertační práce je poodkrýt genetické pozadí metabolického syndromu a to za pomoci komparativní transkriptomické analýzy relevantních orgánů geneticky definovaných potkaních modelů. K popisu genetické architektury metabolického syndromu jsme provedli tři nezávislé experimenty. Nejprve jsme pomocí komparativní transkriptomické analýzy mezi levými srdečními komorami kmene SHR a jeho minimálního kongenního kmene PD5, charakterizovaným mj. menší mírou fibrózy myokardu, identifikovali zvýšenou expresi genu *Nr4a1/Nur77* u kmene PD5 a dále dysregulaci genů *Nr4a3, Per1* a *KCNA5*. V druhém experimentu jsme pozorovali rozdíly fenotypových profilů potkaních kmenů PD, SHR a BN po podání vysokotukové diety za účelem odhalení podstaty vyšší náchylnosti kmene PD k rozvoji metabolického syndromu. Identifikovali jsme slibný kandidátní gen *Acsm3* (acyl-CoA-synthetase for medium-chain member 3), který kóduje enzym patřící do rodiny syntetáz aktivujících středně dlouhé mastné kyseliny (C4-C14) pro vstup do beta-oxidace. V jaterní tkáni kmene PD není tento gen prakticky exprimován, což jsme potvrdili na mRNA jakož proteinové úrovni.

Cílem třetího experimentu byla identifikace patofyziologických mechanismů vedoucích k diferenciální citlivosti kmenů SHR a PD5 ke glukokortikoidy indukovanému metabolickému syndromu. I zde jsme provedli komparativní transkriptomickou analýzu jaterní tkáně potkanů PD5 a SHR před a po podání dexamethasonu odkrývající možné genetické determinanty, proteomická analýza nám poté pomohla určit potenciální cíle *Plzf* jakožto genu důležitého pro tento aspekt metabolického syndromu.

Pomocí kombinovaného přístupu užití geneticky definovaných modelů a transkriptomických esejí jsme identifikovali několik metabolických drah s potenciální rolí v patogenezi metabolického syndromu a zároveň jsme odhalili několik kandidátních genů.

Klíčová slova: hypertenze, metabolický syndrom, kongenní kmen, SHR, PD, PD5, kandidátní geny, *Nur77, Acsm3, Plzf*.

6. Abstract

Metabolic syndrome (MetS) is a worldwide highly prevalent disease defined as a clustering of at least three of the following conditions: central obesity, hypertension, diabetes, high level of low-density lipoproteins, low level of high-density lipoprotein or high level cholesterol. MetS is a multifactorial disease which is caused by both environmental factors and a heritable component. Unfortunately, because of its ever rising worldwide incidence MetS emerges as a worldwide epidemic and a heavy socioeconomic burden. In order to effectively fight the MetS pandemic, it is vital to dissect the genetic background and mechanisms that underlie MetS and its individual components, a goal that is profoundly benefitted by physiological and genetic studies in animal models of MetS.

The aim of this thesis was to dissect the genetic background of metabolic syndrome by using comparative transcriptomic analysis in relevant organs obtained from genetically defined rodent models. Each of our genetically defined rat strains is phenotypically distinct in terms of manifesting individual components of MetS. We present three separate transcriptomic experiments in order to unravel the genetic background of MetS. First, we performed the global comparative transcriptomic analysis of left ventricular tissue from SHR and SHR-derived minimal congenic strain PD5 with attenuated cardiac fibrosis. An overexpression of nuclear orphan receptor *Nur77/Nr4a1* in PD5 and dysregulation of *Nr4a3, Per1* and *Kcna5* were revealed. In the second experiment, we observed phenotypic changes in PD, SHR and BN rat strains, respectively, after high fat diet administration, with subsequent transcriptomic analysis so as to find the pathophysiologic and genetic background of higher susceptibility of PD strain to MetS. A promising candidate gene contributing to higher susceptibility of PD rats to MetS is *Acsm3* (coding for acyl-CoA-synthetase for medium-chain member 3), which belongs to a family of enzymes activating medium chain fatty acids (C4-C14) to beta-oxidation, and which was absent in liver of PD on both mRNA and protein levels. In the third experiment we tried to unravel mechanisms underlying differential liability of SHR and PD5 to glucocorticoid induced metabolic syndrome. We performed comparative transcriptomic analysis of PD5 and SHR liver tissue after dexamethasone treatment unraveling potential genetic determinants; furthermore, we performed a proteomic analysis unraveling potential targets of *Plzf* as a possible candidate gene responsible for this aspect of metabolic syndrome.

Using defined rodent models and transcriptomic approach we mapped several key pathophysiological pathways accountable for development of MetS features and unraveled several candidate genes in the context of these pathways.
Key words: metabolic syndrome, hypertension, congenic strain, SHR, PD, PD5, candidate genes, *Nur77, Acsm3, Plzf*

7. Introduction

Multifactorial diseases are the most prevalent medical conditions plaguing humanity and causing appalling socio-economic consequences. In each individual, phenotypic expression of multifactorial disease is determined by a complex interaction among environmental factors with genetic background. It is this very interaction and the variability of both the genetic component and environment that makes the dissection of the genetic background of each complex trait particularly challenging.

Metabolic syndrome is probably the most prevalent complex disease worldwide. To understand the clustering of its individual components and their pathophysiology, a wide spectrum of genetically defined rodent models has been developed, from monogenic mutant models, inbred strains selected for one or more traits to population models. These organisms, together with functional and comparative genomic approaches present powerful tools in dissecting the individual genetic components of complex traits.

7.1. Metabolic syndrome

Metabolic syndrome is defined as a clustering of visceral obesity, dyslipidemia, arterial hypertension, insulin resistance and related maladies such as prothrombotic state or sleep apnea syndrome. Metabolic syndrome is probably the most prevalent multifactorial non-communicable disease worldwide according to the WHO (Riley L. et al. 2016). The prevalence of many of the components of the "metabolic syndrome", particularly obesity and diabetes, has grown considerably throughout the Western World since this term was initially suggested by Haller in 1977 (Haller H. et al., 1977) which is an alarming condition given that the metabolic syndrome is an important precursor to cardiovascular disease and other chronic maladies (Grundi SM. et al., 2004; Pucci G. et al., 2017; Deboer MD. et al., 2018),

7.2. History of Metabolic syndrome

The first reported association between diabetes and hypertension was described in the early 20th century by Joslin who first expressed possible causality between these two maladies with Kylin subsequently performing additional studies (Joslin E., 1921, Kylin E., 1923). Throughout the following years additional aspects of metabolic syndrome and their mutual relations and connections to mortality were proposed. In 1956, Vague suggested that abdominal obesity may predispose to diabetes and cardiovascular disease (Vague J. et al.,

1956). An important milestone came in 1988 when Reaven in his now legendary Banting lecture related increased cardiovascular morbidity to clustering of hypertension, insulin resistance with compensatory hyperinsulinemia and dyslipidemia, a condition which he coined with the term syndrome X (Reaven GM., 1988). The last three decades have brought forth a number of definitions and criteria to identify this condition. The first comprehensive definition of MetS was presented in 1998 by the World Health Organization (WHO), (Table 1). On one hand, it assigned insulin resistance a key role in development of MetS and all components of MetS as defined by this definition were exploited in further definitions, on the other hand, it was criticized by many because of insufficient correlation between insulin resistance and microalbuminuria, moreover the clamp technique to analyze insulin resistance was far from appropriate for large-scale surveys (Alberti KG. et al., 2009). Shortly thereafter, the European Group for the study of Insulin Resistance (EGIR) proposed its own definition of Metabolic syndrome omitting the microalbuminuria as an integral part of the syndrome, while introducing different cut-offs from those previously used for the other components of the syndrome (Balkau B. et al., 1999), (Table 1). In a controversial move, the National Cholesterol Education Adult Treatment Panel III report (NCEP:ATPIII, 2001) dropped insulin resistance as a mandatory component of MetS and laid focus on obesity (Table 1); however, obesity defining criteria are not applicable across all ethnic groups. On the other hand, because of its clarity, the NCEP ATP III criteria are probably the most widely used to diagnose MetS worldwide (Table 1). It embraces the crucial features of hyperglycemia/insulin resistance, visceral obesity, dyslipidemia and hypertension. It operates with easily obtainable measurements and laboratory results, which makes it readily available to physicians, promoting its clinical and epidemiological application. It does not require that any specific criterion be met; only that at least three of five criteria are met. Thus, the definition does not build in any preconceived notion of the underlying cause of metabolic syndrome, whether it is insulin resistance or obesity (Huang PL. et al., 2009).

Clinical measure	World Health Organisation 1998	European Group for the Study of Insulin Resistance 1999	Adult Treatment Panel III of the National Cholesterol Education Program 2001	International Diabetes Federation 2005	American Heart Association/National Heart, Lung, and Blood Institute 2005
Criteria	Insulin resistance + any other 2	Insulin resistance + any other 2	Any 3 of 5	Increased WC (population-specific) + any other 2	Any 3 of 5
Insulin resistance	IGT/IFG IR	Plasma insulin > 75th percentile	-	-	-
Blood glucose	IFG/IGT/T2 DM	IFG/IGT (excludes diabetes)	⩾ 110 mg/dL (includes diabetes)	⩾ 100 mg/dL	⩾ 100 mg/dL (includes diabetes)
Dyslipidemia	TG ⩾ 1.69 mmol/L and HDL-C men < 0.90 mmol/L women < 1.01 mmol/L	TG ⩾ 1.69 mmol/L and HDL-C < 1.01 mmol/L in men and women	TG ⩾ 1.69 mmol/L HDL-C men < 1.03 mmol/L women < 1.29 mmol/L	TG ⩾ 1.69 mmol/L or on TG treatment HDL-C men < 1.03 mmol/L women < 1.29 mmol/L Or HDL treatment	TG ⩾ 1.69 mmol/L or on TG treatment HDL-C men < 1.03 mmol/L women < 1.29 mmol/L Or HDL treatment
Blood pressure	⩾ 140/90 mmHg	⩾ 140/90 mmHg or	⩾ 130/85 mmHg or	⩾ 130/85 mmHg or	⩾ 130/85 mmHg or on

		on antihypertensive medications	on antihypertensive medications	on antihypertensive medications	antihypertensive medications
Obesity	Waist: hip ratio men > 0.9 women > 0.85 and/or BMI > 30 kg/m2	WC men ⩾ 94 cm women ⩾ 80 cm	WC men ⩾ 102 cm women ⩾ 88 cm	WC ⩾ 94 cm	WC men ⩾ 102 cm women ⩾ 88 cm
Other	Microalbuminuria	-			

Table 1: Individual definitions of Metabolic syndrome. BMI, body mass index; HDL-C, high-density lipoprotein cholesterol; IFG, impaired fasting glucose; IGT, impaired glucose tolerance; IR, insulin resistance; T2DM, type 2 diabetes mellitus; TG, triglycerides; WC, waist circumference. (Rochlani Y. et al., 2017; Alberti KG. et al., 2009)

7.3. Individual components of the Metabolic syndrome

7.3.1. Hypertension

Almost 80% of individuals with metabolic syndrome suffer from hypertension (Katsimardou A. et al., 2020). As with every other feature of MetS the pathophysiology of hypertension is complex, with every component of metabolic syndrome responsible for its development to a certain extent. However, increased renal sodium reabsorption and impaired pressure natriuresis due to high sympathetic tonus are major contributors to the rise in blood pressure associated with excess weight and metabolic syndrome (Hall JE. et al., 2015).

Adipose tissue was shown to produce increased circulating levels of AngII and aldosterone, and potentially impairs metabolism of AngII (Schütten MT. et al., 2017), furthermore aldosterone overactivity may reduce levels of adiponectin, which has protective properties against obesity-linked complications, such as hypertension (Ohashi K. et al., 2011; Guo C. et al., 2008).

Insulin resistance appears to contribute to hypertension in the context of the metabolic syndrome by increasing the tonus of sympathetic nerves and upregulating AngII receptors (Mancia G. et al., 2007, Nickenig G. et al., 1998.) Besides, insulin resistance reduces nitric oxide synthesis (Andronico G. et al., 1997). These changes subsequently result in tachycardia and inevitably lead to hypertension.

To stress the complexity, there are some minor pathophysiological pathways leading to high blood pressure. For example ectopic adipose tissue accumulation produces higher levels hydroxyeicosatetraenoic acid (20-HETE), a cytochrome P450 (CYP450)-derived arachidonic acid metabolite, which increases large artery stiffness by activation of metalloproteinase 12 (MMP12) and elastin degradation, revealing an important role in interstitial tissue metabolism in hypertension (Soler A. et al., 2018)

7.3.2. Dyslipidemia and components of lipid spectrum disbalance

The major components of dyslipidemia in MetS are characterized by increase in fasting and postprandial triglyceride-rich lipoproteins (TRLs) fraction, decreased high-density lipoprotein (HDL), increased low-density lipoprotein (LDL) fraction, and raised apolipoprotein (apo) B level. This disequilibrium in lipid spectrum accounts for increased atherogenicity of lipid profile leading to cardiovascular morbidity and mortality particularly in obese individuals with metabolic syndrome (Blaton V. et al., 2007). Furthermore high LDL cholesterol and hypertriglyceridemia are independently associated with myocardial infarction or stroke risk in patients with MetS (Anderson JL. et al., 2004). The observed dyslipidemia in MetS may be the natural outcome of the global metabolic effect of insulin resistance (Kolovou GD. et al., 2005).

Under hyperinsulinemic conditions associated with insulin resistance adipocytes increase their lipolytic activity and consequently produce large quantities of free fatty acids (FFA) which in turn diminish the suppressive effect of insulin on VLDL production (Lewis GF. et al., 1995,), moreover insulin resistance further decreases Apo B lipoprotein degradation, and through relative deficiency of lipoprotein lipase leads in the decreased clearance of fasting and postprandial TRLs, and the decreased production of HDL particles (Ruotolo G. et al., 2002; Gorter PM. et al., 2004). These above-mentioned metabolic changes eventually increase VLDL levels, VLDL particles are subsequently converted to LDL particles which are usually of normal levels but of different lipoprotein composition due to higher triacylglycerol component as opposed to healthy individuals. Both LDL and VLDL particles show increased atherogenic properties. (Hegele RA. et al., 2009; Packard CJ. et al., 2003).

7.3.3. Insulin resistance

Insulin resistance is defined as an inability of the organism to adequately respond to insulin and properly dispose of glucose. Insulin resistance is often accompanied by hyperinsulinemia which is recognized as an endogenous pathophysiologic mechanism, raising from insulin resistance and leading to metabolic and endocrine disruption, and plays a pivotal role in impaired glucose homeostasis, MetS, and T2D. (Aronis KN. et al., 2012; Marusić M. et al., 2021). The weakened effect of insulin on peripheral tissues occurs in spite of hyperinsulinemia and subsequent hyperglycaemia confers wide range of peripheral organs and tissues damage (most notably liver, endotelium, kidneys, muscles and vascular beds), and contributes to the development of other components of metabolic syndrome, but also to cardiovascular disease, NAFLD (Boden G. et al., 2008; Shanik MH. et al., 2008;), Alzheimer's disease (Blazques E. et al., 2014; De La Monte SM. et al., 2017), and impaired lung function (Forno E. et al., 2015).

Insulin signaling pathway is triggered after insulin binds membrane insulin receptors subsequently leading to receptor dimerization and autophosphorylation (Figure 1). The ensuing insulin receptor substrate activation (IRS1/IRS2) then splits the pathway in three distinct branches - activated IRS may promote cell proliferation and cell survival through RAS-MAPK pathway, protein synthesis through TSC/mTOR signaling and translocate the glucose membrane receptor to the cell surface via PI3/AKT pathway.

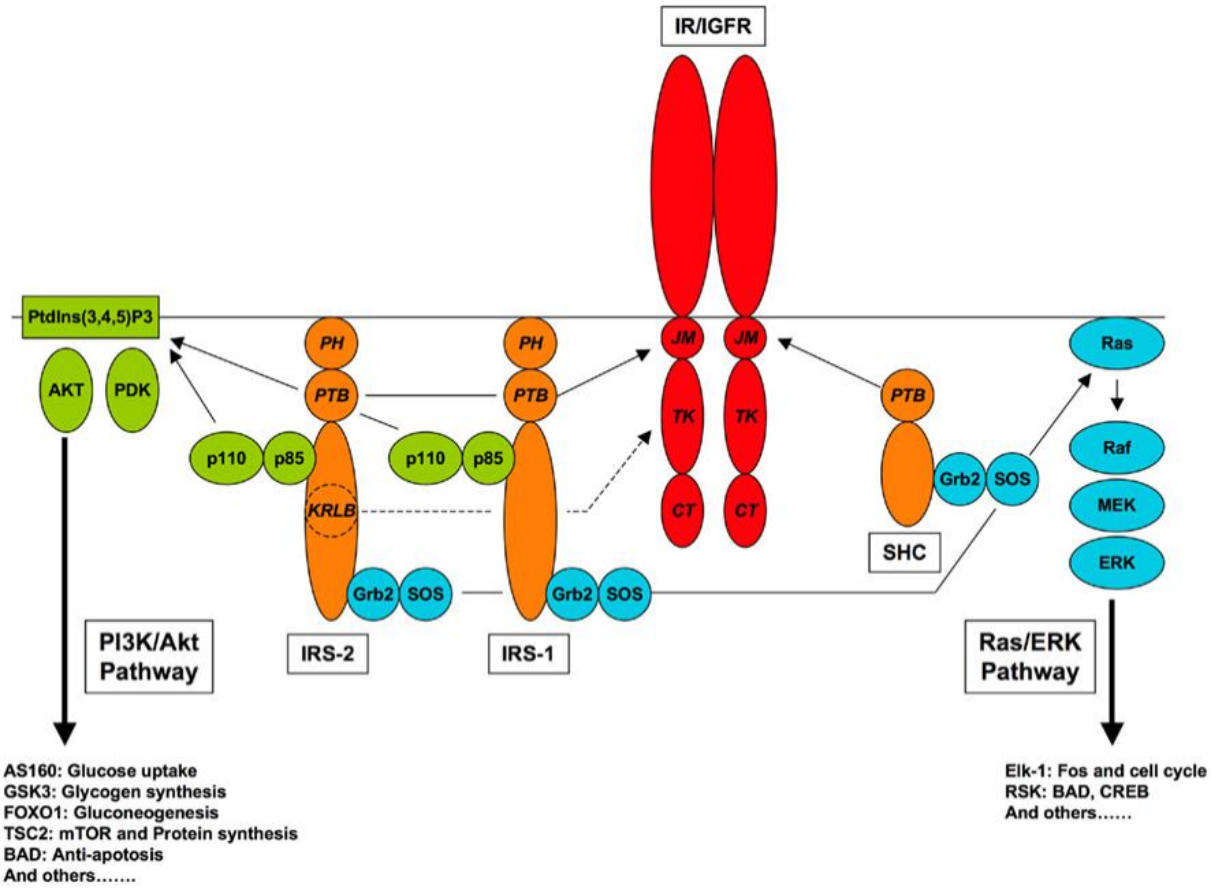

Figure 1: Simplified scheme of the canonical insulin signaling pathway. The picture shows relevant cytosolic parts of the insulin receptor relevant in triggering of the downstream PI3K/Akt and Ras/ERK pathways. Taken from Siddle K. et al. 2012. (JM, juxtamembrane; TK, tyrosine kinase; CT, carboxyl-terminal; PTB, phosphotyrosine-binding; PH, pleckstrin homology, SH2, Src homology-2; KRLB, kinase regulatory loop binding). Taken from auschard MJ. et al., 2012.

On a molecular level, the insulin signaling pathway requires delicate regulation by phosphatases and kinases. Modifications in any of the key steps in the insulin signaling pathway can lead to IR, which is seen on the cellular level due to dysregulation of intracellular signals normally promoted with insulin binding (Marusić M. et al., 2021). Current data suggest that the desensitization of proximal insulin signaling by IRS serine/threonine phosphorylation promoted by Inhibitor of kappa kinase beta (IKK-b), c-Jun-N-terminal kinase (JNK-1), and protein kinase C (PKC) plays a significant role in the pathogenesis of human insulin resistance (Yung JHM. et al., 2020; Polyzos S. et al., 2009; Sha H. et al., 2009).

Higher exposure to leptin associated with leptin resistance in obese individuals, may cause mitigated effect of insulin-mediated activities, such as tyrosine phosphorylation of the

insulin receptor substrate-1 (IRS-1), and down-regulation of gluconeogenesis (Cohen B. et al., 1996).

Other direct pathophysiological mechanisms of insulin resistance include chronic inflammatory reaction mediated by TNF. TNF is produced by macrophages and its level correlates with adipose tissue mass (Weisberg SP. et al., 2003). Along with Il-1 and Il-6 TNF signaling leads to direct phosphorylation IRS substrates on serine and threonine residues in hepatocytes and adipose tissue, impairing downstream signaling, resulting in diminished effects of insulin (Hotamisligil GS. et al., 1995). Wide range of metabolites indirectly cause IR by altering the flux of substrates through multiple metabolic pathways, including lipogenesis, lipid oxidation, protein synthesis and degradation and hepatic gluconeogenesis (Yang Q. et al., 2018). Some leading theories on insulin resistance pathophysiology also center on mitochondrial dysfunction, which could be either caused by oversaturation of superoxide dismutase and other antioxidant mitochondrial enzymes by ROS overproduction (Bhatti JS. et al., 2017), which is seen in excessive NADH and FADH2 production after overnutrition (Masschelin PM. et al., 2020),or the mitochondrial dysfunction can be attributed to primary decline of mitochondrial function (Burkart AM. et al., 2016). Primary inherited or acquired mitochondrial dysfunction was also linked to accumulation of intramyocellular lipids that leads to decreased insulin sensitivity in skeletal muscle, and implies that strategies to accelerate flux through β-oxidation should improve insulin sensitivity. (Lowell BB. et al., 2005)

7.3.4. Obesity

Obesity, defined as BMI ≥ 30 kg/m^2 is present in the majority of people suffering from MetS. (Park YW. et al., 2003). Obesity reflects positive energy imbalance leading to ectopic fat deposition (visceral or subcutaneous) and mirrors metabolic stress which firmly correlates with all features of MetS, therefore it might be perceived as a key component.

Phenotypically, two types of obesity distribution can be discerned – Upper and lower body fat distribution. The upper body fat distribution is seen predominantly in men and is associated with the development of obesity-related comorbidities and even all-cause mortality. In contrast, gluteofemoral fat distribution seen in women protects against insulin resistance as suggested by some authors (Snijder MB. et al., 2004; Yusuf S. et al., 2005). Furthermore, fat mass may not proportionally correlate with metabolic phenotype or insulin resistance; for instance, there is no significant effect of liposuction on insulin action and risk factors for coronary heart disease (Klein S. et al., 2004). Another example may be

individuals with lipodystrophy, a condition with adipose tissue deficiency who suffer from diabetes (Ganda OP. et al., 2000). Interestingly though, insulin resistance was significantly attenuated in lipodystrophic mice after surgical implantation of fat tissue (Gavrilova O. et al., 2000). Peculiarly, thiazolidinediones lead to weight gain although they improve insulin resistance (Fonseca V. et al., 2003). This testifies that simple fat mass volume cannot be the sole factor in developing MetS features, but as above mentioned examples illustrate the adipose tissue distribution and functioning plays an undeniable role (Goossens GH. et al., 2017).

Adipose tissue should not be perceived only as a passive storage of energy, but rather as an organ with complex metabolic and endocrine functions which can contribute to various pathophysiological processes resulting in MetS (Kahn CR. et al., 2019), (Figure 2). Overnutrition results in hypertrophy of subcutaneous adipose tissue with subsequent tissue ischemia and hypoxia which induces necrosis and attracts inflammatory cells leading to noninfectious inflammation . The failure of subcutaneous adipose tissue to expand and buffer excess energy intake leads to ectopic fat accumulation which only aggravates the inflammation process (Goossens GH. et al., 2008; Stinkens R. et al., 2015). This inflammation is promoted by dysregulation of certain inflammatory molecules, among these are Il-6, TNF-alpha, leptin, angiotensinogen and PAI-1. (Berg AH. et al., 2005). These inflammatory molecules, at least experimentally, induce insulin resistance or diabetes (Bełtowski J. et al., 2003), the complex role of adipose tissue is depicted in (Figure 2). Moreover, higher plasma levels of angiotensinogen II which were shown to likely occur in obese individuals and obese subjects with T2DM impair insulin signaling (Henriksen EJ. et al., 2013). The adipose tissue exerts endocrine function via a wide range of tissue hormones as listed in (Table 2). Levels of adiponectin negatively correlate with coronary heart disease (Ouchi N. et al., 2001), hypertension (Chow WS. et al., 2007) and diabetes (Hotta K. et al., 2000). Since adiponectin is an antiinflammatory molecule it underpins the role of inflammation in MetS (Yamauchi T. et al., 2003). On a molecular level angiotensin II? triggers production of reactive oxygen species (ROS) by activating nicotinamide adenine dinucleotide phosphate oxidation (Sachse A. et al., 2007). The ROS cause endothelial injury, mitochondrial dysfunction, oxidation of cell membranes and LDL oxidation. This ROS induced damage in turn activates pro-inflammatory pathways thus closing this self supportive vicious circle. Leptin correlates with adipose tissue volume (Considine RV. et al., 1996) and its levels are proportional to the energy reserves of the organism, it facilitates energy expenditure and enhances tissue inflammation through T lymphocytes (Lord GM. et

al., 1998). Studies show that particularly high levels of leptin exert proinflammatory effect, thus leptin was suggested as an important link among metabolic syndrome, cardiovascular diseases and obesity (Patel SB. et al., 2008).

Increased Expression in MetS (↑)	Decreased Expression in MetS (↓)
Leptin, PAI-1, chemerin	adiponectin
IL-1, IL-6, IL-8, MCP-1, TNF-α	omentin
High sensitivity CRP, fibrinogen	Il-10
Monocytic TLR2 and TLR4	

Table 2: Important adipose tissue hormones dysregulated in MetS (Fahed G. et al., 2022)

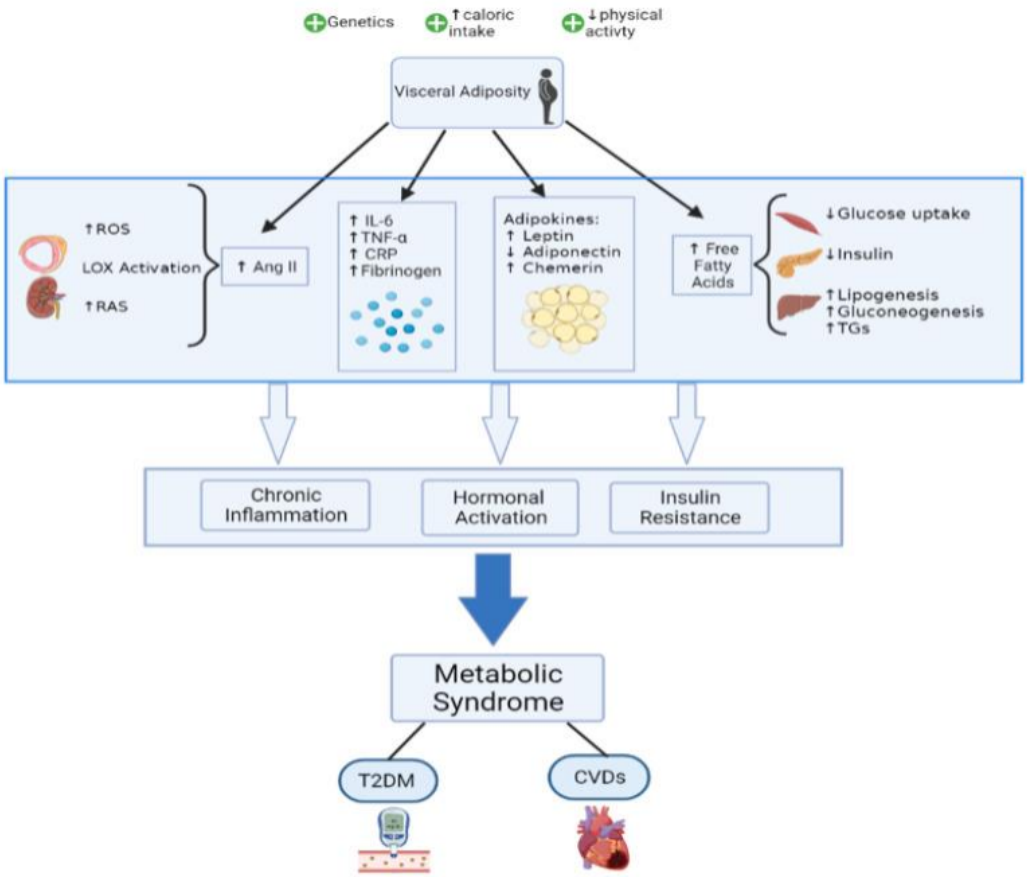

Figure 2: Role of adipose tissue and visceral obesity in metabolic syndrome. Taken from Fahed G. et al. 2022.

7.4. Genetic background of the Metabolic syndrome

MetS is a multifactorial disease with polygenic heritability pattern, and the extent to which every component of MetS will be manifested in each individual is a consequence of complex interaction among genetic background and environmental factors. The evidence of the genetic component of metabolic syndrome was provided with family and twin studies with the heritability ranging from 16 to 60% depending on the observed component (Bellia A. et al., 2009; Carmelli D. et al., 1994; Lin HF. et al., 2006-2012). The challenge to uncover the genetic determinants of MetS has been largely faced with candidate gene association studies, linkage analysis and genome wide association studies GWAS. The candidate gene studies and GWAS in human and murine GWAS have revealed that each of the main components (insulin resistance, obesity, hypertension and dyslipidemia) has a complex genetic background affected by numerous genetic variants, with most individual loci affecting only one or some of the comorbidities that comprise MetS (Abou Ziki MD. et al., 2016). In rodents, genetic studies of outlier strains with extreme forms of MetS have led to identification of variants with large effects. The advantage of this approach is in the effect size of the variants and the potential in characterizing their functional effects in vitro and in vivo (Abou Ziki MD. et al., 2016)

Studies in humans are still challenging even today in the era of large scale omics studies given the complex nature of this disease and numerous environmental factors which are impossible to control in a large population such as diet, energy expenditure or sedentary lifestyle etc. (Brown AE. et al., 2016), for this very reason studies performed on experimental rodent models play an important role in the research of polygenic diseases (Cox RD. et al., 2003; Reese DA. et al., 2005). Most progress has been made in identification of common variants that increase the risk for one or two metabolic risk factors. These GWAS (https://www.ebi.ac.uk/gwas/) have almost exclusively focused on the individual elements of the metabolic syndrome finding at least 56 loci reproducibly associated with obesity, 157 with lipids and over 90 loci associated with hypertension as well as the numerous loci associated with T2D (Brown AE. et al., 2016; Stancakova A. et al., 2014). Despite this though, studies of larger and more homogenous populations are necessary to identify variants that underlie the association of the diverse metabolic traits of this syndrome.

7.5. Methods to unravel the genetic background of complex traits

One of the most burning challenges of current genetics is to determine to what extent and how a certain allele or genetic variant influences a certain phenotype. This task is relatively uncomplicated for genetic variants with strong penetrance, strong phenotype, early onset of manifestation and Mendelian fashion of transmission (e.g.rare monogenic diseases). These rare variants were certainly able to unravel some information about complex traits, but were by far not able to explain gene-environmental interactions or interactions among genes participating on complex traits. For this reason, numerous methods have been developed, the main being the hypothesis-driven candidate gene studies (knock-out, knock-in) and the hypothesis-free GWAS or linkage studies.

7.5.1. Linkage analysis

For decades and particularly in the late 20th century linkage analysis has been a powerful method used for the genetic mapping of Mendelian and complex traits with familial aggregation (Ott J. et al., 2015). It is based on the assumption that genes closely related together on a single chromosome cosegregate as a unit during meiosis. Linkage analysis exploits wide range of markers (single nucleotide polymorphisms - SNPs, microsatellites, restriction fragment length polymorphisms (RFLP), microdeletions or insertions) spread across the genome, each with a high level of heterozygosity which is a necessary requirement for statistical robustness of the study. Subsequently, linkage analysis studies whether the ailment phenotype does cosegregate with any of the markers. In recent years, linkage analysis methods were overshadowed by GWA studies, although with the advent of whole-genome sequencing linkage analysis might yet prove to be a powerful method in detecting rare disease variants (Ott J. et al., 2015).

7.5.2. GWAS

Genome-wide association studies represent the most widely used approach for genetic analyses of common human diseases with multifactorial inheritance (Altshuler D. et al., 2008, Uffelmann E. et al., 2021). They are hypothesis-free observational studies aimed at finding genetic variants (particularly SNPs) at genomic loci spread across the genome that are significantly associated with complex traits in the population. The most commonly used and basic setup of GWA studies is case-control study where group of interest (e.g. individuals with disease) and control group are firstly genotyped for SNPs densely covering

all chromosomes, subsequently for each of these SNPs it is then investigated if the allele frequency is significantly altered between the case and the control group (Clarke GM. et al., 2011), (Figure 3). Potential candidate genes for the multifactorial diseases have been identified on every chromosome of the most commonly used model organisms (Perusse L. et al., 2004), moreover this finding is supported from genome-wide association studies data, what suggests an "omnigenic" hypothesis (Boyle EA. et al., 2017). GWAS have no or limited power to discover the molecular mechanism of the association with the disease for any particular sequence variant (Altshuler D. et al., 2008) ; however, intermediate phenotypes, especially gene expression, are also "mappable" as "eQTLs" using GWAS approach, and coincidence of an eQTL with a physiological QTL can often help to unravel the mechanism of complex disease susceptibility (Zhu Z. et al., 2016)

On the other hand, GWA studies have many limitations - loci displaying pleiotropy i.e. influencing two or more phenotypic traits significantly reduce power of these studies , furthermore it is certainly conceivable that a large number of phenotypically relevant genetic variants may be too rare to be noticed in GWAS and even go unnoticed in estimates of heritability (de Magalhães JP. et al., 2019) or on the contrary, significant loci may be of very little importance in the context of the whole phenotype. Another drawback of these studies poses gene variants which have become fixed, so this loss of variability prevents GWAS from detecting them no matter how significant their gene products are. (de Magalhães JP. et al., 2019).

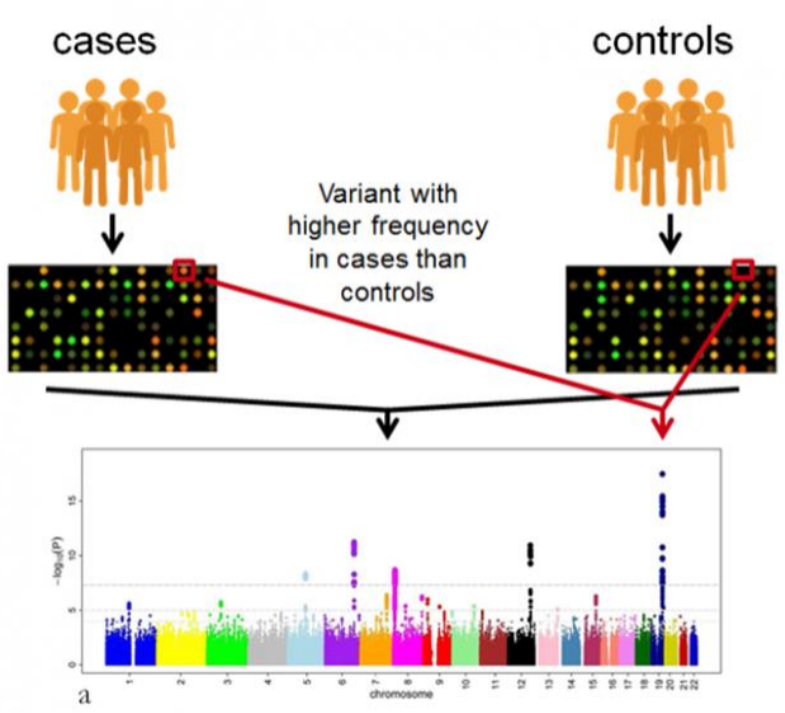

Figure 3: A simplified principle of GWAS. Data sets are sourced from large populations carrying the phenotype of interest. Each individual is genotyped using microarrays to capture common variants, or NGS methods. Genetic association tests are run for each genetic variant, using an appropriate model (for example, additive, non-additive, linear or logistic regression). Results are subject to statistical analyses to assign a *p-value* to each variant. (taken from www.ebi.ac.uk)

7.5.3. Comparative genomics and rodent models of human disease

Comparative genomics is a field of biological research which compares a wide range of genetic features among various species and helps to translate the knowledge obtained from genetically defined organisms to human biology. Genetically defined model (rodent) organisms are indispensable tools in experimental medicine and especially comparative genomics, confer valuable advantages in terms of dissection of genetic background of complex diseases, and as of today rodent models are the most used animal models to study metabolic syndrome (Fuchs T. et al., 2018). Their genes are similar to the human genes 99% of human genes have clearly defined orthologs in other mammals, beyond that and the shared genetic features may usually also involve gene order, regulatory sequences, and other genomic structural landmarks (Xia X. et al., 2013). Moreover, the animal's small space and nutrition requirements make it a cost-efficient model (Vandamme TF. et al., 2014). In general, the advantages of model organism usage confer the possibility of targeted modification of the genome, adjustment of the living and environmental conditions, diet, drug administration or other procedures and subsequently monitoring the effects on the

phenotype of such a change. Such an intervention would naturally be unthinkable and unethical in human research. However since the observed results cannot be directly translated into the human context, careful evaluation is warranted. Because of the above mentioned context various strains have been bred ranging from monogenic mutant models, polygenic models, models with population risk of acquiring metabolic syndrome, to transgene models or inbred congenic models. Each of these strains develop one or more traits underlying MetS (Wong SK. et al., 2016).

7.5.4. Commonly used types of rodent models:

Inbred lines – Inbred population is a genetically homogeneous population, where all individuals are identical and homozygous for every allele of their genome. Inbred strains are established by consecutive sib-pair mating for a minimum of 20 generations (Shinya M., 2016).

Congenic lines – are inbred lines with a part of their genome obtained from a different strain (Lagrange D. et al., 2010).

Transgenic lines – In a strict sense, transgenic lines are inbred lines which differ by a single gene, however recent years have seen rapid growth in popularity of modern genome- editing techniques including ZFNs, TALEN and CRISPR systems which allow not only to knock-in or knock-out genes and generate transgenic lines but also to edit genome on a much smaller scale (Zhang HX, 2019).

Consomic lines – are a special type of congenic strains. The consomic strains contain a whole chromosome obtained from a different strain (Lagrange D. et al., 2010).

Recombinant inbred lines (RILs)- these lines provide a robust mapping population for QTL studies. To generate the RILs the parenteral inbred lines are first crossed, the F1 generation is repeatedly intercrossed in order to further segregate the parental alleles. Selected pairs from the F2 progeny subsequently undergo repeated sibling intercrossing so every individual in the resulting RIL population is homozygous for every locus and represents a unique mix of parental alleles (Figure 4).

Near isogenic lines (NILs)– are a subtype of inbred lines, which are particularly useful for candidate gene approach to dissect the role of target gene or QTL variability on the phenotype. To obtain NILs a donor strain with the phenotype of interest is crossed with control strain (wild-type). The resulting progeny generation backcrossed with the parental

control generation. By repeating this process for a number of generations a population is eventually bred where each individual may contain a single genetic fragment introgressed to an otherwise homogeneous genetic background, (Figure 4). NILs can be used as a mapping population for QTL studies, one particular advantage of NILs is the diminished effect of genetic background since it is homogeneous.

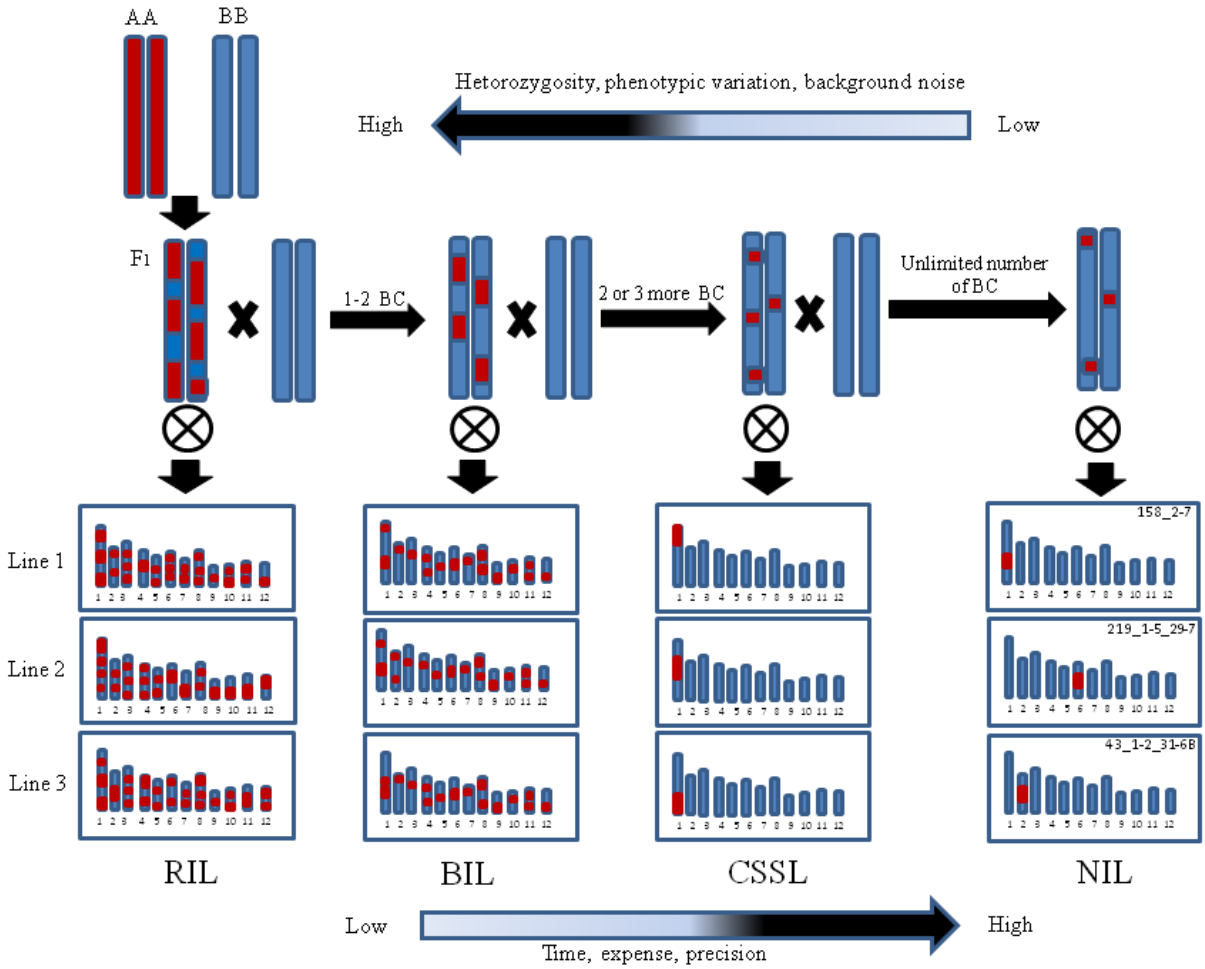

Figure 4: shows different types of mapping populations. RIL - recombinant inbred lines; backcross inbred lines (BILs), chromosome segment substitution lines (CSSLs) and near isogenic lines (NILs) , BC Backcross. Taken from Shakiba E. et al., 2014.

7.5.5. Transcriptome analysis

Transcriptome analysis is a study of transcripts produced by genome transcription by means of high throughput methods. Transcriptome analysis may be performed under various biological conditions and advanced methods such as single cell RNA sequencing enabled us to study single cells. Transcriptome comprises coding and non-coding RNA sequences such as rRNA, tRNA, snRNA, snoRNA, miRNA or lncRNA. This latter group may provide us with insight into the regulation of certain biological processes.

7.5.6. Epigenome analysis

By definition, epigenetics refers to molecular modifications on DNA that can regulate gene expression. These modifications comprise biochemical alterations of the chromatin without changing DNA sequence and are mitotically stable (Holliday R. et al., 2006). There are five main epigenetic mechanisms - DNA methylation/demethylation, histone modifications, chromatin remodeling, non-coding RNA and gene imprinting (Mohn F. et al., 2009) although the latter uses all the previous mechanisms and has a particularly significant role in evolutionary coadaptation and balancing parenteral conflict (Haig D. et al., 2014). Because data have linked epigenome dysregulation with a wide range of maladies including autoimmune disease, diabetes or cancer (Fang J. et al., 2014; Ling C. et al., 2019; Picascia A. et al., 2015;), the epigenome has sparked interest in the scientific community and recent years saw the rise of epigenome analyzing methods such as single cell epigenome sequencing (Armand EJ. et al., 2021) and genome-wide chromatin state annotation using Chromatin immunoprecipitation followed by sequencing (ChIP-seq) (Nakato R. et al., 2021) or bisulfite conversion of genomic DNA combined with next-generation sequencing (BS-seq) which is widely used to measure the methylation state of a whole genome, the methylome (Krueger F. et al., 2012). These novel methods enable systematic analysis of how the epigenomic landscape contributes to cell identity, development, lineage specification, and disease (Nakato R. et al., 2021), but thus far, only a few studies have successfully identified epigenetic regions and individual markers associated with separate MetS components (Akinyemiju T. et al., 2018; Das M. et al., 2016; Nuotio ML. et al., 2020; Zhang Y. et al., 2013).

7.5.7. Multi-omics approach

The advent of new high-throughput technologies accelerated by our need for comprehensive understanding of complex biological processes enabled us to analyze genome-scale quantities of data and at least partially solve some flaws resulting from GWAS and linkage analysis studies. The suffix „-omics" suggests a holistic view on a cluster of molecules (Hasin Y. et al., 2017). Multi-omics aims to combine two or more omics data sets to aid in data analysis, visualization and interpretation to determine the mechanism of a biological process.

The significant data within each omics group (genomics, proteomics, metabolomics, transcriptomics, epigenomics) give us an insight into pathophysiological processes related to disease and may serve as useful markers. Since the first transcriptomic arrays have been

available, it became clear that great proportion of the biologically significant disease mechanisms would be rather related to regulatory changes than changes resulting from mutations in coding regions like those that lead to the truncation of the coded protein, moreover focusing on only single omics group is limited, since it may reflect reactive processes rather than the causative ones.(Hasin Y. et al., 2017).

Accordingly, in order to tackle these large quantities of data and to dissect the genetic component of complex disease, an integration of various omics groups is required. This fusion of individual omics clusters confers a challenge resulting from data heterogeneity, different normalization, visualization etc. among omics groups (Krassowski M. et al., 2020). To tackle these obstacles, various multi-omics tools have been developed and are readily available including mixOmics (Rohart F. et al., 2017), SNF (Wang B. et al., 2014), Paintomics (Hernández-de-Diego R. et al., 2018). In recent years further progress has been made in the field of machine learning where some of its forms like multiview learning emerges as a powerful method for understanding functional multiomics (Nguyen ND. et al., 2020).

7.6. Plzf

The Promyelocytic zinc finger gene (*Plzf*) also known as zinc finger and BTB containing protein 16 *(Zbtb16)* is involved in the regulation of diverse cellular processes, including cell proliferation, apoptosis, differentiation, stem cell maintenance and organ development and seems to act as master regulator (Jin Y. et al., 2017, Liu TM., et al. 2016). In recent years *Plzf* emerged as an important candidate gene in metabolic syndrome development, and was proved to be connected to all features of metabolic syndrome (Šeda O. et al., 2017). Plzf protein is a member of the Krüppel Cys2His2-type zinc-finger protein family and came firstly into main research focus when Grignani (Grignani F. et al., 1998) unveiled its causative role in acute promyelocytic leukemia. Further research recognized *Plzf* as a transcription factor executing its functions either as an activator or repressor, additionally Plzf may interfere with epigenomic landscape (Suliman BA. et al., 2012). Structurally Plzf consists of three main domains. The first domain - bric à brac, tramtrack, and broad protein domain (BTB/POZ) mediates repression of transcription by promoting SMRT/mSin3-HDAC-NCoR corepressor complex. The second domain (RD2) is a target of posttranslational modifications such as acetylation (Guidez F. et al., 2005, Sadler AJ. et al., 2015), ubiquitination (Sobieszczuk DF. et al., 2010) and sumoylation (Kang SI. et al., 2003).

The third domain is DNA binding Krüppel Cys2His2-type zinc-finger domain (Figure 5). This structural scaffold reflects and underpins the role of Plzf as a transcriptional modulator and repressor (Li JY. et al., 1997).

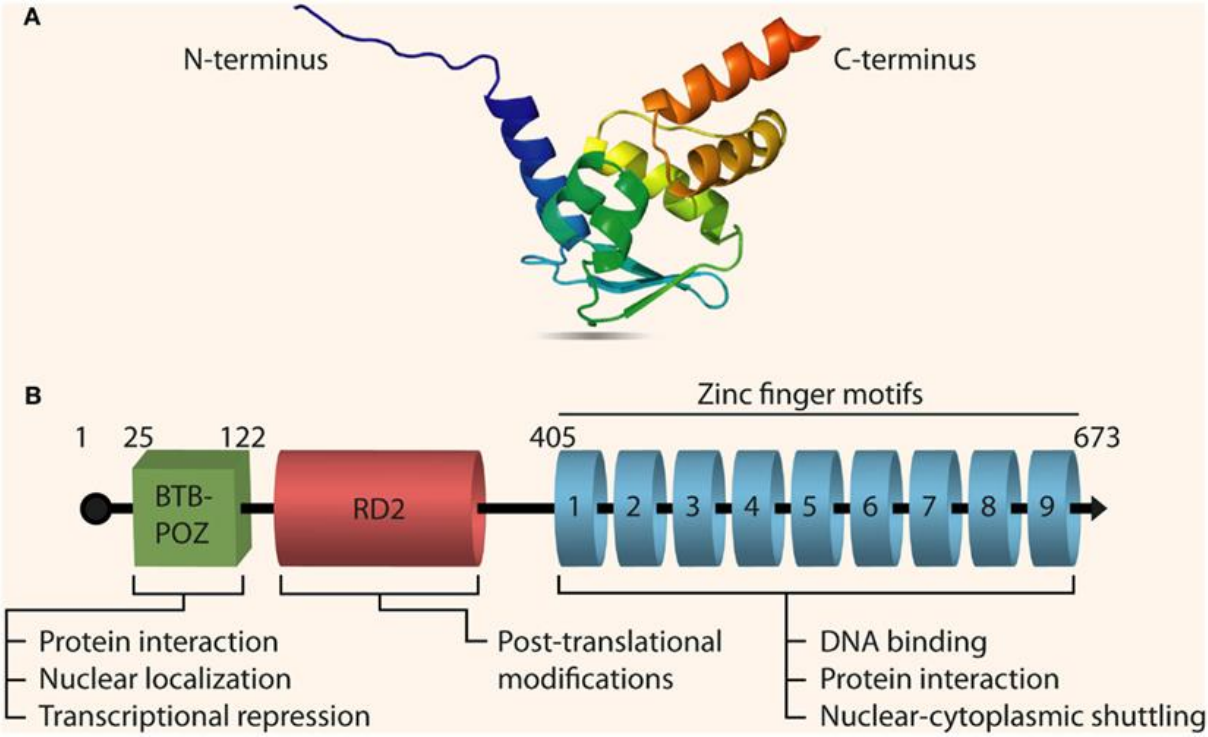

Figure 5: Schematic structure of Plzf. (A) crystal structure of PLZF resolved using X-ray diffraction as published by Li X. et al., 1999; (B)The full-length primary transcript of PLZF (Gene ID: 7704, Transcript ID: ENST00000335953) with its three functional domains: the BTB/POZ domain, the RD2 domain, and the zinc finger domain, taken from Suliman BA. et al., 2012

7.6.1. Plzf in cardiac hypertrophy and hypertension

As mentioned above, Plzf has a multifaceted role in metabolic syndrome. A mounting evidence suggests an important role of Plzf in development of cardiac hypertrophy and arterial hypertension. This could be put down to the fact that Plzf interacts with the renin angiotensin axis by direct action on the AT2 and (pro)renin receptors with subsequent activation of phosphatidylinositol-3 kinase p85α subunit (Ahmed BA. et al., 2011; Funke-Kaiser H. et al., 2010, Shamansurova Z. et al., 2016). Plzf also inhibits Na^+ reuptake in renal epithelial cells upon aldosterone stimulation and hence makes up a negative feedback loop (Naray-Fejes-Toth A. et al., 2008). It was shown that SHR with TALEN targeted *Plzf* exhibited an amelioration of cardiac hypertrophy and increased sensitivity of adipose and muscle tissue to insulin action when compared with wild-type controls (Liška F. et al., 2017).

7.6.2. Plzf in adipose tissue

Large comparative epigenomic analysis of murine and human adipogenesis comparing chromatin state maps, *PPARγ*, *CTCF* localization maps and gene expression profiles from murine and human models of adipogenesis, showing relationship between open chromatin marks and transcription factor motifs identified and validated *Plzf* and *Srf* as regulators of adipogenesis. (Mikkelsen TS. et al., 2010). *Plzf* represses adipogenesis by enhancing cell respiratory capacity, increases mitochondrial count, stimulates thermogenic program in brown adipose tissue (Mikkelsen TS. et al., 2010) and mRNA levels reversely correlate with ectopic fat deposition (Ying F. et al., 2017; Plaisier CL. et al., 2012). *Plzf* is induced in energy consuming tissues (brown adipose tissue) where *Plzf* overexpression activates thermogenic program, including genes involved in fatty acid oxidation, glycolysis and mitochondrial function (Plaisier CL. et al., 2012) but is inhibited in energy storing tissues (white adipose tissue) (Chen S. et al., 2014). Plzf increases the number of mitochondria and the glucose consumption and may reduce the content of the TAG in the cell (Ying F. et al., 2017), this finding was supported by observation in Dgat1-transgenic mice where Plzf was substantially downregulated favoring intramuscular fat deposition (Ying F. et al., 2017).

7.6.3. Plzf in liver tissue

Plzf appears to function primarily as a repressor by recruiting nuclear receptor co-repressors (N-CoRs), histone deacetylases (HDACs) mSin3a, and SMRT via highly conserved residues in its POZ domain (Melnick A. et al., 2002). Through this mechanisms, PLZF exerts its epigenic function and maintains propagation of a repressive chromatin environment and further chromatin remodeling activity to cause gene silencing (Guidez F. et al., 2007), This PLZF-mediated transcriptional repression is reversible by HDAC inhibitors (David G. et al., 1998). This repressory function is particularly important during the development of invariant NKT cells where PLZF is expressed and directs their effector program (Klibi J. et al., 2021). In particular Invariant natural killer T (*i*NKT) cells are sensitive to lipid tissue antigens, which mediates immune liver tissue inflammation and by some authors may be a reason for NAFLD development (Crosby CM. et al., 2018). Recent study conducted by (Hu H. et al., 2022) stressed an important activator role of Plzf. According to the paper, the Plzf activatory function is dependent on switching between acetylation and phosphorylation state. Activated Plzf then binds to SREBP-1c promotor and activates lipogenic genes (Hu H. et al., 2022). This finding was supported by observation in C57BL/6J mice displaying fatty liver

phenotype and overexpressed PLZF, while the knockdown of hepatic Plzf leads to a contrary effect on hepatic steatosis (Hu H. et al. 2022), moreover Plzf promotes gluconeogenic gene expression and hepatic glucose output leading to hyperglycemia and enhancing insulin resistance probably by decreasing phosphorylation of IRS1, Akt and FoxO1 a key elements in insulin signaling cascade and stimulates hepatic glucose synthesis as PPARγ coactivator (Chen S. et al., 2014). This finding is supported by restoring glucose homeostasis and insulin sensitivity in db/db mice with hepatic PLZF knockout (Chen S. et al., 2014). While all this data imply robust evidence of the involvement of the Plzf in all attributes of metabolic syndrome, backed by the data from animal models, the underlying mechanisms remain still elusive.

7.6.4. Plzf in metabolic syndrome

The first insight into the genetic architecture of metabolic syndrome provided linkage studies in recombinant inbred strains and in F2 populations derived from the SHR and normotensive strains which mapped possible quantitative trait loci (QTLs) on chromosomes 1, 2, 4, 8, 13, 16, 19 and 20 (Křen V. et al., 1997) . This approach however, could not discern between falsely positive linkages and genuine QTLs containing molecular determinants responsible for manifestation of metabolic syndrome. To tackle this problem, a set of recombinant inbred strains was produced by transferring single chromosome regions of the corresponding chromosome regions from an appropriate normotensive strain onto the SHR genetic background to establish to what extent the individual QTLs affect observed phenotype (Šeda O. et al. 2005). Introgression of a 30cM segment derived from chromosome 8 of the normotensive BN-Lx strain onto the SHR background resulted in substantial reductions in systolic and diastolic blood pressure and cardiac mass. (Křen V. et al., 1997). The consequent process focused on identification of causative alleles which were deemed to be trapped within the recombinant segment of chromosome 8. For that purpose, a set of congenic sublines was produced, which differed in the lengths of their respective recombinant segments. The differential segment of SHR-Lx PD5 congenic substrain [SHR.PD(D8Rat42-D8Arb23)/Cub] harbors a short segment of PD origin which was precisely mapped using high density recombinant markers and contains just 7 genes: P*lzf*, *Htr3a*, *Htr3b*, *Usp28*, *Zw10*, *Tmprss5*, and *Drd2.* (Liška F. et al., 2014). In spite of this minute genomic difference from its SHR progenitor strain, SHR-Lx PD5 rats displayed lower total body weight, postprandial triglyceride concentrations and a tendency towards and enhanced glucose tolerance (Šeda O. et al., 2005) which indicated a presence of

causative allele trapped within the congenic segment. Dexamethasone administration led to significant elevation of TAG in SHR-Lx PD5 (Šeda O. et al., 2005). Sequencing unraveled an intronic deletion in the Plzf gene which is unique to the PD/Cub strain and is not present in any other normotensive or hypertensive rat strain (Liška F. et al. 2014). These findings helped to establish Plzf as a candidate gene in metabolic syndrome pathophysiology. Because the Plzf targeted allele is semilethal, morphologically normal heterozygous rats were used for metabolic and hemodynamic analyses. SHR-Plzf+/− heterozygotes versus SHR wild-type controls exhibited reduced body weight and relative weight of epididymal fat, lower serum and liver triglycerides and cholesterol, and better glucose tolerance. In addition, SHR-Plzf+/− rats exhibited significantly increased sensitivity of adipose and muscle tissue to insulin action when compared with wild-type controls. Blood pressure was comparable in SHR versus SHR-Plzf+/- (Liška F. et al., 2017). As a follow up to further dissect the role of Plzf, a single gene congenic strain was produced (SHR-Lx.PD5$^{PD\text{-}Zbtb16}$), harboring *Plzf* of PD origin on SHR background. This novel strain displayed markedly increased plasma TG and diminished insulin sensitivity of skeletal muscle tissue after dexamethasone admission in comparison to other novel minimal congenic strain SHR-Lx.PD5$^{SHR\text{-}Zbtb16}$ with *Plzf* of SHR origin (Krupková M. et al., 2018) .

7.6.5. Plzf as pleomorphic factor

Plzf is expressed in various cell types across different tissues (Uhlen M. et al., 2005). As a powerful transcription factor, Plzf regulates a wide spectrum of biological processes from cell proliferation, differentiation, spermatogenesis, limb development to stem cell maintenance and innate immune cell development (Liška F. et al., 2009; Suliman BA. et al., 2012; Jin Y. et al., 2017). PLZF has a specific, non-redundant and vital function for the development of a complete immune system (Alonzo ES. et al., 2011) and is particularly essential for the correct development of natural killer T cells (Kovalovsky D. et al., 2008). Emerging evidence also shows that PLZF regulates the balance of self-renewal and differentiation in stem cells (Liu TM., et al. 2016). Hematopoietic stem cells harboring inactivated Plzf displayed decreased repopulation potential, present an amplified aging phenotype, suggesting that Plzf controls age-related pathway (Vincent-Fabert C. et al., 2016). Plzf is also an important gene in oncology research. Although its role in oncogenesis was primarily uncovered with promyelocytic leukemia (Chen Z. et al., 1993; Jansen JH., et al., 2001) , recent findings underline the role of Plzf in various solid tumors

particularly as a tumor suppressor gene (Table 4) since it regulates the cell cycle and apoptosis in various cell types (Suliman BA. et al., 2012)

Alteration of Plzf expression in solid tumors	
Upregulated	**Downregulated**
Clear cell renal cell carcinoma	Hepatocellular carcinoma
Colon cancer	Lung cancer
Glioblastoma	Melanoma
Testicular seminoma	Pancreatic cancer
	Prostate cancer
	Thyroid carcinoma

Table 3: Relative alterations in Plzf expression in various tumors compared to respective. It implicates important role of Plzf in oncogenesis and underlines its pleiotropic function. Taken from Jin Y. et al., 2017)

8. The aims of the thesis

The chief goal of this work was to identify genetic determinants underlying metabolic syndrome and to dissect the role of Plzf within the complex network of these determinants.

1, elucidate the genetic background leading to amelioration of blood pressure and cardiac fibrosis in SHR minimal congenic strain PD5

2, compare transcriptional and phenotypic changes in PD and SHR rat strains after high fat diet and unravel pathophysiological mechanisms underlying PD susceptibility to metabolic syndrome.

3, compare transcriptional and phenotypic changes in PD5 and SHR rat strains before and after dexamethasone administration in order to uncover the role of Plzf in glucocorticoid induced metabolic syndrome.

9. Ethic statement

All experiments were performed according to the guidelines of the Declaration of Helsinki and in agreement with the Animal Protection Law of the Czech Republic (311/1997) which is in compliance with the European Community Council recommendations for the use of laboratory animals 86/609/ECC and were evaluated and approved by the Ethical committee of the First Faculty of Medicine and the Ministry of Education, Youth and Sports of the Czech Republic (protocol ID MSMT-1461/2015-17). Animals were held under temperature and humidity controlled conditions on a 12-h light/dark cycle. At all times, the animals had free access to food and water. There were no unexpected deaths throughout the experiment. All efforts were made to minimize suffering of the experimental animals.

10. Methods

10.1. Rodent models of metabolic syndrome

10.1.1. Spontaneously hypertensive rat SHR

Spontaneously hypertensive rat (SHR/OlaIpcv, RGDID 631848) is probably the most studied rodent model of essential hypertension and metabolic syndrome. SHR is a polygenic, highly inbred model of metabolic syndrome which shows marked hypertension, dyslipidemia, insulin resistance and is predisposed to left ventricular hypertrophy and myocardial fibrosis, in general however, is not considered obese. It was created in Japan in the sixties by crossing outbred Wistar Kyoto hypertensive rats (Okamoto K. et al., 1963) and has ever since been preserved by brother sister mating. So far, dysregulation of several genes involved in the pathogenesis of MetS components have been identified *(cd36, ogn, srebp, folr1*). (Pravenec M. et al., 1990, 2007, 2010, 2016; Aitman TJ. et al., 1999).

10.1.2. Polydactylous rat, PD strain

Polydactylous rat (PD/Cub, RGDID 728161) is a result of random breeding of a polydactylous pair of Wistar-Kyoto rats with leg malformation and subsequent brother sister mating. It is a well defined luxate syndrome model with markedly high triglyceridemia and insulin resistance even with comparison with SHR, but lacks hypertension (Šedová L. et al., 2000). Polydactylous rat is particularly sensitive to aggravation of insulin resistance and triacylglycerolaemia after a diet rich in carbohydrates, as opposed to Brown Norway. (Šeda O. et al., 2005)

10.1.3. Brown Norway strain

Brown Norway (BN/Cub, RGDID 737899) was derived from a brown mutation in a pen-bred colony in 1958 by Billingham and Silvers (Billingham RE. et al., 1959). The rats were brought from the USA to the Institute of Biology, First Faculty of Medicine in Prague in 1964 and bred since by brother x sister mating for more than 100 generations. Brown Norway strain is suitable to use as an experimental control having normal metabolic profile and normotension (Šeda O. et al., 2002).

10.1.4. PD5 rat strain

PD5 formally described as SHR.PD (D8Rat42-D8Arb23)/Cub (RGD ID: 1641851) is a minimal congenic strain derived from SHR rat strain. PD5 strain has been established by

introgression of a small segment of chromosome 8 from the PD/Cub strain, on the genetic background of SHR by repeated backcrossing. Using the high definition marker-assisted approach the congenic segment was identified as containing 788 kbp (chr8:51,897,776-52,685,422 according to the rat reference genome version 3.4), encompassing 7 genes: *Plzf, Htr3a, Htr3b, Usp28, Zw10, Tmprss5*, and *Drd2*. *Drd2* is represented in the segment only by its promoter, first noncoding exon, and part of the first intron. By sequencing the congenic segment a deletion in the noncoding sequence (with possible enhancer function) of *Plzf* was revealed (Liška F. et al., 2014). From the phenotypic point of view PD5 displays significantly lower blood pressure, heart weight (Křen V. et al., 1997), lesser tendency to myocardial fibrotization (Liška F. et al., 2014) and lower triacylglycerol and cholesterol levels (Krupková M. et al., 2014), when compared to SHR.

10.2. Experimental protocols and designs

10.2.1. Comparative transcriptome analysis of PD5 vs SHR heart tissue

Our aim in the first project was to elucidate the genetic background leading to amelioration of blood pressure and cardiac fibrosis in SHR minimal congenic strain PD5, and dissect the involved profibrotic pathways. For that purpose we used SHR and its minimal congenic strain PD5. Only male rats were used. Both strains were bred in-house. Rats were kept under 12 h light-dark cycle, fed standard laboratory chow and given access to water ad libitum. At 2 months of age rats were anesthetized and decapitated. Complete organs were weighed, left ventricular myocardium was snap frozen in liquid nitrogen, and used for further analysis.

10.2.2. Determining the effect of high fat diet on PD and SHR strains metabolic parameters and liver transcriptomes

In our second project, our goal was to dissect the genetic architecture responsible for PD susceptibility to metabolic syndrome and compare the transcriptional and phenotypic changes in PD and SHR rat strains without intervention and after a high fat diet. Thus Adult male rats of BN (n = 8), SHR (n = 6), and PD (n = 7) strains were used. Until the age of 6 months, they were fed a standard chow (Ssniff R-Z) diet ad libitum. Then, after an overnight fasting period, we recorded the body weight and fasting glycemia, and performed the oral glucose tolerance test (OGTT) (3 g/kg body weight, 30% aqueous solution; Ascensia Elite Blood Glucose Meter; Bayer HealthCare, Mishawaka, IN, USA). Subsequently, rats were fed HFD (Ssniff EF R/M with 30% fat, containing saturated fatty acids (FAs), short- to long-chain FAs, corresponding to approximately 50% of energy, for four weeks. Rat males had

free access to food (except the initial and final overnight fasting period) and water, and they were held under humidity- and temperature-controlled conditions on a 12-12-h light-dark cycle. Diet consumption was measured as the difference in weight of the feeding dose of pellets and remaining pellets after 3–4 days (twice each week). After 4 weeks (after overnight fasting period), the oral glucose tolerance test was performed again, and each male's body weight was recorded. After, males were sacrificed by decapitation and their blood serum and tissues were collected for further analyses.

10.2.3. Comparative transcriptomic analysis of SHR and PD5 strains after dexamethasone admission and Plzf proteomic study.

Here, we intended to relate the transcriptomic alterations with the phenotypic changes in PD5 and SHR rat strains after dexamethasone admission in order to fully elucidate the role of Plzf in development of metabolic syndrome. Only male SHR (n=14) and male PD5 (n=19) were used. Rats were kept under 12 h light-dark cycle, fed standard laboratory chow and given access to water ad libitum. After 12 months, both strains were divided into two groups with one group from each strain receiving DEX (Dexamed, Medochemie) in drinking water (2.6 μg/ml) for 3 days SHR standard diet n=7; SHR dexamethasone n=7; PD5 standard diet n=10; PD5 dexamethasone n=9). Subsequently the oral glucose tolerance test (OGTT) was performed after overnight fasting. Blood for glycaemia determination was drawn from the tail at intervals of 0, 30, 60 and 120 minutes after the intragastric glucose administration to conscious rats (3 g/kg total body weight, 30% aqueous solution). After that all rats were anesthetized and decapitated.

10.2.4. Tissue Collection

Selected tissues (liver, heart, kidneys, adrenal glands, brown fat tissue, epididymal fat tissue, retroperitoneal fat tissue, soleus muscle, and diaphragm) were dissected and weighed (except the diaphragm). The tissues were flash-frozen in liquid nitrogen and stored at −80 °C for future analysis.

10.2.5. Biochemical Parameters

10.2.5.1. Lipidogram

0,5ml blood samples were harvested immediately after decapitation. The whole blood was then centrifuged at 3000x g for 15 minutes, after that the plasma was harvested and freezed in -20°C until further analysis. The serum lipoprotein distribution was evaluated using gel-

permeation high-performance liquid chromatography (GP-HPLC) and LipoSEARCH® algorithm (Toyobo Inc., Japan), (Hara I. et al., 1986; Okazaki M. et al., 2016; Toshima G. et al., 2013). With this technique, the serum lipoproteins were separated according to their size in SkylightPakLP1-AA gel permeation columns (Skylight Biotech Inc., Japan, 300 mm × 4.6 mm I.D.). The resulting effluent was divided in two equal parallel columns and loaded in two reactor coils (PTFE; 25 m × 0.18 mm I.D.) prior to measuring the content of cholesterol and triglyceride of each lipoprotein subfraction by enzymatic degradation in each of the two parallel columns using commercially available kits (Roche Diagnostics, Basel, Germany). After the enzymatic degradation, an absorbance at 550 nm was continuously monitored, and the sizes of each lipoprotein was determined by their retention times of the peaks observed on a chromatogram using a linear calibration curve (Usui S. et al., 2000; Toshima G. et al., 2013). The resulting chromatogram is a composite picture of each sample where every lipoprotein particle is classified in one of the 4 major classes and in one of the 20 lipoprotein subfractions according to cholesterol, TG content and their size using the Gaussian curve fitting technique (Beaufrère H. et al., 2020; Okazaki M. et al., 2016; Toshima G. et al., 2013), (Supplementary table 8). The measurement was performed in an external laboratory.

10.2.5.2. Free fatty acids (FFA)

Serum levels of Free fatty acid before and after feeding HFD were analyzed using commercially available acyl-CoA oxidase-based colorimetric kits (Roche Diagnostics, Basel, Germany). Briefly, the levels of FFA are determined by coupled two-step enzymatic reaction, where Acyl-CoA synthetase in the presence of ATP firstly catalyzes fatty acid acylation of coenzyme A. The Acyl-CoA is oxidized by Acyl CoA Oxidase in the subsequent reaction, thus producing hydrogen peroxide which then reacts with the kit's Colorimetric Probe. The colorimetric dye is measured on the spectrophotometer in the visible wavelength range at 546 nm. The measurement was performed in an external laboratory.

10.2.5.3. Insulin

Insulin levels before and after HFD feeding were determined using the Rat Insulin ELISA kit (Mercodia AB, Uppsala, Sweden). The measurement was performed in an external laboratory.

10.2.5.4. Adiponectin

Adiponectin serum levels before and after HFD feeding were determined using the Rat Adiponectin ELISA kit (MyBioSource, San Diego, CA, USA). The measurement was performed in an external laboratory.

10.2.5.5. C-peptide, GIP, GLP-1, Glucagon, Leptin, PP, and PYY

Levels of C-Peptide 2, GIP, GLP-1, glucagon, insulin, leptin, PP, and PYY before and after HFD were assessed via Milliplex Metabolic Hormone MAGNETIC kit using the BioPlex 200 system (Bio-Rad Laboratories, Inc., Hercules, CA, USA, Merck Millipore Corp., Billerica, MA, USA). The measurement was performed in an external laboratory.

10.2.5.6. Cytokines

The cytokine profiles of male rats before and after HFD were assessed via Bio-Plex Pro™ Rat Cytokine 23-Plex Assay (Bio-Rad Laboratories, Inc., Hercules, CA, USA, Luminex Corporation, Austin, TX, USA) for levels of G-CSF, GM-CSF, GRO/KC, IFN-γ, IL-1α, IL-1β, IL-2, IL-4, IL-5, IL-6, IL-7, IL-10, IL-12p70, IL-13, IL-17, IL-18, M-CSF, MCP-1, MIP-1α, MIP-3α, RANTES, TNF-α, and VEGF using the BioPlex system (Bio-Rad Laboratories, Inc., Hercules, CA, USA). The measurement was performed in an external laboratory.

10.2.5.7. Lipid Levels in Liver Tissue

In order to determine TAG, DAG and cholesterol in the liver, the tissues were powdered under liquid N2 and extracted for 16 h in chloroform:methanol followed by the addition of 2% KH2PO4. The solution was then centrifuged. samples were extracted in a chloroform/methanol mixture. The resulting pellet was dissolved in isopropyl alcohol, after which the TAG content was determined by enzymatic assay (Erba-Lachema, Brno, Czech Republic). Briefly, the TAG content was lyzed to free fatty acids and glycerol, which was oxidized and reacted with to generate fluorescence. The hepatic diacylglycerols were separated using a modified Folche extraction method (HÜTTL M. et al., 2020) using chloroform/methanol solution, followed by thin-layer chromatography and its quantitative content was determined by enzymatic assay (Erba-Lachema, Brno, Czech Republic).

10.2.6. Gene Expression

10.2.6.1. RNA Isolation

For RNA isolation and purification we used RNeasy Plus Mini Kit (Qiagen, Hilden, Germany). Total RNA from relevant organs (liver, heart, kidneys, adrenal glands, brown fat tissue, epididymal fat tissue, retroperitoneal fat tissue, soleus muscle, and diaphragm) was used. Tissues were homogenized in Trizol (Thermo Fisher Scientific, Waltham, MA, USA) using TissueLyser LT (Qiagen, Hilden, Germany). 200µl Chloroform was added per RNA sample and the mixture was incubated at room temperature for 10 minutes, then centrifuged in a cooled centrifuge (4°C) at 12000 g for 15 minutes to achieve phase separation. The aqueous phase was mixed 1:1 with 70% ethanol, vigorously shaken and 500µl of the mixture was applied to RNeasy mini spin columns centrifuged at 8000 g at room temperature for 15 s and the flowthrough was discarded. Three consecutive steps of centrifugation at room temperature at 8000g for 15s each with buffer addition in the following order (RW1, RPE and RPE buffer) was followed by centrifugation at 8000 g for 2 min and centrifugation at maximum speed for 2 minutes. In each of these steps the flowthrough was discarded. Finally the RNA was eluted physically in RNAse free water by centrifugation of the spin mini columns at room temperature at 8000g for 60s. Obtained RNA was quantified and purity was assessed by spectrophotometry (Eppendorf BioPhotometer©, Hamburg, Germany) at 260/280 nm OD

10.2.6.2. RNA Integrity

The quality of the isolated RNA was assessed as a measure of integrity using an Agilent Bioanalyzer 2100 on RNA-6000 Nano-LabChip (Agilent, Böblingen, Germany). which is an microfluidics-based automated electrophoresis system for the sample quality control of RNA, DNA or protein biomolecules. In the first step 1 µl of the RNA 6000 Nano dye concentrate is added to 65 µl of the prefiltered Agilent RNA 6000 nano gel matrix and spinned for 10 minutes at room temperature at 13000 g. The gel dye mix is then loaded onto the RNA chip , pressed in the priming station to ensure the evenly distribution of the mix and RNA 6000 nano marker and RNA ladder are consequently pipeted in respective wells on the chip. RNA samples are heat denatured (70 °C, 2 minutes) before loading 1 µl of the RNA sample in denoted wells. The chip is vortexed in a proprietary IKA vortex mixer© and analyzed in the Agilent 2100 bioanalyzer. As an objective quantification of integrity output this system provides RIN (RNA integrity number) ranging from 1 (completely degraded

RNA) to 10 being high quality RNA. Only samples showing RNA integrity numbers (RIN) above 8 were used for further analysis.

10.2.6.3. Gene Expression

The transcriptome was assessed using Affymetrix GeneChip® Rat Gene 2.1 arrays (Affymetrix, Santa Clara, CA, USA). Only good-quality RNA was isolated from liver or heart tissue obtained from SHR, PD/Cub, Brown Norway and PD5 strains and was used in our respective experiments. For the first experiment 3 SHR and 3 PD5 male rats were used, in the second experiment we chose 4 male rats from each strain (SHR, PD/Cub and BN), for the third experiment we used 3 male rats from each strain and diet (SHR, SHR + dexamethasone, PD5, PD5 + dexamethasone). The isolation was performed by the Trizol (Thermo Fisher Scientific, Waltham, MA, USA) extraction method as described above following preclearing Qiagen RNeasy Mini kit® (Qiagen, Hilden, Germany) and precipitation by 3M NaOAc. In our experiment we opted for the two- cycle target labeling protocol. In the first cycle of the reaction the RNA was reverse-transcribed by incubation for 1 hour in cycler at 42°C for using T7-oligo(Dt) primers (which adds T7 promotor to the 5´end of the cDNA), Superscript II reverse and first-strand Master mix (Affymetrix, Santa Clara, CA, USA), after 1 hour the mix was heated to 70°C in order to deactivate the polymerase. The ensuing single stranded cDNA is incubated 2 hours at 16°C, then 10 minutes at 75°C with E.Coli DNA polymerase I, RNase H (which helps to simultaneously degrade the RNA) and First cycle second strand master mix. This RNase mediated synthesis creates the second-strand cDNA which serves as a template for complementary RNA (cRNA) synthesis. Briefly, the second-strand cDNA is incubated for 16 hours at 37°C with IVT Master Mix (MEGAscript® T7 Kit, Thermo Fisher Scientific, Waltham, MA, USA) after the incubation the samples are mixed with ethanol and IVT cRNA Binding Buffer, loaded onto purification spin columns and repeatedly centrifuged. The yield of the cRNA was determined on a spectrophotometer (Eppendorf BioPhotometer©, Hamburg, Germany) at 260/280 nm OD. In the second cycle of the reaction the purified cRNA from the previous reaction is incubated with random primers and Second-Cycle, First-Strand Master Mix© containing Superscript II polymerase. The mix is then incubated for 1 hour at 42°C, cooled and incubated for additional 20 minutes at 37°C with RNase H, thus a first-strand cDNA is synthesized, which consequently serves as a template for second-strand cDNA synthesis. In this reaction first strand cDNA is incubated for 2 hours at 16°C with T7 Oligo (dT) primers and Second-Cycle, Second-Strand Master Mix containing E.coli polymerase I, after

incubation T7 polymerase is added to the mixture and incubated for 10 minutes at 16°C, the resulting double stranded cDNA is loaded in the presence of cDNA Binding Buffer to the cDNA Cleanup Spin Column and centrifuge for 1 minute at ≥ 8000 x g. The cDNA is eluted from the column using an elution buffer. The buffers are proprietary to the kit (GeneChip cleanup module, Thermo Fisher Scientific, Waltham, MA, USA)

In the next step the cRNA was biotin labeled (with covalently bounded fluorescent marker by terminal deoxynucleotidyl transferase, purified, fragmented by DNA glycosylase and apurin/apyrimidinic endonuclease (APE1) which cleaves uracil nucleotides. The fragments were denatured at 99°C and hybridized onto the chip according to the manufacturer's protocol. This reaction is carried by Expression console software (Affymetrix, Santa Clara, CA, USA) was used to perform quality control.

10.2.6.4. Transcriptomic enrichment analysis and annotation clustering

In the first experiment, differential gene expression between strains was determined using PARTEK Genomics Suite 6.6 (Partek, St. Louis, MO, USA) software. We considered a p value lower than 0.05 as well as fold change <-1.5 or >1.5 with subsequent false discovery rate (FDR) correction, applying Benjamini-Hochberg procedure, where α=0.05 (5 % FDR) The data harvested in the second and third experiment , Transcriptome Analysis Console (TAC version 4.0.1, Affymetrix, Santa Clara, CA, USA) was used for data normalization, statistical analysis, and pathway enrichment using the robust multiarray average method (RMA). The transcriptomic data sets from each experiment were enriched for Gene ontology ("GO") terms by DAVID (Dennis G. et al., 2003) a web based annotation tool, Gene ontology terms were divided into 3 main GO categories which were GO molecular function, GO cellular compartment and GO biological process. The microarray data discussed in this publication has been deposited in NCBI's Gene Expression Omnibus (Edgar R. et al., 2002) and are accessible through GEO Serie accession number GSE16417 (first experiment), GSE126709 (second experiment) and GSE234984 (third experiment).

10.2.6.5. RT-PCR

In total 1 µg of total RNA was used to synthesize cDNA using SuperScript III reverse transcriptase (Invitrogen, Carlsbad, CA, USA). In the first part of the protocol 5µl of the RNA is mixed with 1µl oligo(DT) primers (Thermo Fisher Scientific, Waltham, MA, USA) which are complementary to the 3´mRNA poly(A) ending, 1µl dNTP and 6µl of RNAse free water. This mixture was denatured for 5 minutes at 65°C. In the next step 4µl of 5x FS

reaction buffer, 1µl of DTT, 1µl of RNaseOUT™ and 1µl of SuperScript III reverse transcriptase are added and cycled in labcycler (SensoQuest, Göttingen, Germany) for 60 min at 50°C and 15 min at 75°C. Along the reaction, two negative controls were made: negative control 1 without reverse transcriptase and negative control 2 without RNA. The resulting cDNA was diluted in a nuclease free water to a concentration c = 5 ng/µl and then used as a template in quantitative real-time PCR (qPCR) reactions.

10.2.6.6. qPCR

The different expression of candidate genes was verified by quantitative real-time PCR (qPCR). Primers for qPCR reactions were designed using PrimerBLAST (Ye J. et al., 2012) to span at least one exon–exon junction, with every amplicon within 70 to 200 bp range. All primers are listed in (Supplementary tables 1-3). All samples were used in triplicates. *Per1* and *Gadph* was amplified using the TaqMan® Gene Expression Master Mix (Applied Biosystems), *Acsl5, Acsm2a, Acsm3, Aox1, Apol, Casp12, Cd36, Ces2e, Crh, Cyp2b1, Cyp7b1,Doc2a, GCA, Insig1, KCNA5, Lepr, Lmod, Nox4, Npy, NR4a1, NR4a3,Oxt, Ppia, Pomc, Scd1, Rgs16, Sirt3, Slc17a2, Ugt2a3, Vas,* were amplified using the Power-up SYBRGreen master mix (Thermo Fisher Scientific, Waltham, MA, USA). For primer sequence see (Supplementary tables 1 – 3). Amplification was performed according to the respective manufacturer's instructions. Amplification was done in Applied Biosystems® 7900HT Real-Time PCR cycler system. Results were analyzed using the Livak (Livak K. et al., 2001) analysis method with every expression compared to glyceraldehyde 3-phosphate dehydrogenase (*Gapdh*) or cyclophilin (*Ppia*) as a reference gene expression.

10.2.7. DNA Sequencing

Sequencing of *Acsm3* in PD strain: Because of the impossibility of amplifying cDNA (absence of cDNA of *Acsm3* in liver tissue from PD), genomic DNA was used for sequencing of *Acsm3*. Long-range PCR products were sequenced on an Illumina MiSeq using the Nextera XT DNA Library Preparation Kit (Illumina), for primers see (Supplementary table 4). Bioinformatic analysis was done with the help of Galaxy (https://usegalaxy.org). Mapping was done by BWA-MEM (Burrows-Wheeler Aligner). Duplicated reads were removed by Picard (http://broadinstitute.github.io/picard/). FreeBayes was used to identify sequence variants (Garrison E. et al., 2012). IGV (Integrated Genome Viewer) was used for data visualization.

10.2.8. Western Blotting

Tissues were homogenized in aqueous buffer EBC (50 mM Tris pH 8, 120 mM NaCl and 0.5 % NP-40) supplemented by protease inhibitor cocktail Complete (Roche, Basel, Switzerland) and 35 µl β-mercaptoethanol per 10 ml of solution using TissueLyser (Qiagen, Hilden, Germany). N-terminal rabbit monoclonal anti-Nra4a1 antibody (anti-Nur77; ab109180) was purchased from Abcam (Cambridge, UK), mouse monoclonal Acsm3 antibody (G-8; sc-377173) was purchased from Santa Cruz Biotechnologies, Inc., Dallas, TX, USA, N-terminal rabbit monoclonal anti-Plzf antibody (ab189849) was purchased from Abcam (Cambridge, UK). As controls mouse anti-αtubulin (B-5-2-1) was purchased from Sigma-Aldrich (St. Louis, MO, USA), mouse monoclonal Vinculin antibody (VLN01) was purchased from Thermo Fisher Scientific, Waltham, MA, USA. Tissue lysates (for every experiment 3 samples from each strain) were run on SDS-PAGE (12% separating gel) in 1x tris-glycine SDS at 200 V for 100 min (ACSM3) or 110 min (PLZF) respectively, the control antibodies were run for the same time as respective target antibody. The separated proteins were heat denatured and blotted onto PVDF membranes Immobilon P (EMD Millipore Biosciences, Billerica, MA, USA) preincubated in 100% methanol for 10 min and PBS buffer with 10% Tween-20 acting as a detergent for additional 10 minutes. The blotting itself was performed in 1 tris-glycine SDS buffer with 20% methanol for 75 min at 60 V. After blotting, nonspecific empty sites were blocked by incubation in 5% milk solution for 2 hours at room temperature. Membranes were incubated overnight at 4 °C with primary antibodies at a final dilution of 1:3000 NR4A1, 1:3000 PLZF, 1:10000 α-tubulin, 1:200 ACSM3 and 1:10,000 Vinculin. Adding PBS buffer with 10% Tween-20 after incubation washed away non-bound primary antibodies. Secondary anti-mouse (ACSM3, Vinkulin, α-tubulin) or anti-rabbit (PLZF) antibodies (Mouse Ig NA931, Rabbit Ig NA934, GE Healthcare, Chicago,IL, USA) were bound and signal was detected after 2 hour incubation in room temperature using an ECL Prime chemiluminescent detection kit and Hyperfilm ECL (all from GE Healthcare Bio-Sciences, Chicago, IL, USA). Developed hyperfilms were scanned and densitometry was performed in ImageJ (Schneider CA. et al., 2012).

10.2.9. Luciferase assay

10.2.9.1. Recombinant Plzf construct preparation

Genomic DNA obtained from SHR liver tissue was used to amplify 5 constructs in total. The respective relation of the constructs and their design is depicted in (Figure 6). Constructs denoted as “A (all)”, “L (left)”, “R (right)” and “Full” were spanning the intronic deletion

of Plzf. While “R” corresponded to the most conserved region of intronic deletion, the “A” segment was congruous with the whole span of the deletion, and the “L “ was analogous to the least conserved sequence of the intronic deletion. The constructs “out” and “full” correspond to the highly conserved sequence 5′ up before the intronic deletion, furthermore the “full” construct spaned over the most conserved part of the intronic deletion. PCR products and plasmids pGL4.10 and pGL4.23 (Promega, Madison, WI, USA, Figure 7) were cut with appropriate restriction endonucleases (Supplementary table 6), ligated and electroporated in E. coli TOP10 cells (ThermoFisher). The vector pGL4.10 is a promotorless vector designed to measure the activity of promoter and enhancer sequences with a luciferase assay, the vector pGL4.23 contains a minimal promoter for measuring the activity of transcriptional response elements. The backbone of these vectors encodes luc2 gene encoding luciferase enzyme and an ampicillin resistance gene to allow for selection in E. coli (Figure 7). The bacteria were inoculated onto Petri dishes containing Luria Broth (LB) with ampicillin cultivated overnight at 37 degrees. The following day selected colonies were transferred in a liquid LB medium and propagated for an additional day. The amplified bacteria were centrifuged and the plasmid DNA was isolated from the pellets by standard alkaline method with QIAGEN® Plasmid Mini kit (Qiagen, Hilden, Germany). The correct sequence and orientation of the constructs cloned in the plasmids was verified by restriction analysis and sequencing (Next generation sequencing, Iluminna).

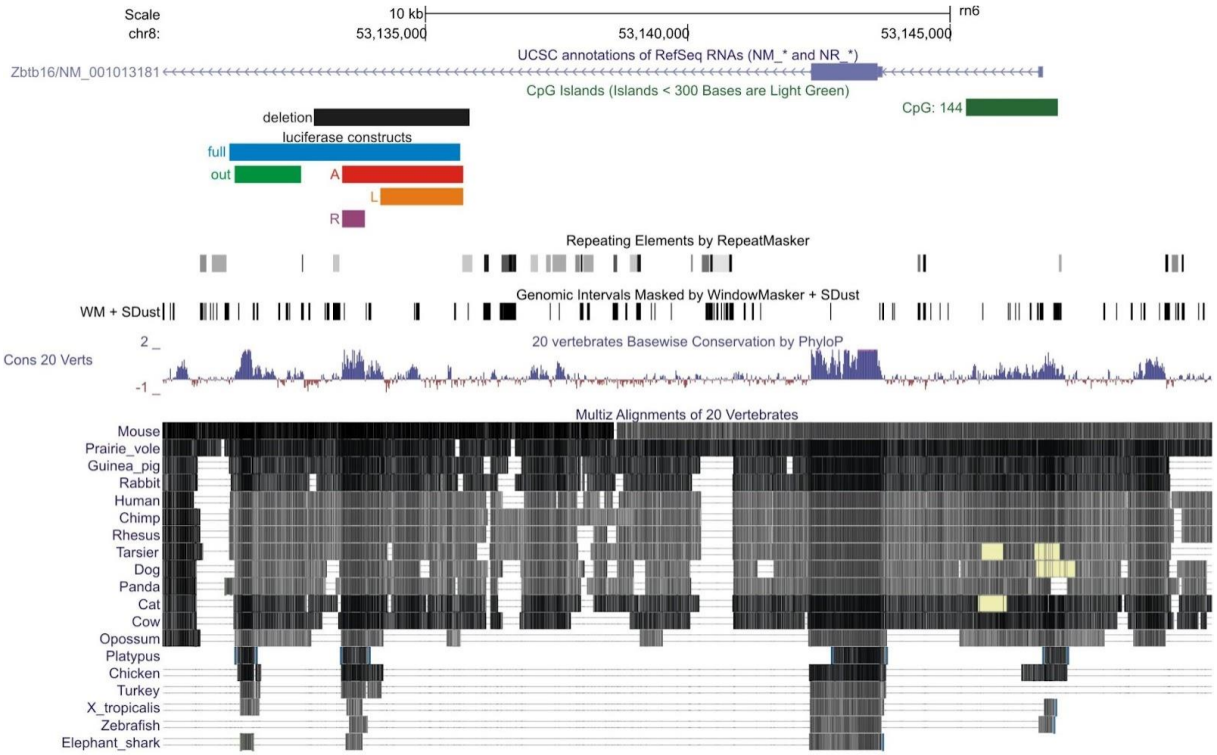

Figure 6. Scheme depicts relation of recombinant constructs to Plzf coding sequence and its conserved domains.

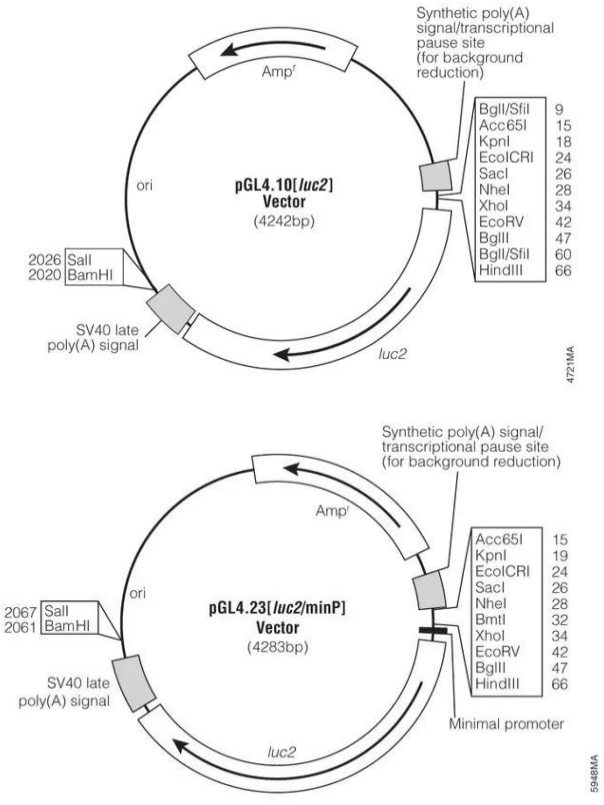

Figure 7:. Scheme of pGL4.10 and pGL4.23 vectors. Taken from Promega.com.

10.2.9.2. Cell cultures

Human cervical hepatocellular carcinoma (HepG2) cells purchased from Sigma-Aldrich (St. Louis, MO, USA) or HEK293 cell purchased from Thermofisher (Waltham, Massachusetts) were grown in D-MEM supplemented with 10% fetal bovine serum (FBS), penicillin (100 IU/mL) and streptomycin (100 mg/mL) at 37 °C in 5% CO_2 humidified atmosphere. Both cell types were grown without dexamethasone and with added dexamethasone in final concentration of 110nM. Transfections were carried out using ViaFect (E4981, Promega) according to the manufacturer's protocol. Briefly 10µl of the signature ViaFect™ transfection reagent is incubated with 0.1µl of the DNA. After 20 minute incubation at room temperature the mixture is added to cells (100µl) and returned to the incubator for additional 24–48 hours.

10.2.9.3. Luciferase reporter assay

The firefly luciferase reporter pGL4.10 and pGL4.23 constructs were co-transfected with Renilla luciferase reporter vector pGL4.74 into HepG2 cells by ViaFect (E4981, Promega Madison, WI, USA) or to HEK293 cells (derived from human embryonic kidney tissue). The reporter vector pGl4.74 is engineered to serve as an internal control since it produces luciferase by induction of a "renilla promoter" in *hRluc* gene. After 24 h cells were lysed, luciferase activity was measured according to Dual-Glo®Luciferase Assay System protocol (E2920, Promega, Madison, WI, USA), and the Infinite 200® luminometer (Tecan, Männedorf, Switzerland). Briefly, after cell lysis luciferin is added which serves as a substrate for firefly luciferase enzyme, the addition of substrate, Mg+, ATP triggers the bioluminescence reaction, (Figure 8). Luminescence signal from empty vectors was set as threshold for background signal. Data were normalized to renilla luciferase activity induced by addition of substrate coelenterazine and assay was performed in triplicate and repeated at least three times.

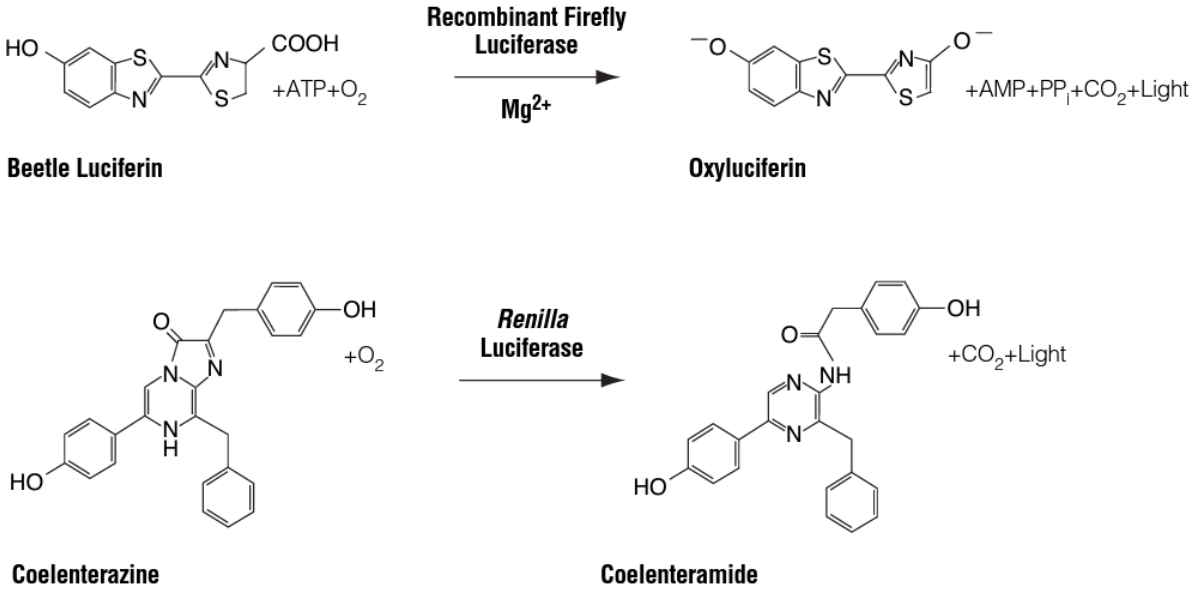

Figure 8: Bioluminescent reaction catalyzed by Renilla and Firefly luciferase. Taken from dual-Glo Luciferase Assay System Technical Manual TM058, Promega.

10.2.10. GST pull-down assay

10.2.10.1. Cloning, production and purification of Plzf domains and GST-fusion proteins

Three Plzf constructs encompassing whole gene Plzf, BTB and Zinc finger domains were prepared by standard PCR using cDNA obtained from BN heart tissues. The amplified constructs were restricted with a combination of restriction endonucleases (EcoRI +HindIII for pET42b plasmid, BTB and ZF domain; EcoRI+SalI for construct ALL). For primers see (Supplementary table 5). Constructs were ligated to pET42b plasmids and were in vivo amplified using E. coli cells. pET42b plasmid distincts itself by incorporated schistosomal glutathione-S-transferase (GST•Tag) coding sequence as a fusion partner to GST pulldown assays. The cells were grown on Luria Bertani medium enriched with Kanamycin thus selecting cells with incorporated plasmid since the plasmid encodes Kanamycin resistance gene at 37 degrees for 16 hours with subsequent further propagation in liquid LB medium for an additional day. Grown cells were harvested by centrifugation, lysed and plasmids were isolated by standard alkaline method with QIAGEN® Plasmid Mini kit (Qiagen, Hilden, Germany). Plasmids were sequenced on an Illumina MiSeq using the Nextera XT DNA Library Preparation Kit (Illumina). The Plzf constructs and cassettes for prokaryotic protein expression are shown in (Figure 9). Sequence-verified constructs were re-transformed in the expression cells Rosetta(DE3)pLysS cellsThe cells carry a chromosomal copy of the T7

RNA polymerase gene under control of the lacUV5 promoter, which enables these cells to facilitate eukaryotic protein expression which are rarely expressed in prokaryotic cell and divert the bacterial translation apparatus to produce dominantly the recombinant protein.Rosetta(DE3)pLysS cells also contain plasmid pLysSRARE which encodes gene for chloramphenicol resistance, tRNAs which are essential for eukaryotic protein expression and a lysozyme (T7 polymerase inhibitor), (Figure 10). The cells were grown for 16 hours in LB medium containing kanamycin (50ml/ml) and chloramphenicol (33mg/ml) at 37 degrees celsius, with shaking at 250 rpm to an OD600 of approximately 0.5 what indicates the end of the exponential phase. The expression of the recombinant constructs was induced by addition of 1mM IPTG which is a strong inducer of lacUV5 promoter which in turn induces the expression of the T7 RNA polymerase. The protein production was conducted at 37 °C and lasted for 3 hours. The fusion proteins were purified by affinity chromatography using Glutathione HiCap Matrix (Quiagen, Hilden, Germany). The columns are first equilibrated with PBS-EW buffer (1x PBS, 1mM DTT, 1mM EDTA). The cells were lysed (1x PBS, protease inhibitor, DNaseI (QIAGEN), RNase A (Fermentas, ThermoFisher scientific) and then poured onto the resin thus enabling the GST-tagged proteins to enzymatically bind onto the matrix, then two washing with PBS-EW buffer is followed by elution of the tagged proteins by TNGT buffer (50 mM Tris-HCl, 150 mM NaCl, 15% glycerol, 0.5% Triton X-100, 10 mM imidazole [pH 7.5]). The pure fusion proteins were analyzed by sodium dodecyl sulfate polyacrylamide gel electrophoresis (SDS-PAGE). The concentration of the protein samples was determined using spectrophotometry.

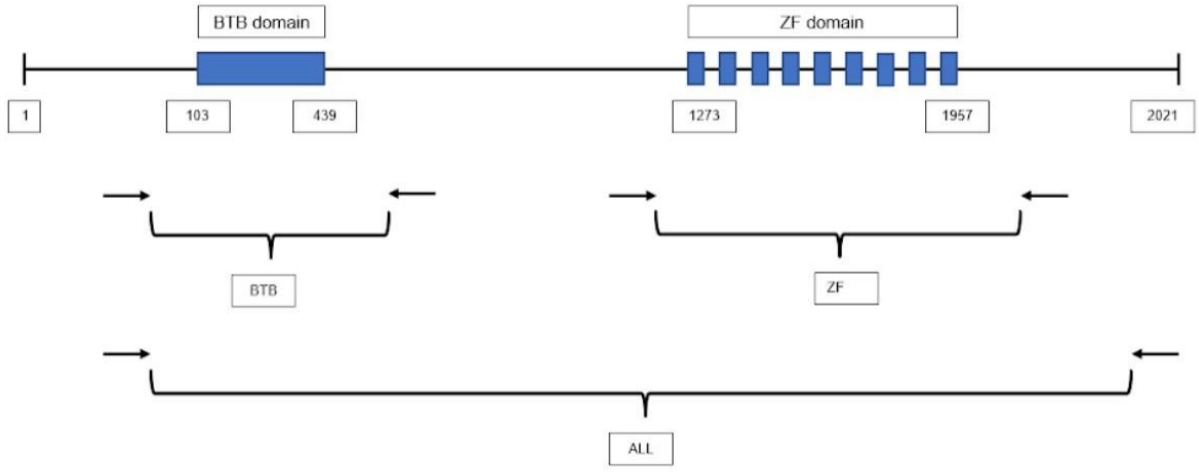

Figure 9: Simplified scheme of *Plzf* coding sequence and recombinant constructs.

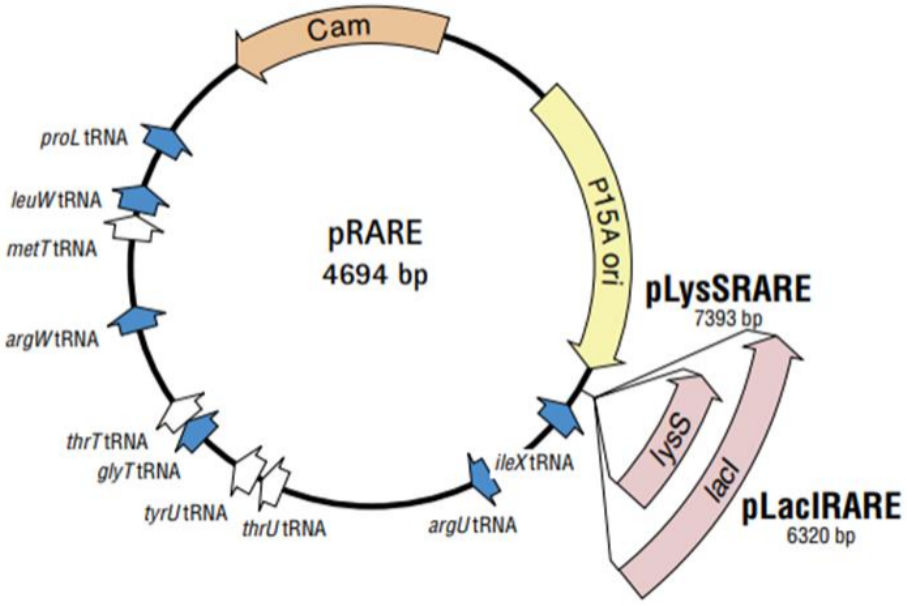

Figure 10: Plasmid pRARE essentially constructed in Rosetta(DE3) pLysS. Taken from: Novagen brochure - Competent cells.

10.2.10.2. Liver tissue prey protein lysate preparation

Male SHR liver tissue on standard laboratory chow was snap frozen, homogenized in liquid nitrogen and resuspended in Tris/NaCl based GST pull down binding and wash buffer (50mM Tris-Hcl, 200mM NaCl, 1mM DTT, 1mM MgCl2, Igepal 0,05%, protease inhibitors). Protein lysate was subsequently pre-cleared on the glutathione matrix in order to eliminate any nonspecific binding of protein lysate onto the GST assay.

10.2.10.3. Pull-down assay

Three GST-tagged fusion proteins were used in the experiment: GST-tagged BTB domain, GST-tagged Plzf zinc finger domain, GST-tagged full-length Plzf sequence and GST-tagged empty plasmid as a positive control to prove the binding ability of GST to bind on the matrix. As a negative control, we added prey protein lysate on the HiCap matrix without adding either GST tagged bait protein or GST non tagged control. The GST-tagged fusion proteins purified previously(see 10.2.10.1) were again were again immobilized (25 µg each) on the glutathione matrix. Subsequently they were incubated with precleared liver protein lysate at 4 °C overnight in the TN1 buffer (50mM Tris-HCl pH 8.0, 200mM NaCl, 0,05% Igepal CA-630/NP-40, 1mM DTT, 1mM $MgCl_2$, protease inhibitors). The reaction mixtures were

washed three times with the same buffer TN1. Bound GST fusion proteins were eluted by 500 µl of 50mM Tris, pH 8, 400mM. NaCl, 50mM reduced glutathione and 1mM DTT. 100µl was used for further analysis.

10.2.10.4. Protein Digestion

Eluted proteins were reduced by boiling at 95°C for 10 min in 100mM TEAB containing 2% SDC, 40mM chloroacetamide, 10mM TCEP. Samples were further precleared using paramagnetic beads, termed single-Pot Solid-Phase-enhanced Sample Preparation (SP3) according to Hughes (Hughes CS. et al., 2014, 2019). The preclearing step is vital for the depletion of contaminating substances while at the same time reducing sample losses. Briefly 5 µl of SP3 beads was added to 30 µg of protein in the lysis buffer and filled to 50 µl with 100mM TEAB. Protein binding was induced by addition of ethanol to 60 % (vol./vol.) final concentration. Samples were mixed and incubated for 5 min at room temperature. After binding, the tubes were placed into a magnetic rack and the unbound supernatant was discarded. Beads were subsequently washed two times with 180 µl of 80% ethanol. All rinses were carried out while tubes were mounted on the magnetic rack. After washing, samples were digested with trypsin (trypsin/protein ratio 1/30) reconstituted in 100mM TEAB at 37°C overnight. After digestion samples were acidified with TFA to 1% final concentration and peptides were desalted using in-house made stage tips packed with C18 disks (Empore) according to Rappsilber (Rappsilber J. et al., 2007). This experiment was performed in an external laboratory.

10.2.10.5. nLC-MS 2 Analysis

Nano Reversed phase column (EASY-Spray column, 50 cm x 75 µm ID, PepMap C18, 2 µm particles, 100 Å pore size) was used for LC/MS analysis. Mobile phase buffer A was composed of water and 0.1% formic acid. Mobile phase B was composed of acetonitrile and 0.1% formic acid. Samples were loaded onto the trap column (Acclaim PepMap300, C18, 5 µm, 300 Å Wide Pore, 300 µm x 5 mm, 5 Cartridges) for 4 min at 15 µl/min. Loading buffer was composed of water, 2% acetonitrile and 0.1% trifluoroacetic acid. Peptides were eluted with Mobile phase B gradient from 4% to 35% B in 60 min. Eluting peptide cations were converted to gas-phase ions by electrospray ionization and analyzed on a Thermo Orbitrap Fusion (Q-OT- qIT, Thermo). Survey scans of peptide precursors from 350 to 1400 m/z were performed at 120K resolution (at 200 m/z) with a 5 × 10 5 ion count target. Tandem MS was performed by isolation at 1,5 Th with the quadrupole, HCD fragmentation with normalized

collision energy of 30, and rapid scan MS analysis in the ion trap. The MS/MS ion count target was set to 10 4 and the max injection time was 35 ms. Only those precursors with charge state 2–6 were sampled for MS/MS. The dynamic exclusion duration was set to 45 s with a 10 ppm tolerance around the selected precursor and its isotopes. Monoisotopic precursor selection was turned on. The instrument was run in top speed mode with 2 s cycles.(Hebert AS. et al., 2014). The data were analyzed using the Andromeda search engine by label-free quantification (LFQ) algorithms in Max-Quant v1.6.3.4 . The enzyme specificity of trypsin was set as C-terminal Arg and Lys residues. MethylThio was the fixed modification,while N-terminal protein acetylation and methionine oxidation were variable modifications. The false discovery rate (FDR) parameter was set to 1% for both proteins and peptides.The measurement was performed in an external laboratory.

10.2.10.6. Data analysis

All data were analyzed and quantified with the MaxQuant software (version 2.0.2.0)(Cox J. et al., 2014). The false discovery rate (FDR) was set to 1% for both proteins and peptides and we specified a minimum peptide length of seven amino acids. The Andromeda search engine (Cox J. et al., 2011) was used for the MS/MS spectra search against the Rattus norvegicus database (downloaded from uniport.org in September 2022, containing 22 909) and database containing individual sequences of used protein constructs. Enzyme specificity was set as C- terminal to Arg and Lys, also allowing cleavage at proline bonds and a maximum of two missed cleavages. Dithiomethylation of cysteine was selected as fixed modification and N-terminal protein acetylation and methionine oxidation as variable modifications. The "match between runs" feature of MaxQuant was used to transfer identifications to other LC-MS/MS runs based on their masses and retention time (maximum deviation 0.7 min) and this was also used in quantification experiments. Quantifications were performed with the label-free algorithms described recently (Rappsilber J. et al., 2007). Data analysis was performed using Perseus 1.6.15.0 software (Tyanova S. et al., 2016). Proteins with intensities above control GST or below detection were not counted. This analysis was performed in an external laboratory.

10.2.11. Statistical Analysis

Statistical evaluation of morphometric data and metabolic parameters was performed using STATISTICA 12 (TIBCO Software, Palo Alto, CA, USA). Data are presented as arithmetic

means ± SEM if not indicated otherwise. The groups were compared by using ANOVA (analysis of variance–tissue weight, insulin levels, gene expression in selected tissues), ANOVA for repeated measurements (oGTT, AUC before and after exposure to HFD, animal weight), and general linear model ANOVA (lipoprotein fractions, with 3 factors–strain, cholesterol or TAG, fraction) if the variances within each group were similar. In case of different variances within the group, the nonparametric test (Kruskal–Wallis test) was used. The comparison was followed by the post-hoc Tukey test. The cutoff for the significant results was determined as a *p*-value lower than 0.05. In the case of gene expression data (lined up by their *p*-value), false discovery rate (FDR) correction was conducted, applying the Benjamini–Hochberg procedure, where $\alpha = 0.05$ (5 % FDR). The FDR procedure was repeated for post-hoc comparison of each of the two strains, and a fold change cutoff <-1.2 or >1.2 was applied. For the qPCR experiment, the cycle threshold (Ct) values of selected genes were normalized relative to the expression of the peptidylprolyl isomerase A (*Ppia*) (cyclophilin) gene (for liver tissue) and ribosomal protein L41 (*Rpl41*) gene (for epididymal fat tissue), which served as the internal control, with results being determined in triplicates. Relative quantification was performed using the ΔΔCt method. Statistical analysis was performed using ANOVA on the normally distributed ΔΔCt values.

11. Results

11.1. Results - experiment 1

11.1.1. Total body and organ weight

Adult male rats of SHR (n = 8), and PD5 (n = 8) strains fed a standard laboratory chow were used.The rats were decapitated at the age of 2 months and their organs weighed. The SHR strain displayed a significantly larger total body weight compared to PD5, which projected into the proportionally increased absolute weights of the individual organs namely heart, liver, soleus muscle. Both the absolute and relative weight of the kidneys was significantly larger in SHR, (Figure

11).

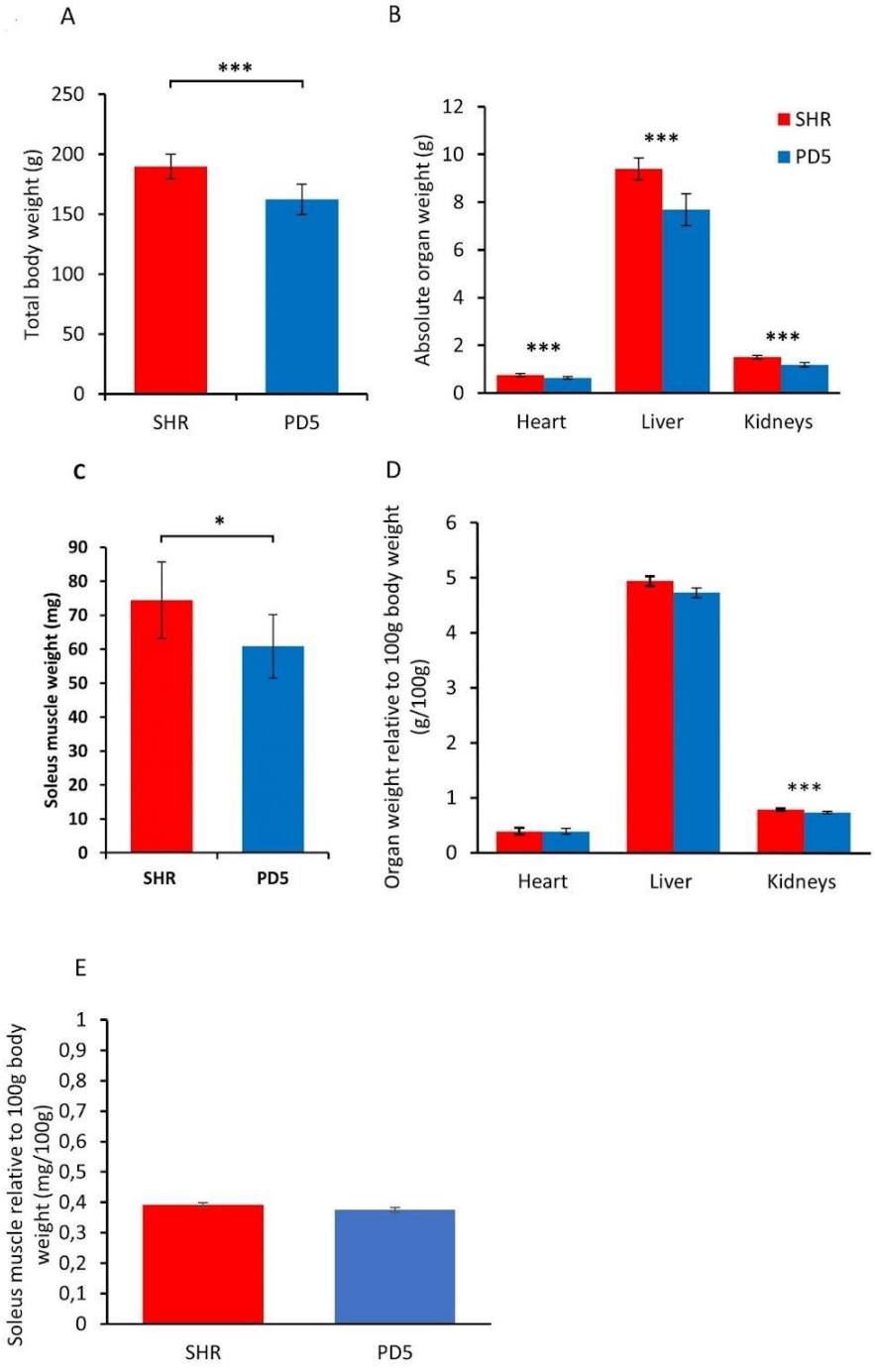

Figure 11: morphometric profile of adult male rats-PD5 (blue, n = 8), SHR (red, n = 8). (a) Total body weight. (b)and (c) Relative tissue weights per 100 g body weight after HFD. (d) and (e) Relative tissue weights per 100g body weight Data are presented as arithmetic means ± SEM. Statistical significance levels are indicated as follows: * $p < 0.05$, ** $p < 0.01$, *** $p < 0.001$

11.1.2. Dissection of differentially expressed genes

In total, eight samples of myocardium, four of each strain, were used for microarray experiments. The raw data were corrected for multiple comparison bias using Benjamini-Hochberg procedure. After the FDR correction (set to 5%) , 18 probes sets (about 0.008 % of 220,232) were identified as significantly differentially expressed between the SHR and PD5. These probe sets represented 10 up-regulated and 8 down-regulated known genes or loci in PD5 compared to SHR (Table 5).

Downregulated in PD5	Upregulated in PD5
Crlf1, Dusp2, Dvl1, Kcna5, LOC500300 Nfkbia, Pax3, *Per1*	*Col9a1, E9PT29_RAT, Epha7, Ephb3, Nr4a1, Nr4a3, Ptprt, Reln, Smg6*, *Tiam1*

Table 5: Table shows downregulated resp. upregulated significantly expressed genes in SHR, PD5 heart tissue

11.1.3. Bioinformatic analysis

To obtain a more in-depth understanding of the above mentioned differentially expressed genes as to their function we performed a Gene ontology (GO function) enrichment of these 18 significantly differentially expressed genes using DAVID. Gene ontology terms were divided into 3 main GO categories which were GO molecular function, GO cellular compartment and GO biological process. Within the molecular function subgroup the top five enriched terms were as follows: GO:0005515 protein binding, GO:0051393 alpha-actinin binding, GO:0035259 glucocorticoid receptor binding, GO:0048365 Rac GTPase binding, GO:0005003 ephrin receptor activity. Within the biological process subgroup the top five enriched terms were as follows: GO:0016477 cell migration, GO:0048013 ephrin receptor signaling pathway, GO:0007411 axon guidance, GO:0045893 positive regulation of transcription, DNA-templated, GO:0071376 cellular response to corticotropin-releasing hormone stimulus. As far as the GO cellular compartment is concerned only three terms – GO:0043025 neuronal cell body, GO:0030425 dendrite, GO:0005737 cytoplasm were enriched. None of the GO terms reached statistical significance.

11.1.4. Confirmation of differentially expressed genes

To validate the transcriptomic data, we selected four differentially expressed genes for qPCR analysis (Per1, Kcna5, Nr3a4 and Nr3a1). All the observed results were in a good concordance with the microarray data (Figure 12). We were able to confirm Nr4a1

upregulation in PD5 compared to SHR also on protein level using Western blotting (Figure. 13).

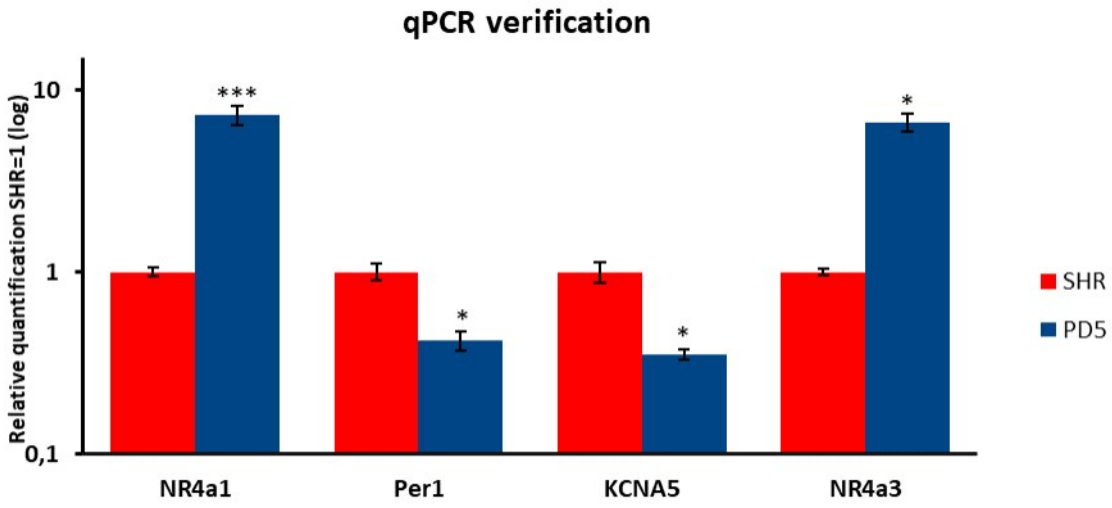

Figure 12: qPCR validation of microarray results of heart tissue of SHR (n=6) and PD5 (n=6) rat strains: Nr4a1 – nuclear receptor subfamily 4 group A member 1, Nr4a3 – nuclear receptor subfamily 4 group A member 3, Kcna5 – potassium VoltageGated Channel Subfamily A Member 5, Per1 – period circadian regulator 1, Data are presented as arithmetic means ± SEM. Statistical significance levels for the factor strain of one-way ANOVA are indicated for pair-wise post hoc Tukey's test as follows: * $p < 0.05$, ** $p < 0.01$, *** $p < 0.001$.

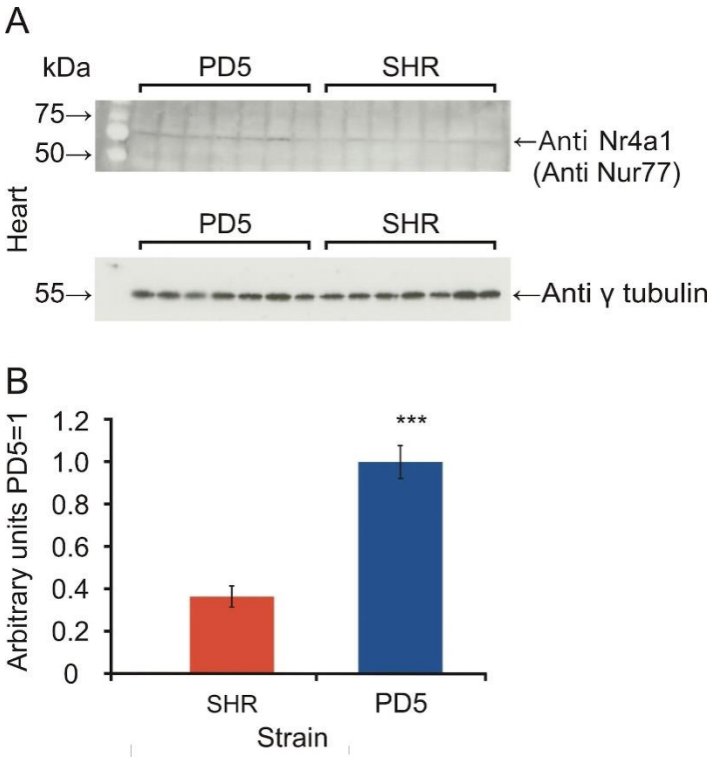

Figure 13: Western blot of Nr4a1 protein (nuclear receptor 4 alpha 1, also known as Nur77) shows upregulation in the minimal congenic strain PD5 compared to SHR. Western blotting using N-terminal antiNur77 antibody in the heart (A), Densitometry data (representing means ± S.E.M, ***=p<0.001; n=7 for both SHR and PD5

rat strains (B). Theoretical molecular weight of unmodified Nr4a1 is 64 kDa. We observed the signal consistently at slightly >60 kDa.

11.1.5. Pathway analysis of differentially expressed genes

In silico analysis using Ingenuity Pathway analysis (IPA; Qiagen) was performed to get a better understanding of the mutual interactions among these transcripts (Figure 14). This analysis uncovered a wide range of possible interactions of these genes and pathways responsible for blood pressure regulation and other components of metabolic syndrome. Particularly interesting is the interaction with eNOS signaling pathway, renin-angiotensin signaling, as well as VEGF signaling pathways.

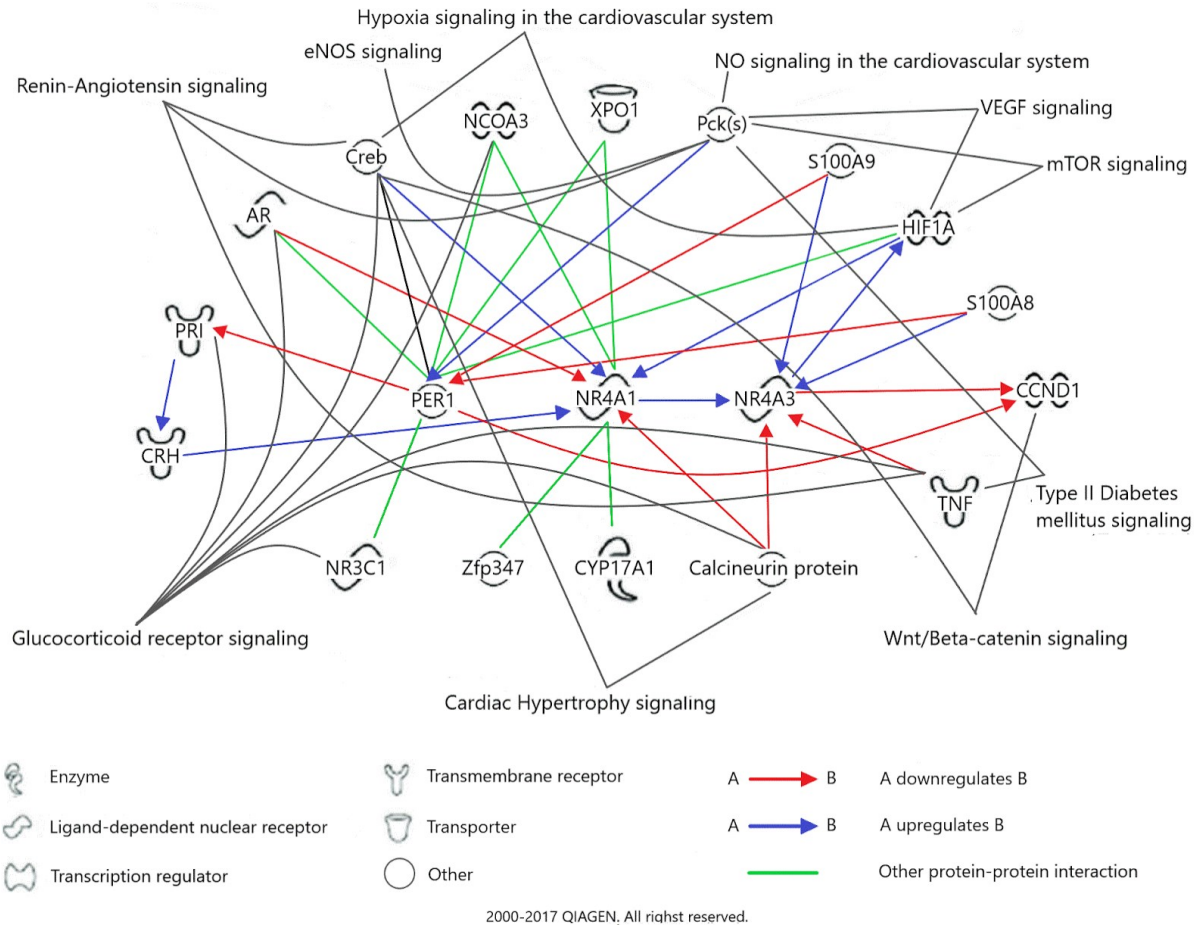

Figure 14: The highest-score network derived using the set of transcripts verified by qPCR derived using Ingenuity Pathway Analysis, and showing significant STRAIN (PD5 * SHR) interaction

11.2. Results - experiment 2

11.2.1. Biometrical analysis of SHR, PD/Cub and BN

11.2.1.1. Total body weight

Adult male rats of BN (n = 8), SHR (n = 6), and PD (n = 7) strain were used. Until the age of 6 months, they were fed a standard chow (ssniff R-Z) diet ad libitum. Then, after an overnight fasting period, we recorded the body weight. Initially, we did not observe any significant difference in total body weight between PD and SHR strain, however the PD strain male rats had significantly higher total body weight than BN strain (Figure 15). After 6 months we administered a high fat diet (Supplementary table 7) for 28 days, which led to further weight gain in all strains. Notably, while PD strain gained weight continuously till the end of the experiment, the BN and SHR strains reached plateau within 7th and 14th day of the experiment (Figure 15a). At the end of the experiment, the most significant gain was by far observed in PD strain, while in BN the weight gain was only moderate. SHR weight gain was more profound than in BN strain albeit not as in PD strain (Figure 15b).

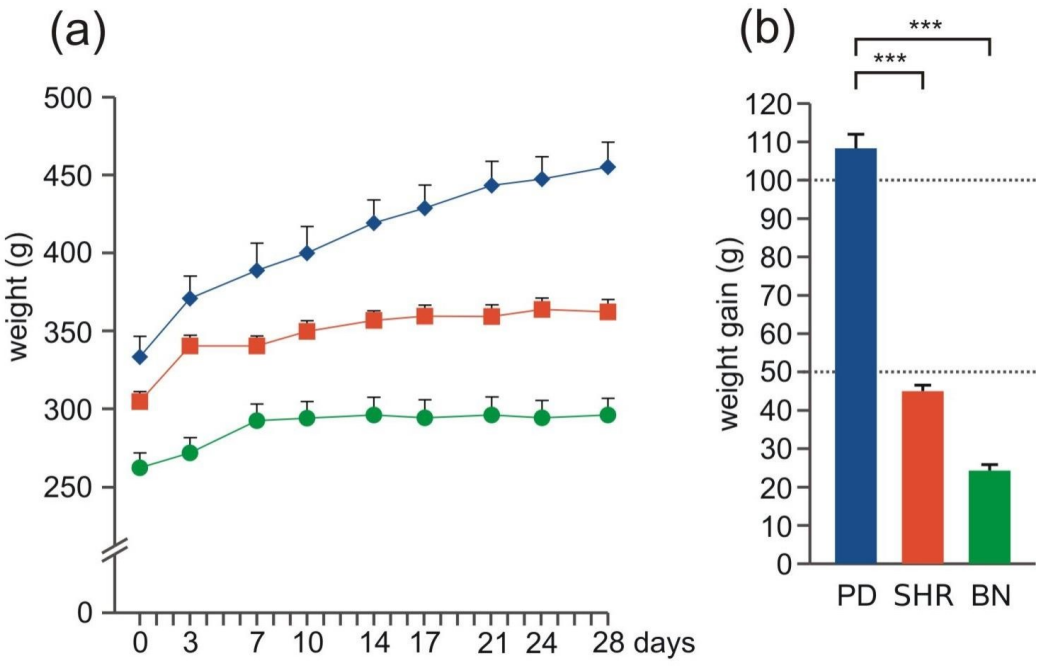

Figure 15: Morphometric profile of adult male rats-PD (blue, n = 7), SHR (red, n = 6), and BN (green, n = 8). (a) Time course of body weight during HFD feeding. (b) Absolute weight gain during HFD feeding. Data are presented as arithmetic means ± SEM. Statistical significance levels for the factor strain of repeated

measurements ANOVA (strain), or for the absolute weight gain one-way ANOVA (strain) with pair-wise post hoc Tukey's test as follows: * $p < 0.05$, ** $p < 0.01$, *** $p < 0.001$. ns. = not significant.

11.2.1.2. Organ weight

The weight of individual organs was measured as a relative weight to 100g of total body weight (Figure 16). After 4 weeks of high fat diet (HFD) administration, we collected heart, liver, kidneys, adrenals, soleus muscle, retroperitoneal, epididymal and brown fat tissue. PD strain displayed the largest relative weight of fat depots (retroperitoneal, epididymal and brown fat tissue), which was the largest significant difference among the organs. The PD strain also has markedly elevated relative liver tissue. SHR showed a larger relative weight in all three adipose tissues to BN, and although the difference was statistically significant it was not as profound as in PD strain. SHR strain had a larger relative heart and kidney weight in comparison to PD and BN strains, heart weight may be attributable to essential hypertension (Liška F. et al., 2017). Both PD and SHR strains showed lower relative weight of adrenals and soleus muscle. This can be explained by the larger adiposity of these strains. The relative organ weight differences among strains is depicted in (Figure 16).

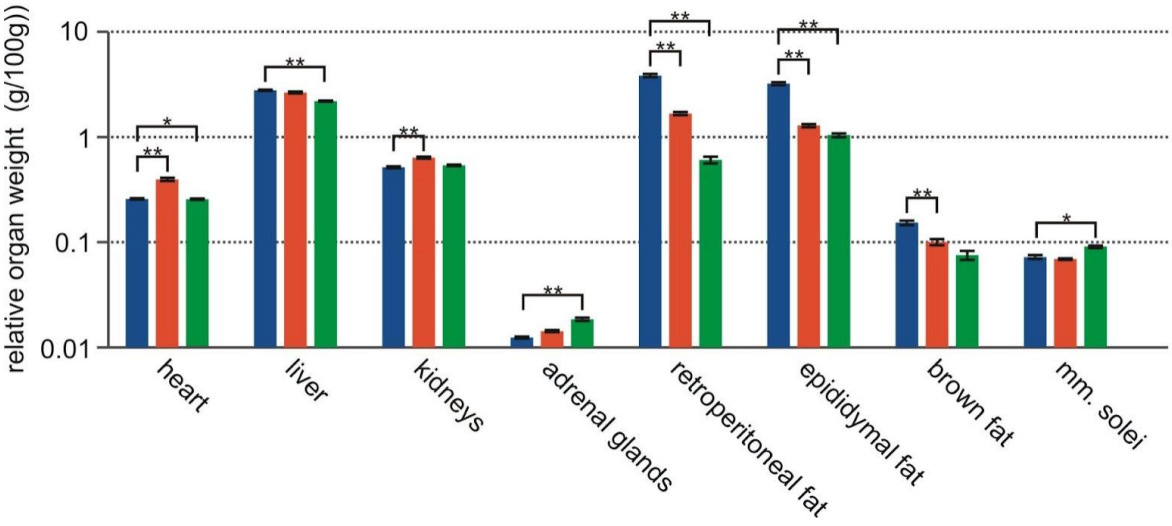

Figure 16: Morphometric profile of adult male rats-PD (blue, n = 7), SHR (red, n = 6), and BN (green, n = 8). Relative tissue weights per 100 g body weight after HFD. Data are presented as arithmetic means ± SEM. Statistical significance levels for one-way ANOVA (strain) with post hoc Tukey's test as follows: * $p < 0.05$, ** $p < 0.01$, *** $p < 0.001$., ns. = not significant.

11.2.1.3. Diet consumption

We measured the amount of consumed diet to ascertain the origin of the increased adiposity of PD and SHR in comparison to BN (Figure 17). Indeed, the largest diet consumption was

observed in PD strain (significantly more compared to both SHR and BN) while SHR animals consumed an intermediate amount of the high fat diet. This correlates well with weight gain, we can thus conclude that increased intake was the major reason for weight gain in PD and SHR (Figure 17).

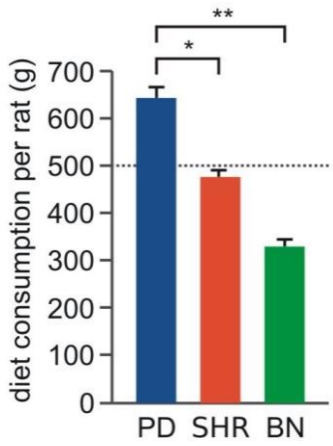

Figure 17: Consumed diet amount per rat of each strain during HFD feeding of adult male rats-PD (blue, n = 7), SHR (red, n = 6), and BN (green, n = 8). Data are presented as arithmetic means ± SEM. Statistical significance levels for one-way ANOVA (strain) with post hoc Tukey's test as follows: * $p < 0.05$, ** $p < 0.01$, *** $p < 0.001$., ns. = not significant.

11.3.1. Metabolic profiling

No significant differences in glycemia (fasting and all measurements during OGTT) were found among the three strains before feeding HFD (Figure 18a). After four weeks of HFD administration we observed elevated fasting glycemia in the PD strain although it did not reach statistical significance (Figure 18b). However; the glycemia during the whole course of OGTT was profoundly elevated in PD in comparison to BN and SHR strains. There was no difference in values of glycemia between SHR and BN strains (Figure 18a-c).

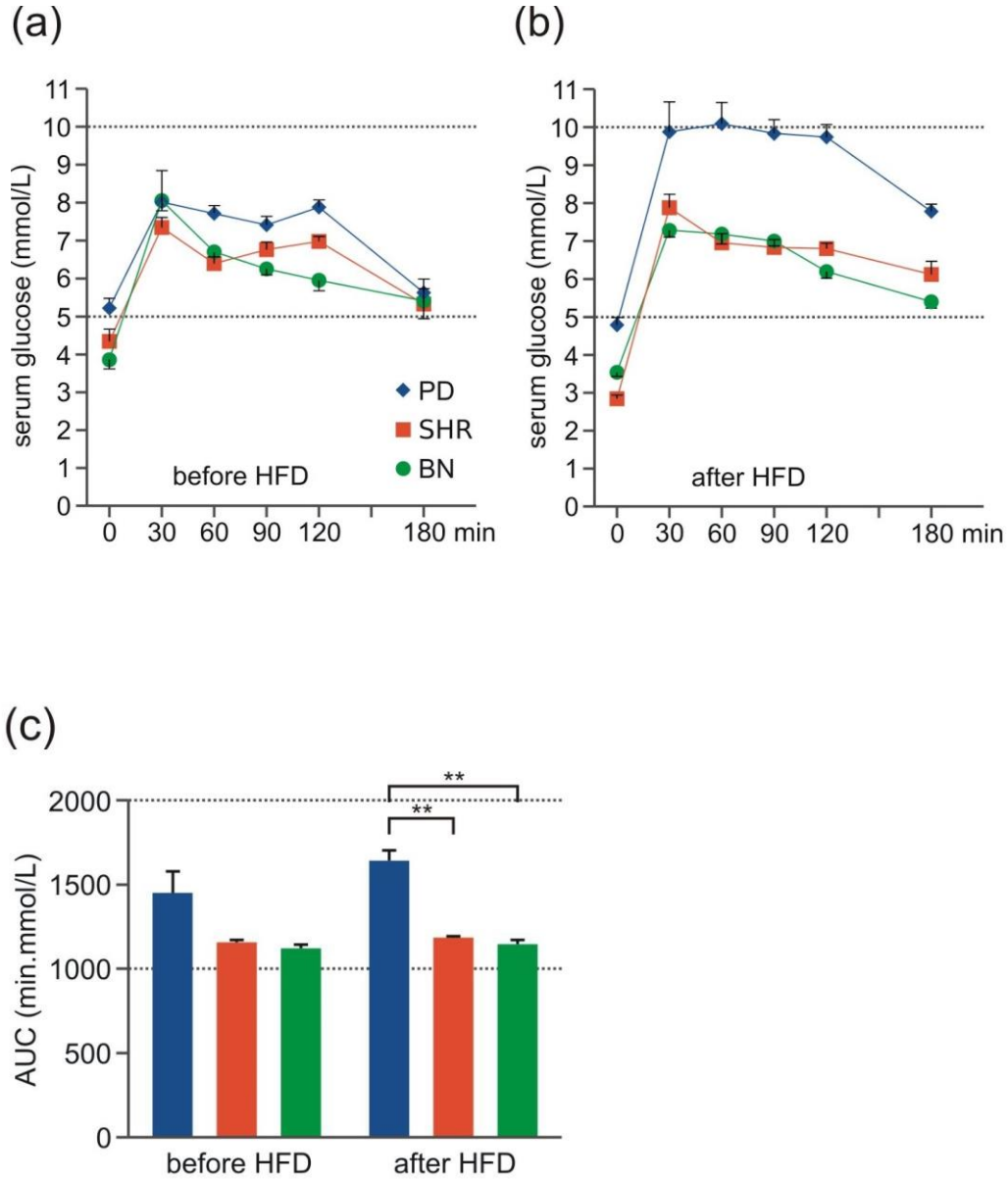

Figure 18: Oral glucose tolerance test of adult male rats-PD (blue, n = 7), SHR (red, n = 6), and BN (green, n = 8). (a) Oral glucose tolerance test (OGTT)-time course of glucose level before HFD. (b) OGTT-time course of glucose level after HFD. (c) The area under the curve (AUC) of OGTT before and after HFD. Data are presented as arithmetic means ± SEM. Statistical significance levels for the factor strain of repeated measurements ANOVA (strain) or two-way ANOVA (AUC) are indicated for pair-wise post hoc Tukey's test as follows: * $p < 0.05$, ** $p < 0.01$, *** $p < 0.001$. For post-hoc OGTT and weight, the upper symbol corresponds to PD vs. SHR comparison, the bottom symbol represents PD vs. BN comparison, ns. = not significant.

11.3.1.1. Insulinemia

The levels of fasting insulinemia both before and after a high fat diet mirrored the levels of glycemia as described above. We did not observe a significant difference among strains in

fasting insulinemia, however, after HFDI there was a markedly elevated level of fasting insulinemia in PD strain (Figure 19).

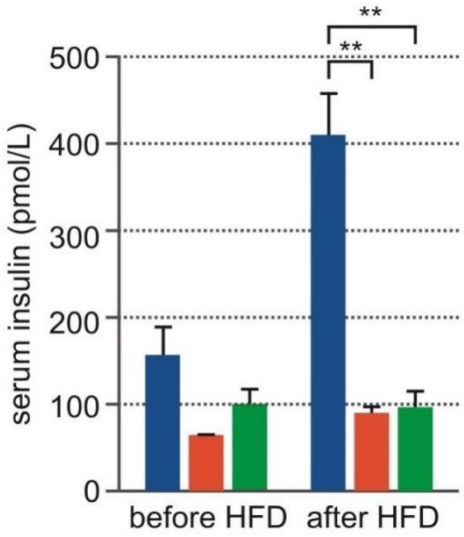

Figure 19: Serum insulin levels before and after 4 weeks of HFD administration in PD (blue, before HFD n=3, after HFD HFDn=7), SHR (orange, before HFD n=3, after HFD n=6) and BN (green, before HFD n=3, after HFD n=8). Data are presented as arithmetic means ± SEM. Statistical significance levels for one way ANOVA (factor strain) o are indicated for unequal N Honestly significance test as follows: * $p < 0.05$, ** $p < 0.01$.

11.3.1.2. Lipidogram

No significant differences in total cholesterol and TAG levels were found before HFD. The cholesterol levels increased in chylomicrons and very low-density lipoprotein (VLDL) particles (fractions 1–5, i.e., particles with diameter >44.5 nm) of the PD strain after HFD administration however the increase was relatively modest, reaching statistical significance only in ANOVA but not in post-hoc comparison of individual groups (Supplementary table 8). On the other hand, there was an order of magnitude increase of total TAG levels due to their accumulation in chylomicron and VLDL fractions in PD compared to the other strains after HFD. After HFD, we found a significant decrease in the FFA level in PD and SHR, but PD compared to SHR and BN still manifested the significantly highest FFA level (Figure 20;).

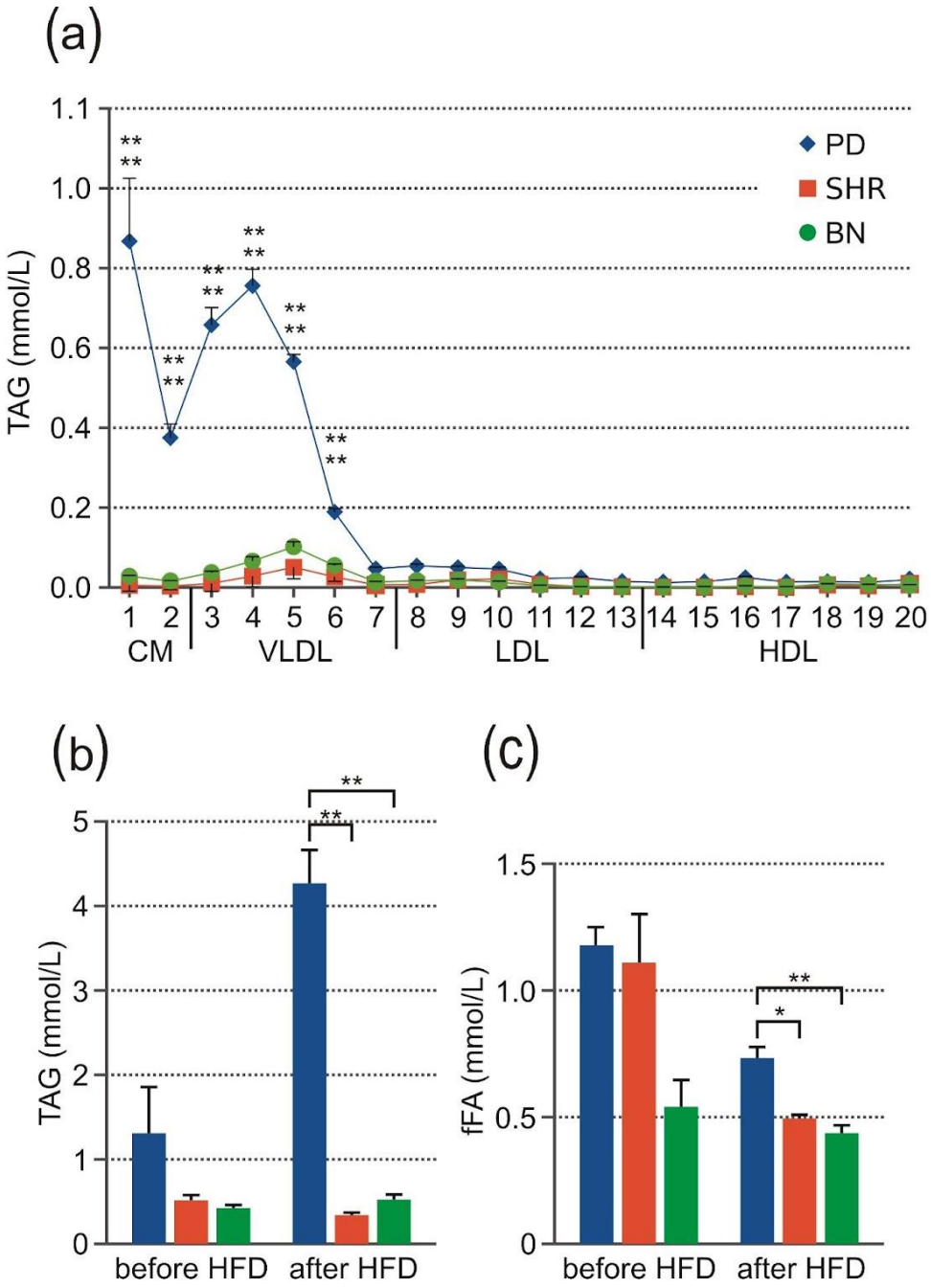

Figure 20: Triacylglycerol and free fatty acid levels.-PD (blue, before HFD n = 3; after HFD n=7), SHR (red, before HFD n = 3; after HFD n=7), and BN (green, before HFD n = 3; after HFD n=8). (a) TAG levels after HFD in 20 lipoprotein fractions. (b) Total TAG levels before and after HFD. (c) Free FAs before and after HFD. Data are presented as arithmetic means ± SEM. Statistical significance levels for the factor strain of repeated measurements ANOVA (TAG in 20 lipoprotein fractions) or one-way ANOVA (total TAG, fFAs) are indicated for pair-wise post hoc Tukey's test as follows: * $p < 0.05$, ** $p < 0.01$. For post-hoc TAG levels, the upper symbol corresponds to PD vs. SHR comparison, the bottom symbol represents PD vs. BN comparison, CM chylomicrons, VLDL very low density lipoproteins, LDL low density lipopoproteins, HDL high density lipoproteins.

11.3.1.3. Adiponectin levels in serum

Adiponectin is a tissue hormone which negatively correlates with white adipose tissue and has anti-inflammatory effects and increases insulin sensitivity. There was no significant difference in adiponectin levels among strains before or after HFD administration (Figure 21; Supplementary table 10).

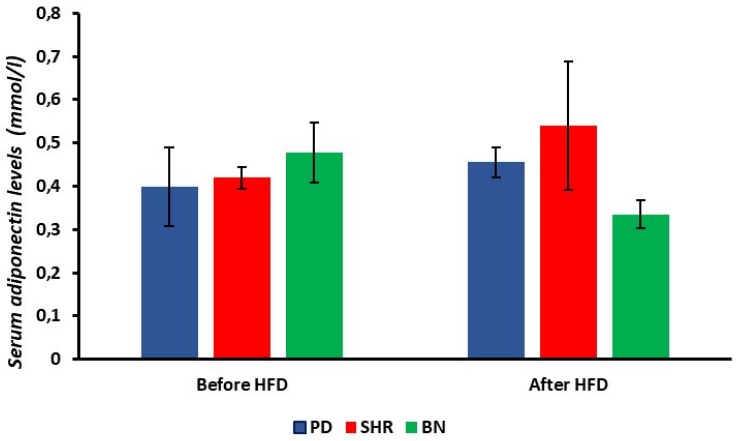

Figure 21: Adiponectin levels in adult male rats before and after high fat diet (HFD) rats-PD (blue, before HFD n = 3; after HFD n=6), SHR (orange, before HFD n = 5; after HFD n=4), and BN (green, before HFD n = 5; after HFD n=8). Data are presented as arithmetic means ± SEM. Statistical analysis was performed using one factor ANOVA (strain) with post hoc HSD for unequal n. None of the differences reached statistical significance.

11.3.1.4. Leptin levels in serum

The serum leptin level before HFD feeding was significantly higher in PD compared to the other strains (Figure 22a). After HFD administration, there was no significant difference between the PD and BN strain and only subtly higher leptinemia in PD compared to SHR, which did not reach statistical significance. Interestingly though, after correction to the white adipose tissue amount, represented by the sum of retroperitoneal and epididymal fat, we found a significantly lower leptin level in PD compared to the other strains (Figure 22b), which may indicate that the leptin level does not correspond to the amount of fat tissue.

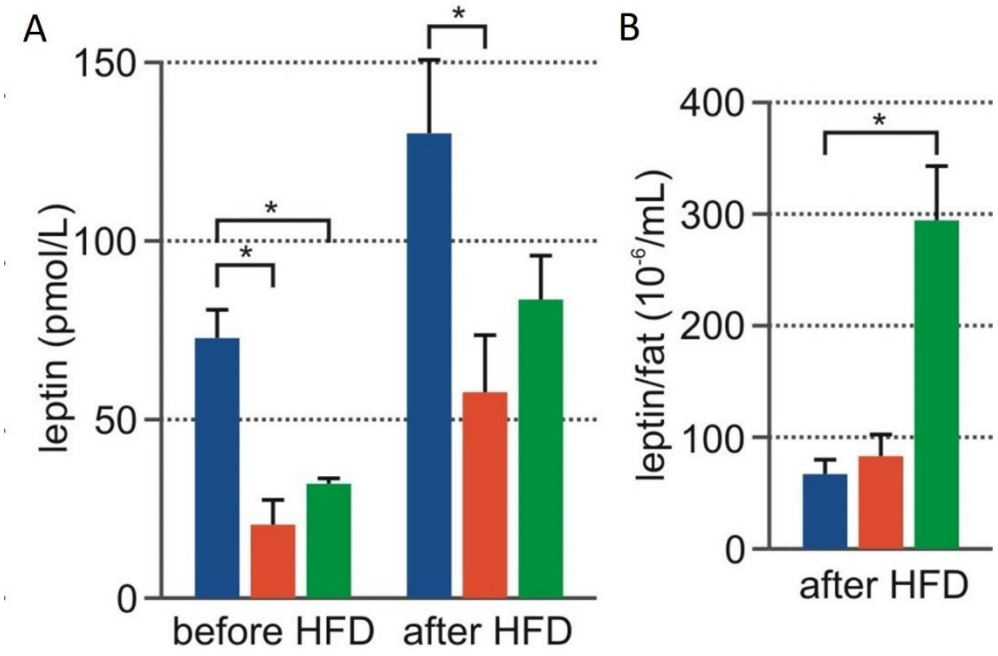

Figure 22: Serum leptin levels in PD PD (blue, before HFD n = 5; after HFD n=5), SHR (orange, before HFD n = 4; after HFD n=5), and BN (green, before HFD n = 3; after HFD n=5). (A) Absolute serum leptin levels before and after 4 week HFD administration. (B) Relative serum leptin levels related to the adipose tissue. Data are presented as arithmetic means ± SEM. Statistical analysis was performed using one factor ANOVA (strain) with post hoc HSD for unequal n.. Statistical significance levels for the factor strain of repeated measurements ANOVA (TAG in 20 lipoprotein fractions) or one-way ANOVA (total TAG, fFAs) are indicated for pair-wise post hoc Tukey's test as follows: * $p < 0.05$, ** $p < 0.01$.

11.3.1.5. Serum cytokine levels

No significant differences among the three strains were found in cytokine levels (MCP-1, IL-1a, IL-1b, IL-2, IL-4, IL-5, IL-6, IL-7, IL-10, IL-12, IL-13, IL-17 IL-18, G-CSF, GM-CSF, GRO/KC, IFN-γ, M-CSF, MIP-1a, MIP-3a, RANTES, TNF-α, VEGF) before and after HFD (Figure 23a-d, Supplementary table 9). However, increased RANTES and decreased VEGF in PD after diet administration showed marginal significance, but neither observation reached significance in ANOVA. This finding may indicate lack of systemic inflammatory response.

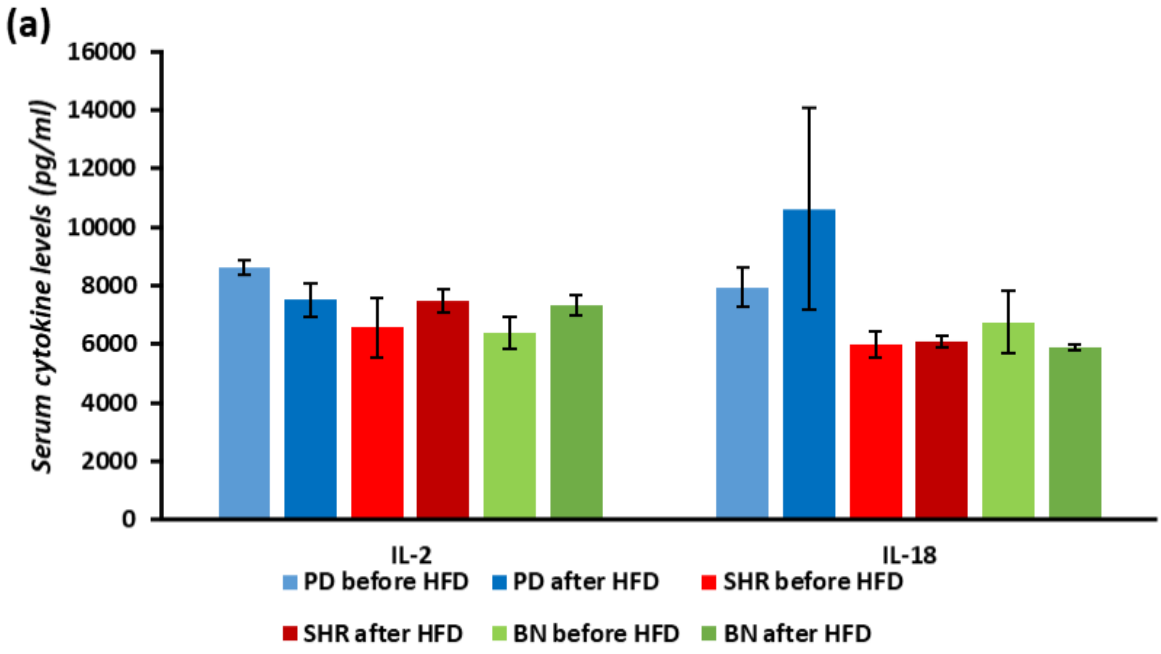
(a)
Serum cytokine levels (pg/ml)
16000
14000
12000
10000
8000
6000
4000
2000
0
IL-2
IL-18
PD before HFD
PD after HFD
SHR before HFD
SHR after HFD
BN before HFD
BN after HFD

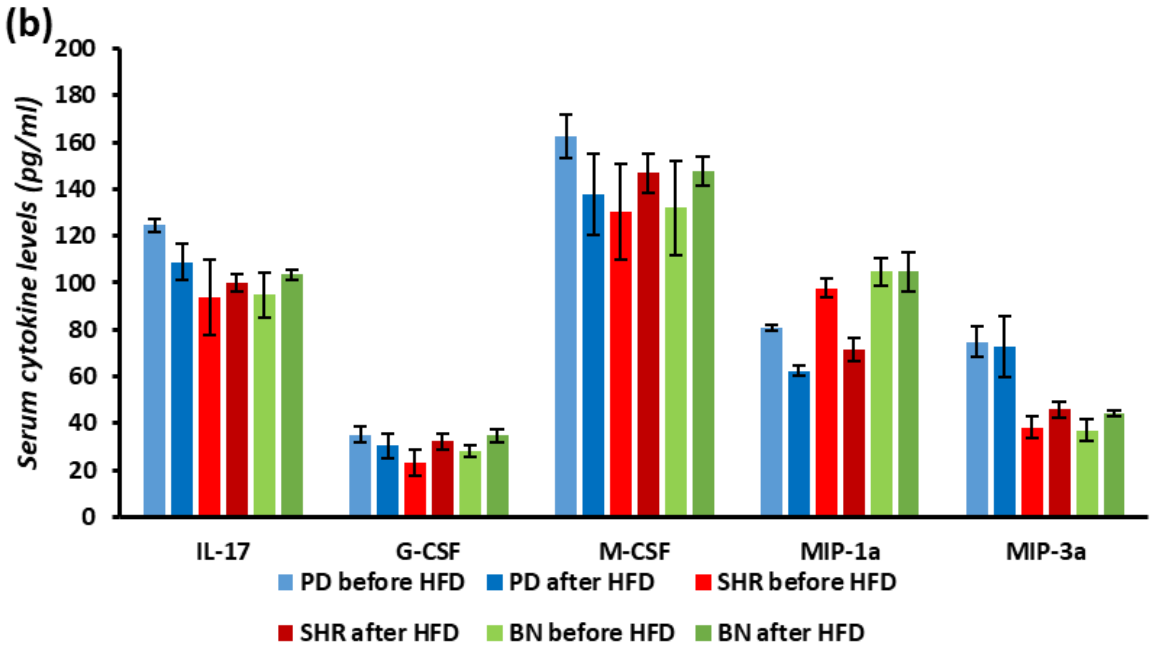
(b)
Serum cytokine levels (pg/ml)
200
180
160
140
120
100
80
60
40
20
0
IL-17
G-CSF
M-CSF
MIP-1a
MIP-3a
PD before HFD
PD after HFD
SHR before HFD
SHR after HFD
BN before HFD
BN after HFD

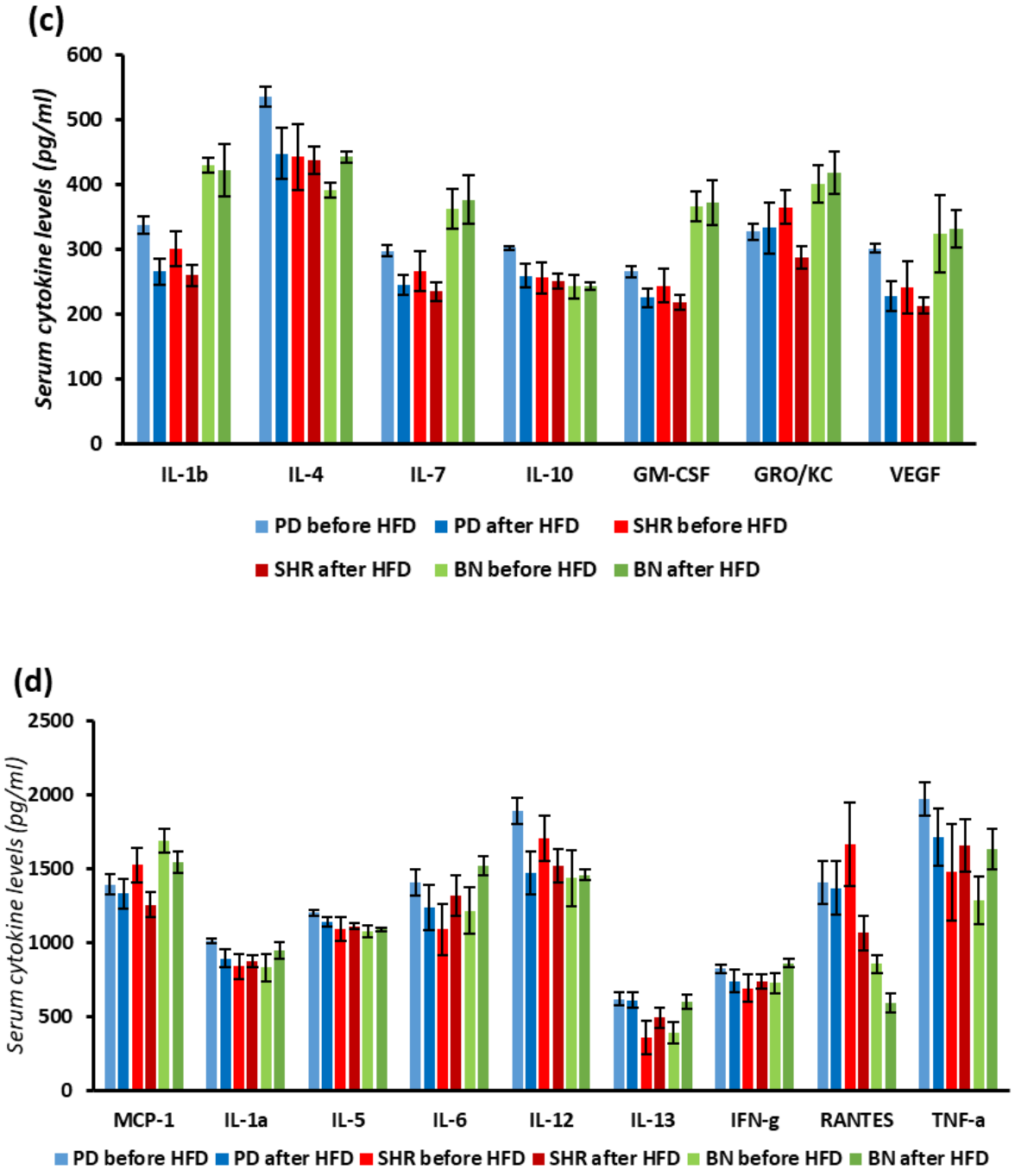

Figure 23: Cytokine levels in adult male rats before and after high fat diet (HFD) rats-PD before HFD (light blue, n = 5), PD after HFD (dark blue, n=5), SHR before HFD (light red, n = 4), SHR after HFD (dark red, n=5), BN before HFD (light green, n = 3) and BN after HFD (dark green, n=5) . (a) Il-2, Il-18 (b) Il-17, G-CSF, M-CSF, MIP-1a, MIP-3a (c) Il-1b, Il-4, Il-7, Il-10,GM-CSF, GRO/KC, VEGF (d) MCP-1, Il-1a, Il-5, Il-6, Il-12, Il-13, IFN-g, RANTES, TNF-a. Data are presented as arithmetic means ± SEM. Statistical analysis was performed using two-way ANOVA (strain and diet) with post hoc HSD for unequal n. None of the sample mean differences reached statistical significance.

11.3.1.6. Serum levels of C-peptide, glukagon, GIP, GLP-1, PP and PYY

No significant differences among the three strains were found in the serum levels of C-peptide, glukagon, GIP, GLP-1, PP or PYY before and after HFD (Figure 24, Supplementary table 10).

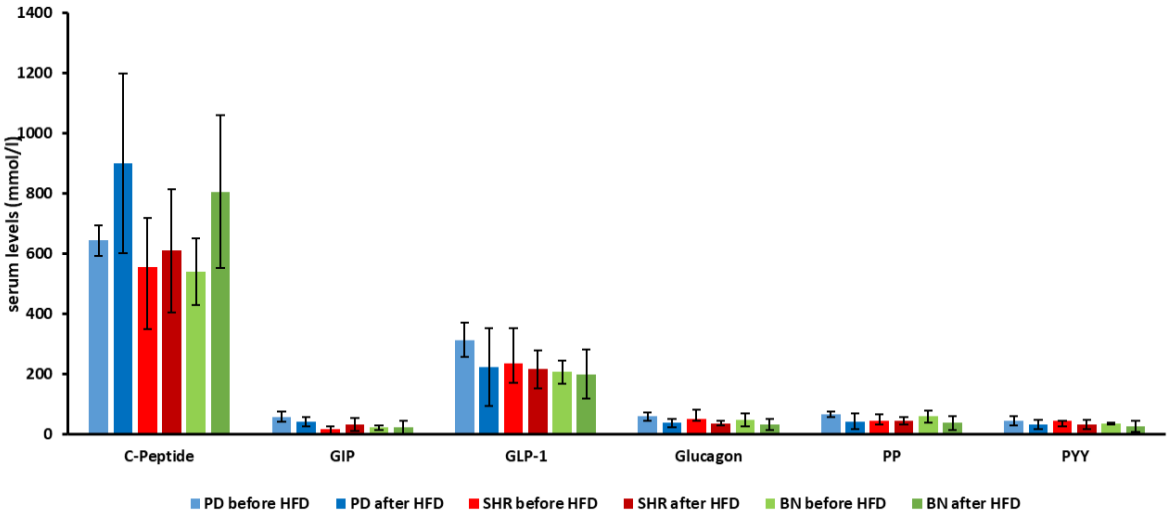

Figure 24: Serum levels of C-peptide, GIP, GLP-1, Glukagon, PP and PYY in adult male rats before and after high fat diet (HFD) rats-PD (before HFD n = 5; after HFD n=4 for glukagon, n=3 for PYY, n=5 for others , SHR (before HFD n = 3 for PP; n=2 for PYY; n=4 for others; after HFD n=4 for glukagon and PP, n=3 for PYY, n=5 for others), and BN (before HFD n = 2 for PYY, n=3 for others; after HFD n=4 for glukagon and PP, n=2 for PYY, n=5 for others). Data are presented as arithmetic means ± SEM. Statistical analysis was performed using two-way ANOVA (strain and diet) with post hoc HSD for unequal n. None of the sample mean differences reached statistical significance.

11.3.1.7. Lipid Levels in Liver Tissue after HFD Feeding

There was no significant difference of the cholesterol content of liver tissue between PD and other strains (Figure 25). Hepatic TAG levels were the highest in SHR compared to PD but not significant compared to BN. On the other hand, thin-layer chromatography assessment of diacylglycerols (DAG), lipotoxic intermediates of TAG metabolism, revealed a significantly lower amount of DAG in SHR liver compared to the other two strains.

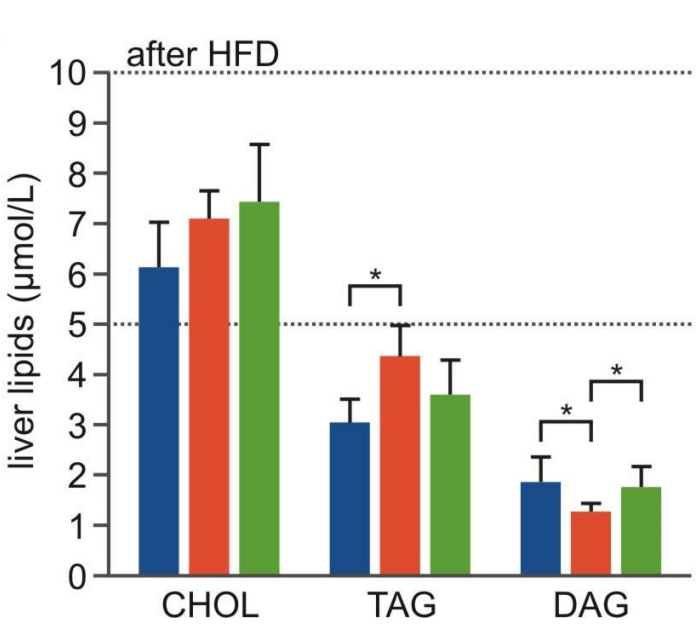

Figure 25: Cholesterol, TAG, and DAG levels in liver tissue of PD (blue, n=7), SHR (orange, n=6) and BN (green n=8) after 4HFD exposition for 4 weeks. Data are presented as arithmetic means ± SEM. Statistical significance levels for one-way ANOVA (factor strain) are indicated for HSD (honestly significant difference) for unequal N as follows: * $p < 0.05$, ** $p < 0.01$.

11.3.2. Analysis of hepatic transcriptome

We found in total 5480 differentially expressed genes, after multiple comparison correction using the Hochberg–Benjamini procedure at a significance level of 0.05, In each post-hoc pairwise comparison of strains, we found 2636 for BN vs. PD (1064 upregulated in PD, 1572 downregulated in PD), 1906 for BN vs. SHR (936 downregulated in SHR, 970 upregulated in SHR), and 938 for PD vs. SHR (620 downregulated in PD, 318 upregulated in PD), (Figure 26). The GO term enrichment analysis of the differentially expressed genes is provided in (Supplementary figures 1-3) and (Supplementary tables 11-13) respectively.

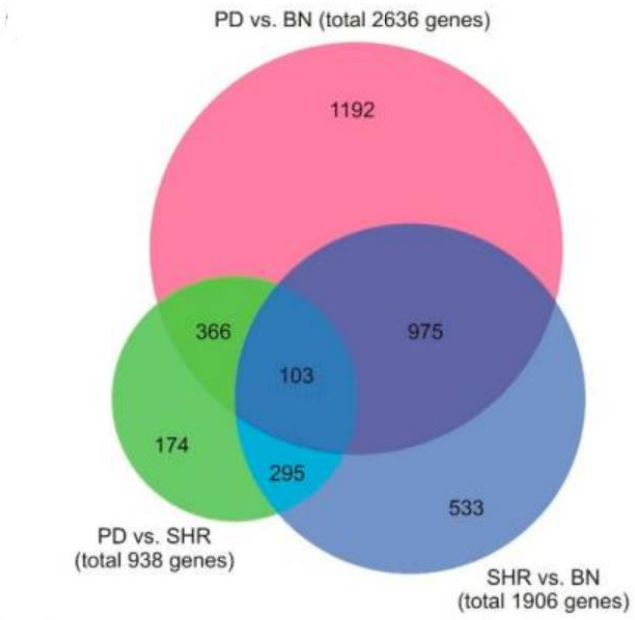

Figure 26:. Differentially expressed genes in the liver after HFD. Venn diagram expressing number of differentially expressed genes for each comparison and the number of overlapping genes (i.e. differentially expressed in more groups). Circles are scaled according to the number of genes, overlapping regions are not to scale

11.3.3. Pathway Analysis

Transcriptome analysis for the PD vs. SHR differentially expressed genes indicated significant enrichment of the pathways related to tryptophan metabolism, beta oxidation, retinol metabolism, and fatty acid biosynthesis (Figure 27a). Interestingly, the same pathways were also the most significantly enriched for the SHR vs. BN comparison (Figure 27b), albeit with a different mix of enriched genes. In the PD vs. BN differentially expressed genes pathway enrichment analysis, the highest scoring results were rhodopsin-like G-protein-coupled receptors, proteasome degradation, fatty acid biosynthesis, cytoplasmic ribosomal proteins, and glucuronidation (Figure 27c). Interestingly, in both SHR vs. PD and SHR vs. BN comparisons, SHR displayed overexpression of complement activation, focal adhesion, and interferon signaling, and none of these pathways were significantly enriched in PD vs. BN comparison (Supplementary tables 11-13).

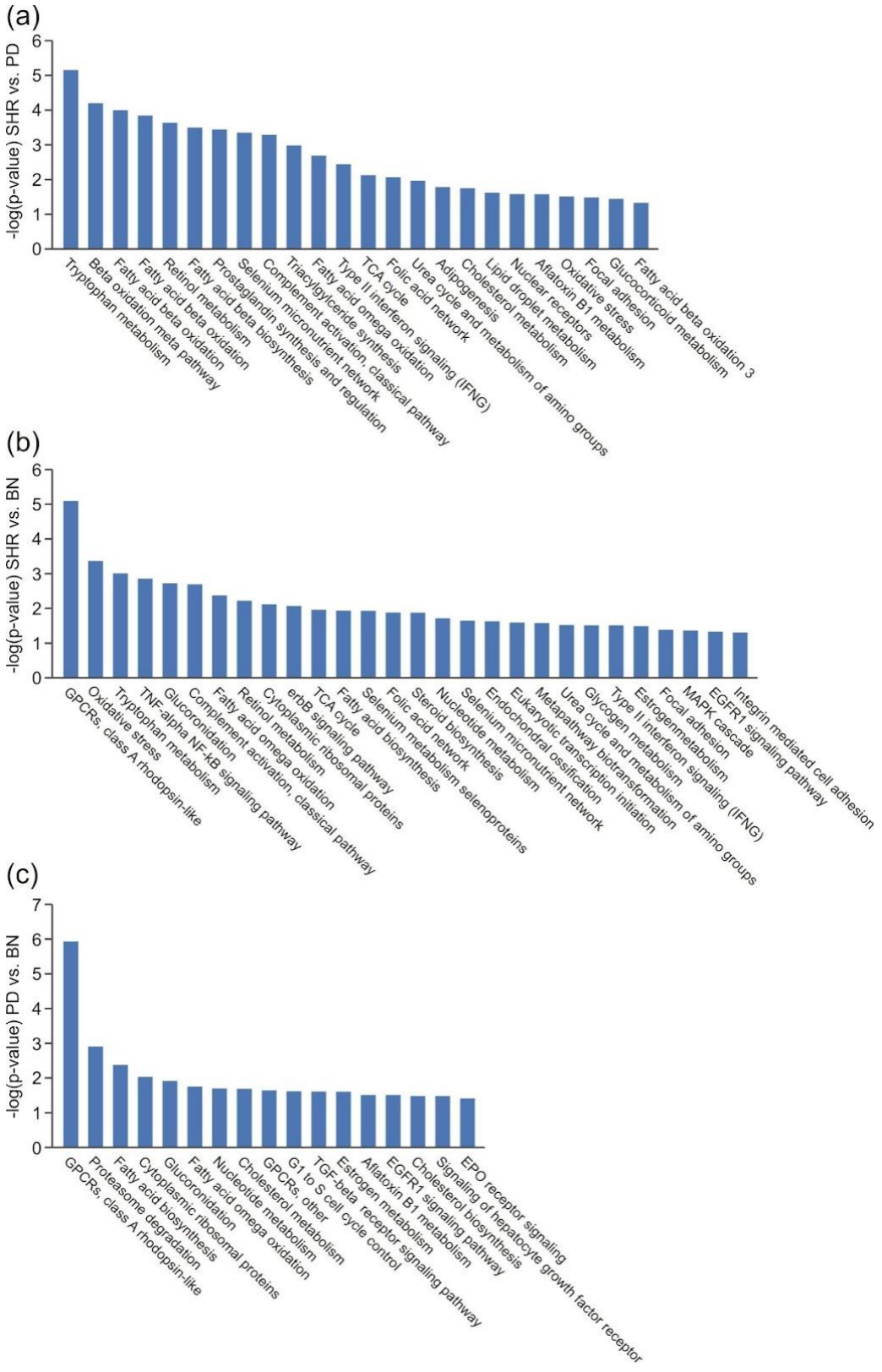

Figure 27: Differentially expressed genes in the liver after HFD. Pathway enrichment analysis using Transcriptomic analysis console software (a-c). (a) Pathway enrichment analysis-SHR vs. PD comparison. (b) Pathway enrichment analysis—SHR vs. BN comparison. (c) Pathway enrichment analysis − PD vs. BN comparison.

11.3.4. Expression of selected genes in liver tissue quantified by qPCR

We confirmed differential expression for 13 protein-coding genes with connection to MetS traits development using qPCR. After finding that *Acsm3* (acylCoA-synthetase for medium-chain family member 3) hepatic expression was absent in the PD strain, we also measured the expression of three other closely related acyl-CoA-synthetases, which were not differentially expressed in the microarray data. The most substantial difference in expression was seen in *Scd1* (stearoyl-CoA-desaturase 1, Figure 28), which was overexpressed in PD compared to the other strains (26-fold and 16-fold, compared to BN and SHR, respectively). We noticed significant downregulation in PD of genes involved in activation of FAs–*Acsm3* (acyl-CoA-synthetase medium-chain family member 3), *Acsm2a* (acyl-CoA-synthetase medium-chain family member 2A), especially the *Acsm3* gene, which was completely/nearly completely absent, as shown by failure of amplification by standard RT-PCR techniques (Figure 28). The expression levels of the remaining genes are shown in (Figure 28).

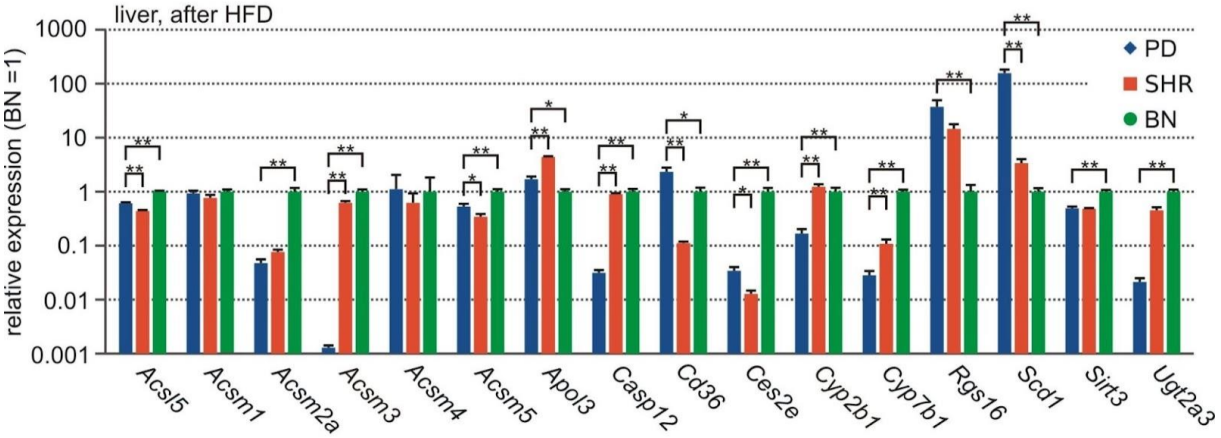

Figure 28: Gene expression (qPCR) after HFD in adult male rats liver tissue. PD (blue, n = 7), SHR (red, n = 6), and BN (green, n = 8). Data are presented as arithmetic means ± SEM. Statistical significance levels for the factor strain of one-way ANOVA are indicated for pair-wise post hoc Tukey's test as follows: * $p < 0.05$, ** $p < 0.01$.

11.3.5. Expression of selected genes in epididymal adipose tissue quantified by qPCR

Since many of the genes differentially expressed in the liver exhibit a close connection to lipid metabolism, we measured the expression of selected genes (*Acsl5, Acsm2a, Acsm3, Casp12, Rgs16, Scd1, Sirt3*) in epididymal fat tissue using qPCR. We found a significantly higher expression of *Scd1* in PD compared to other strains; no other significant result was found. *Acsm3* and *Acsm2a* were practically not expressed in epididymal fat tissue (Figure 29a). Because we observed deregulated leptin levels in the PD strain, we determined *Lep*

gene expression in epididymal fat tissue, which correlated with fat tissue mass in the strains (Figure 29b).

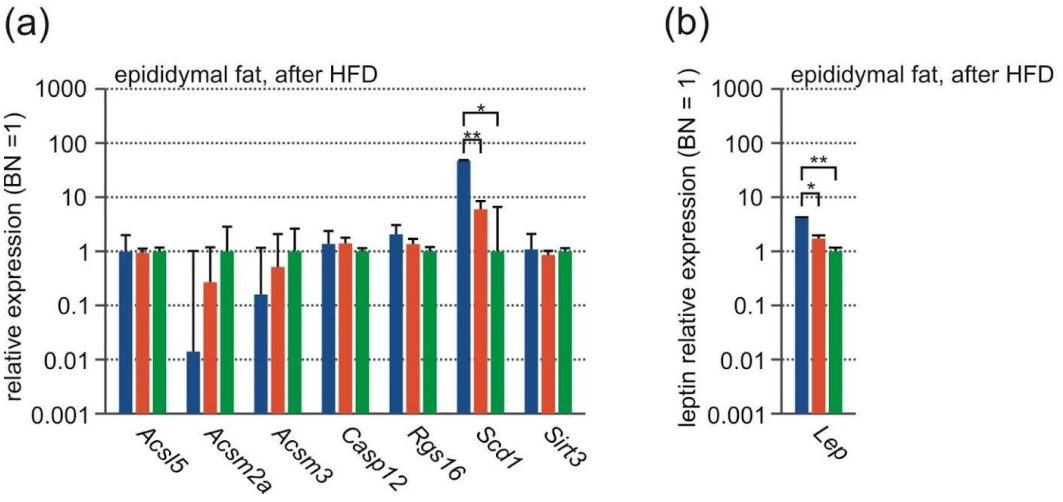

Figure 29: Gene expression (qPCR) after HFD in adult male rats-PD (blue, n = 7), SHR (red, n = 6), and BN (green, n = 8). (a) Epididymal fat tissue. (b) Leptin expression in epididymal fat. Data are presented as arithmetic means ± SEM. Statistical significance levels for the factor strain of one-way ANOVA are indicated for pair-wise post hoc Tukey's test as follows: * $p < 0.05$, ** $p < 0.01$.

11.3.6. Sequencing of *Acsm3*

The absence of *Acsm3* expression in the liver of the PD strain compared to SHR and BN strains (Figure 30a) suggests a sequence variant in a tissue-specific cis-regulatory element (e.g., promoter, enhancer, differential splice site) precluding liver expression. However, sequencing of genomic DNA of the PD strain did not reveal any causal mutation in the *Acsm3* coding sequence, and core promoter, which might conclusively explain the absence of transcript and ACSM3 protein, however a deletion was found within L1-rn element in intron 1 - a LINE element as depicted in(Figure 30b).

(a)

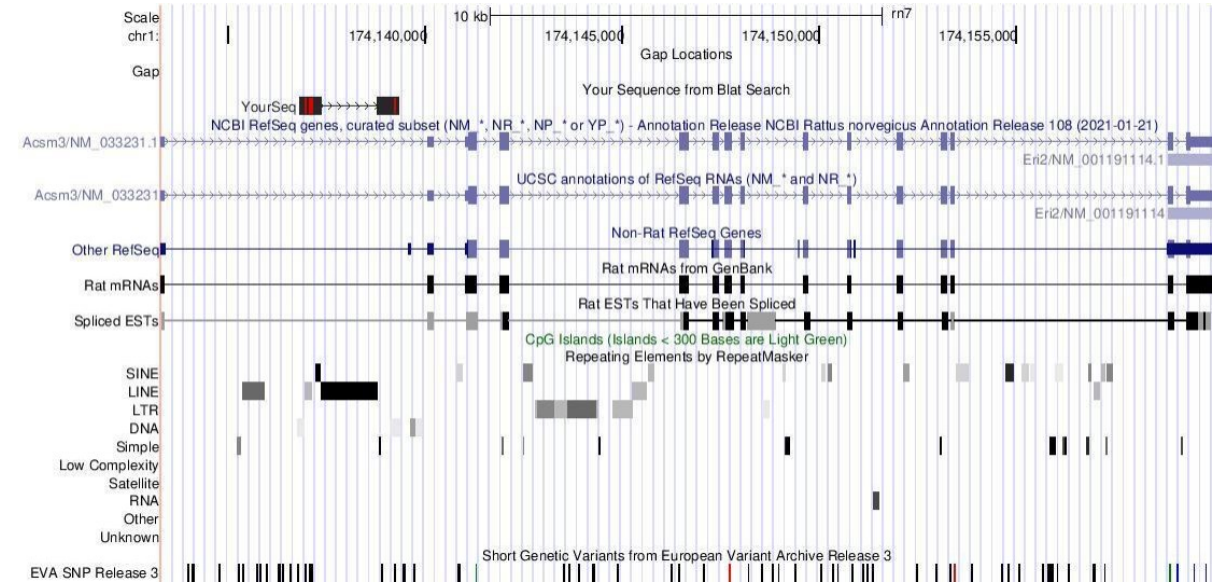

(b)

Figure 30: L1Rn deletion in the first intron of *Acsm3* gene in PD strain. A) Shows position of the mutation in rat genome. Source: Rat Genome Browser, www.genome-euro.ucsc.edu. (The annotation track ”your sequence” corresponds to the region depicted in B). B) Sequencing data for individual strains in the following order PD – SHR – BN. Sequencing data mapped on rat genome using BWA-MEM on Galaxy server and visualized using IGV.

11.3.7. Acsm3 RT-PCR

To confirm the absence of *Acm3* liver expression in PD we performed RT-PCR of *Acsm3* which showed no detectable cDNA, which suggests the absence of mRNA, (Figure 31).

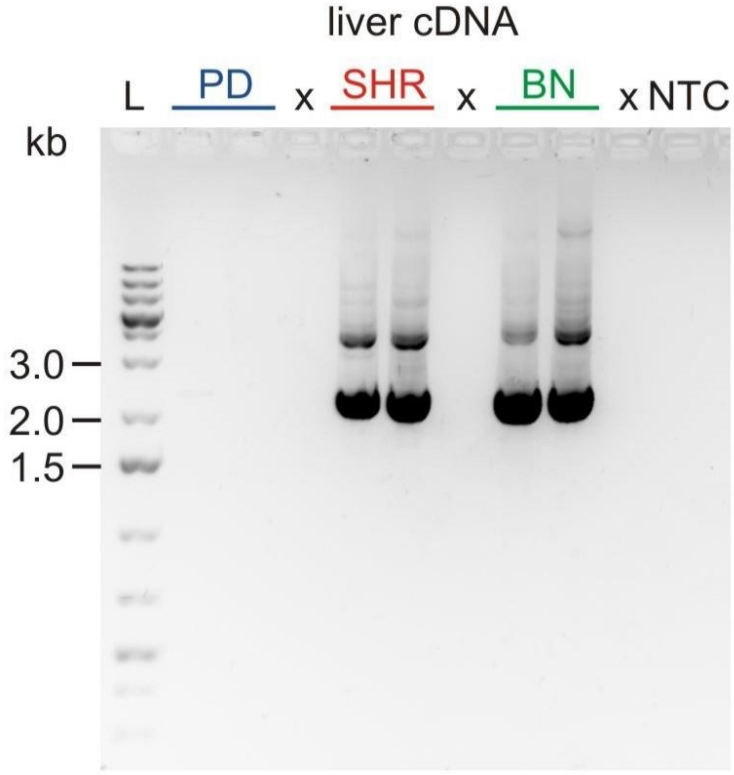

Figure 31: Expression of Acsm3 in the liver of adult male rats-PD (blue, n=2), SHR (red, n=2), and BN (green, n=2); after HFD. RT-PCR of Acsm3, visualized on gel electrophoresis (two representative samples for each strain). Primers flank the complete coding sequence; the expected size of the PCR product is 2296 bp.

11.3.8. Western Blot Analysis

The absence of *Acsm3* liver expression in PD on the mRNA level prompted us to test the expression of the protein. Western blot analysis of liver tissue lysates proved the absence of ACSM3 protein in PD, (Figure 32).

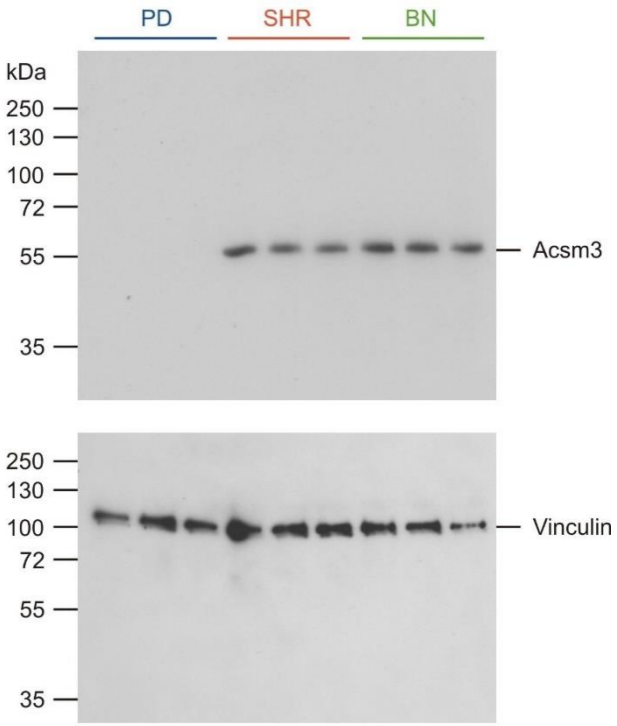

Figure 32: Expression of Acsm3 in the liver of adult male rats-PD (blue, n=3), SHR (red, n=3), and BN (green, n=3); after HFD. Western blotting of ACSM3 (expected molecular weight of the mature polypeptide 63.2 kDa). Vinculin (expected molecular weight 116.6 kDa) was used as the loading control (three representative samples for each strain).

11.4. Results - experiment 3

In this study our aim was to assess the function of the deleted intronic sequence of *Plzf* in PD5 strain. In particular, we wanted to establish its role in metabolism and to determine its molecular role in terms of its possible activity as an enhancer.

11.4.1. Organ and total body weight profile of SHR and PD5

We compared male rats from each strain without intervention and with dexamethasone (SHR=7; SHR +DEX=7; PD5=10; PD5 + DEX=9; total 34 rats) at the age of 12 months. We measured total body weight (Figure 33) and relative weight to 100mg of the total body weight across a spectrum of organs including heart, liver, kidney, adrenal gland, retroperitoneal fat and epididymal fat (Figure 34). The total body weight values in SHR+dexamethasone group were the highest in comparison with other groups (Figure 33).

Dexamethasone profoundly boosted relative weight of liver as well as both fat depots (retroperitoneal and epididymal adipose tissue) in SHR strain. In PD5 dexamethasone failed to boost body weight gain in comparison to SHR strain.The administration of dexamethasone led to increase of relative liver weight as well as increase in both fat depots weight (Figure 34). However, this stimulating effect was displayed in SHR, but was either absent or mitigated and nonsignificant in PD5 strains.

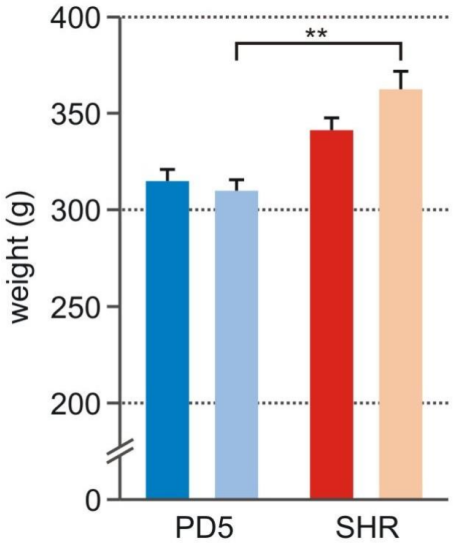

Figure 33: Animal weight of PD5 and SHR males fed with standard diet without dexamethasone (blue, STD; PD5 STD n=10, SHR STD n=7) and standard diet with dexamethasone treatment (orange, STD+DEX; PD5 STD+DEX n=9, SHR STD+DEX, n=7). Data are presented as arithmetic means ± SEM. For better readability, y axis is not to scale (interrupted). Statistical significance levels for the factor strain and dexamethasone treatment of two-factor ANOVA (factor strain, factor dexamethasone exposure) are indicated for pairwise post hoc unequal N HSD test (honestly significant difference) as follows: * $p < 0.05$, ** $p < 0.01$,*** $p < 0.001$.

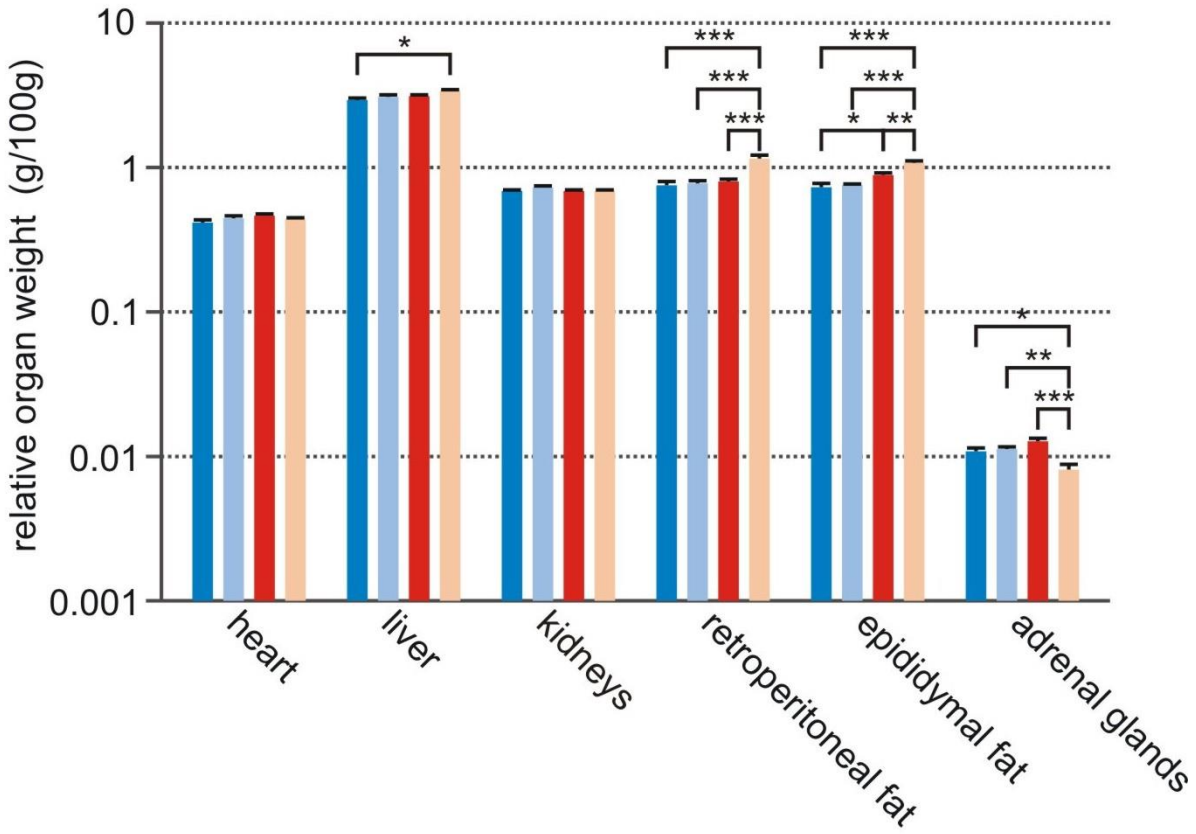

Figure 34: Relative tissue weights per 100 g body weight for PD5 STD (n=10), PD5 STD+DEX (n=9), SHR STD (n=7), SHR STD+DEX (n=7). Data are presented as arithmetic means ± SEM in logarithmic scale. Statistical significance levels for the factor strain and dexamethasone treatment of two-factor ANOVA (factor strain, factor dexamethasone) are indicated for pair-wise post hoc unequal N HSD test (honestly significant difference)as follows: * $p < 0.05$, ** $p < 0.01$, *** $p < 0.001$.

11.4.2. Metabolic profile of SHR and PD5

Oral glucose tolerance test (OGTT) showed higher glucose concentrations in SHR compared to PD5, furthermore the dexamethasone admission deteriorated OGTT in both strains however, the difference was strikingly pronounced in SHR where even the base-line fasting glucose was almost two-fold higher than in SHR without intervention and PD5 under both conditions (Figure 35 and 36). The glycemic curves showed similar patterns in both strains and conditions, in the first 30 min of OGTT the glucose concentrations rose more substantially in SHR and SHR + dexamethasone compared to PD5 and PD5 + dexamethasone, reaching their peak values in 30 to 60 min of OGTT (Figure 35).

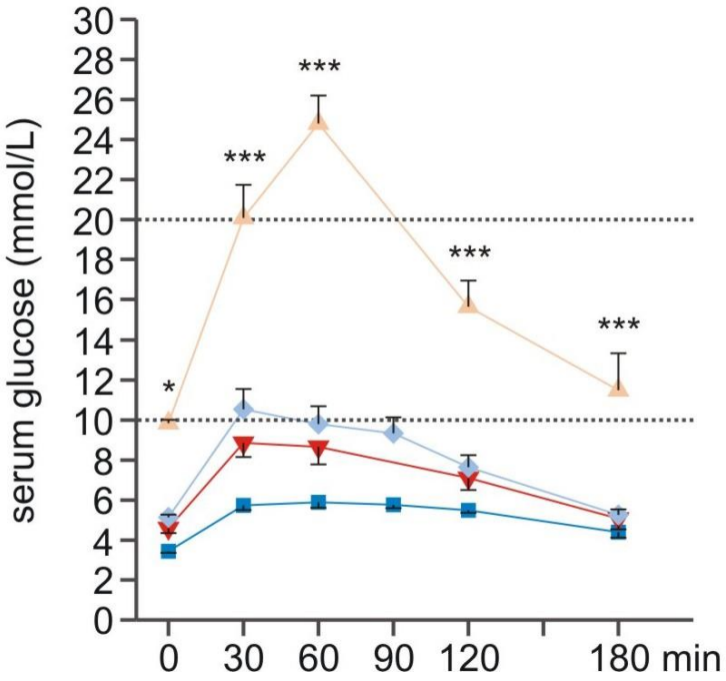

Figure 35: The course of glycaemic curves in SHR STD (n=7), SHR STD + DEX (n=7), PD5 STD (n=10) and PD5 STD+DEX (n=9) male rats during the oral glucose tolerance test. Data are expressed as mean ± S.E.M. Significance levels for OGTT are given for repeated measurements ANOVA (factor strain, factor dexamethasone) with post hoc unequal N HSD (honestly significant difference) as follows: * $P < 0.05$; **$P < 0.01$, *** $P < 0.001$ for SHR vs. PD5 after dexamethasone administration. Red inverted triangles SHR STD, pink triangles SHR DEX, blue squares PD5 STD, light blue diamonds PD5 DEX

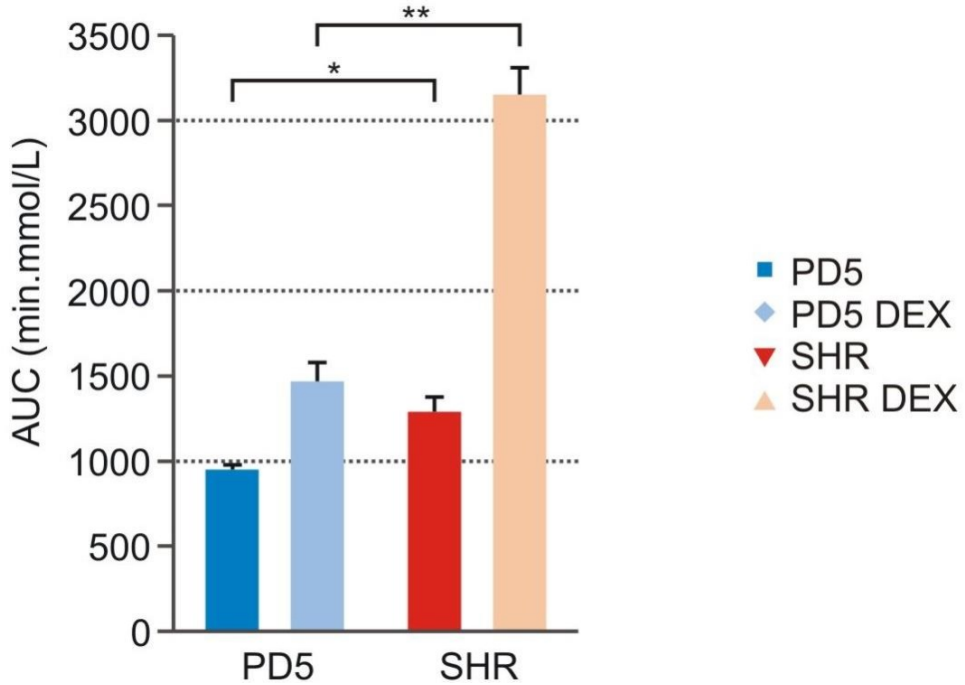

Figure 36: The area under the curve (AUC) of OGTT in SHR STD (n=7), SHR STD+DEX (n=7), PD5 STD (n=10) and PD5 STD+DEX (n=9) male rats. Data are presented as arithmetic means ± SEM. Statistical

significance levels for two-factor ANOVA (factor strain and factor dexamethasone) with post hoc unequal N HSD (honestly significant difference) are indicated as follows: * $p < 0.05$, ** $p < 0.01$, *** $p < 0.001$.

11.4.3. Liver transcriptome

To dissect the genetic background of metabolic syndrome in our strains and to unravel the extent to which it is affected by dexamethasone we conducted comparative transcriptomic analysis using the microarray approach. Three livers from each group (SHR; SHR + dexamethasone; PD5; PD5 +dexamethasone) were sampled, thus obtaining four transcriptomic datasets. For each variable in this experiment – strain, dexamethasone treatment and interaction between strain and dexamethasone treatment, separate analyses were conducted. Transcriptomic data were further subjected to Benjamini-Hochberg correction for each variable separately (strain, dexamethasone treatment and interaction). After this FDR correction (set to 15%), 69 (about 0.18% of 36,668) mRNA probe sets were identified as significantly differentially expressed in the strain category, 1794 (about 4.9% of 36,668) probe sets in dexamethasone treatment category and 20 (about 0.05% of 36,668) probe sets in interaction category. These probe sets represented up-regulated as well as down-regulated known genes or loci. Volcano graphs (which plot significance denoted as -log10 p value versus fold-change on y and x axes, respectively) of normalized expression values showed a wide range of differentially expressed genes on genomic scale among individual groups and as expected suggested a larger effect of dexamethasone on observed phenotype (Figure 37). The GO term enrichment analysis of the differentially expressed genes is provided in (Supplementary figures 4-6) and (Supplementary tables 14-16) respectively. The diagrams in (Figure 38 a 39) represent scatter plots analysis between the differentially expressed mRNAs for each respective category and Venn diagrams respectively.

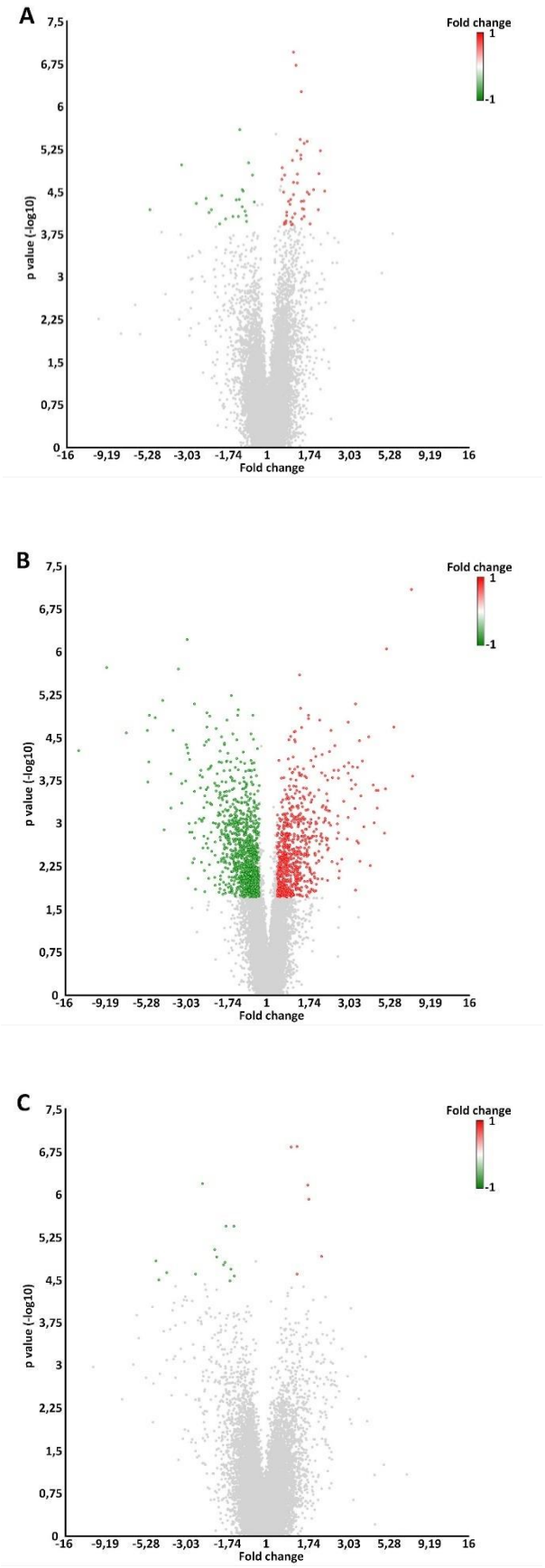

Figure 37: Volcano plots of differentially expressed genes in SHR and PD5 rat liver tissue without intervention and after dexamethasone admission. Significantly differentially expressed genes for strain category (**A**),

dexamethasone treatment category (**B**) and interaction (**C**). Cut-off criteria for DEG (differentially expressed genes) significance was FDR ≤ 15%. The y-axis displays the -log10 q-value for each gene, while the x-axis displays the log2 fold change for that gene relative to strain (**A**), dexamethasone treatment (**B**) or interaction (**C**). Red dots indicate upregulation, green dots indicate downregulation, and gray dots indicate non-significance relative to strain (**A**), dexamethasone treatment (**B**) or interaction (**C**).

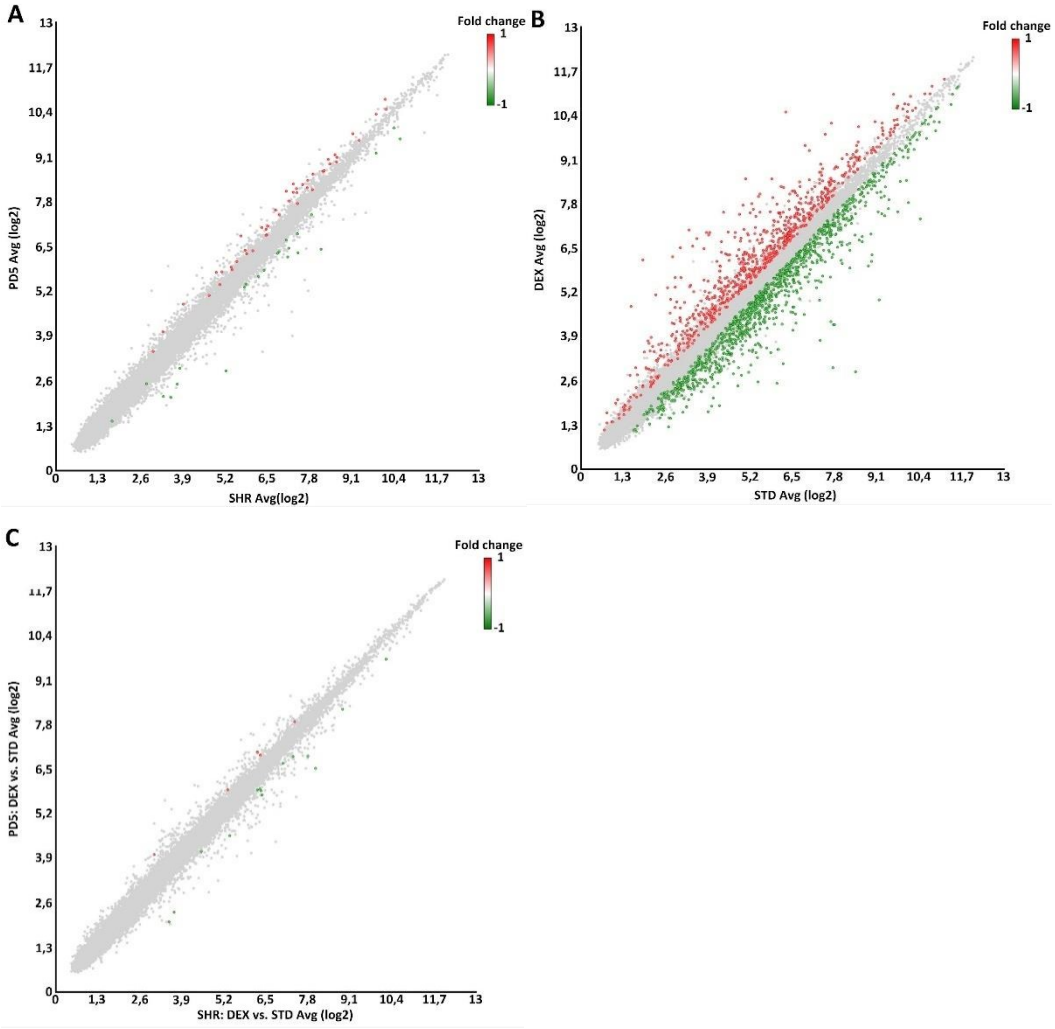

Figure 38: Expression profile alterations of mRNA in SHR and PD5 liver tissue without intervention and after dexamethasone administration. Differentially expressed mRNA is expressed as a scatter for strain (A), dexamethasone treatment (B) and interaction between strain and dexamethasone treatment (C).

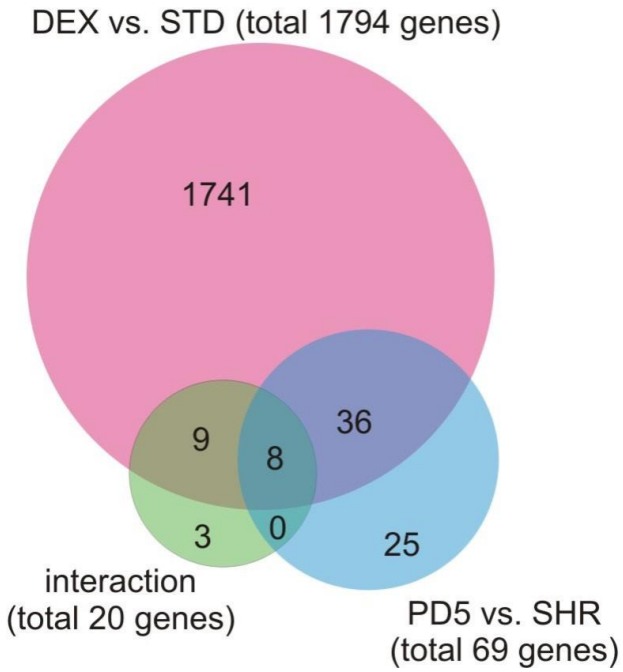

Figure 39: Venn diagram representing the overlapping numbers of significantly differentially expressed genes in individual comparisons – SHR vs. PD5 (pink), dexamethasone vs. standard diet (light blue) and interaction between strain and dexamethasone treatment (light green). Circle diameters correspond approximately to gene number on a logarithmic scale, overlapping regions are not to scale.

11.4.4. Real time PCR confirms differential mRNA expression of Plzf and 6 other selected genes

To confirm the dependability of the results obtained from microarray data and to offer a foundation for further investigation, the expression variations of selected mRNAs showing largest fold changes were studied. *Aox1, Slc17a2, Gca, Doc2a, Lmod2, Nox4,* were analyzed by real-time PCR (Figure 40). All the confirmed mRNAs showed a good consistency with the data acquired by microarray assays.

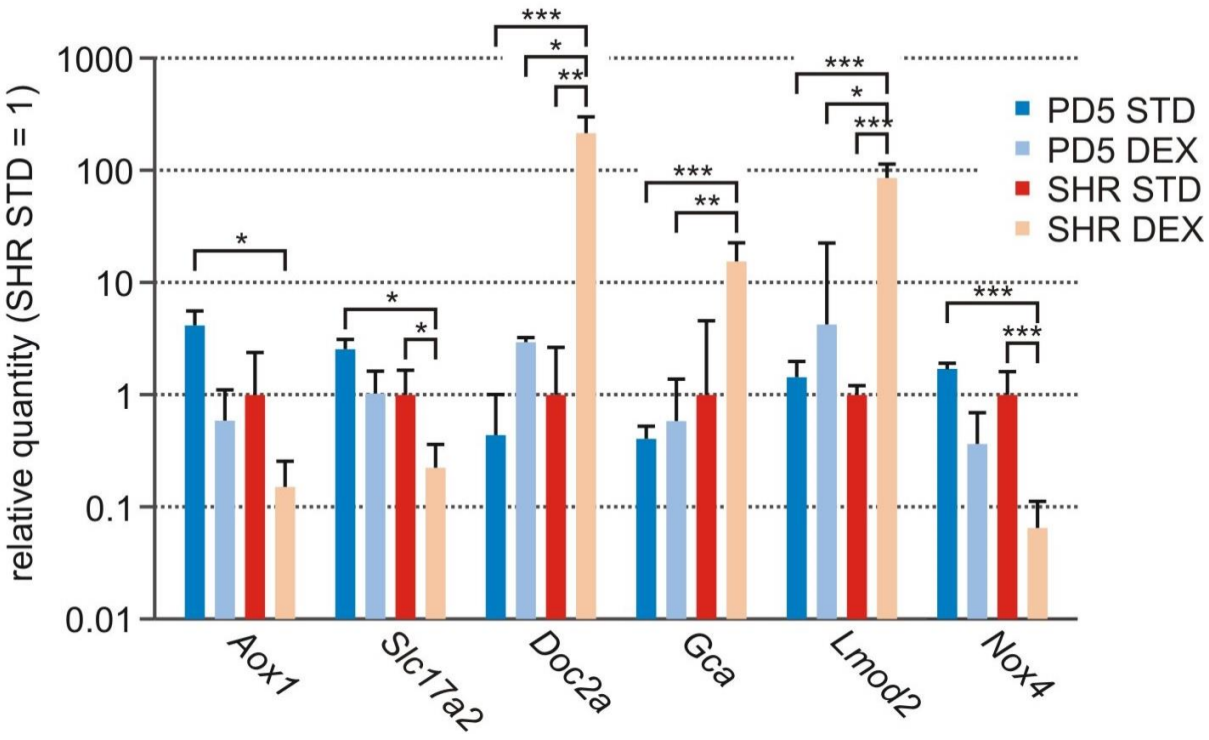

Figure 40: Gene expression (qPCR) in adult male rat liver tissue on standard diet and after dexamethasone administration: PD5 on standard diet (PD5 STD blue, n=6), PD5 on dexamethasone (PD5 DEX light blue, n=6), SHR on standard diet (SHR STD red, n=6), SHR on dexamethasone (SHR DEX beige, n=5) Data are presented as arithmetic means ± SEM. Statistical significance levels for the two factor ANOVA (factor strain and diet) are indicated for pairwise post hoc Tukey's test as follows: * $p < 0.05$, ** $p < 0.01$.

11.4.5. Differentially expressed genes enrichment analysis

In order to set our differentially expressed genes into broader biological context, we predicted their biological function using Gene ontology (GO) terms. GO is the classic cataloging system of gene function (Ashburner M. et al., 2000, Central GO. et al., 2023), which categorizes genes into three main categories – biological process (BP), cellular compartmentation (CC) and molecular function (MF). Enrichment analysis was performed separately for each of our parameters – strain, dexamethasone treatment and interaction respectively. Strain related differentially expressed genes were significantly enriched to following BP GO terms: response to oxidative stress (GO:0006979), cell aging (GO:0007569), response to drug (GO:0042493), glutathione biosynthetic process (GO:0006750) and response to nutrient (GO:0007584). These genes were also significantly enriched for the CC GO term – cytosol (GO:0005829) and the top five enrichment results for MF GO terms were as follows: glutamate-cysteine ligase activity (GO:0004357),

oxidoreductase activity, acting on the CH-CH group of donors, NAD or NADP as acceptor (GO:0016628), flavin adenine dinucleotide binding (GO:0050660), chaperone binding (GO:0051087), oxidoreductase activity, acting on CH-OH group of donors (GO:0016614) (Supplementary figures 4 - 6).

11.4.6. PLZF protein upregulation by dexamethasone treatment is diminished in PD5

While there was no significant difference in expression of Plzf in STD between the strains on the protein level, Western blot analysis of the liver tissue lysates showed upregulation of the Plzf protein after dexamethasone administration in both PD5 and SHR rat strain (Figure 41 and 42). Moreover, the levels of Plzf were significantly higher in SHR, suggesting a possible role of the intronic deletion variant of Plzf in the dexamethasone-induced hyposensitivity in PD5.

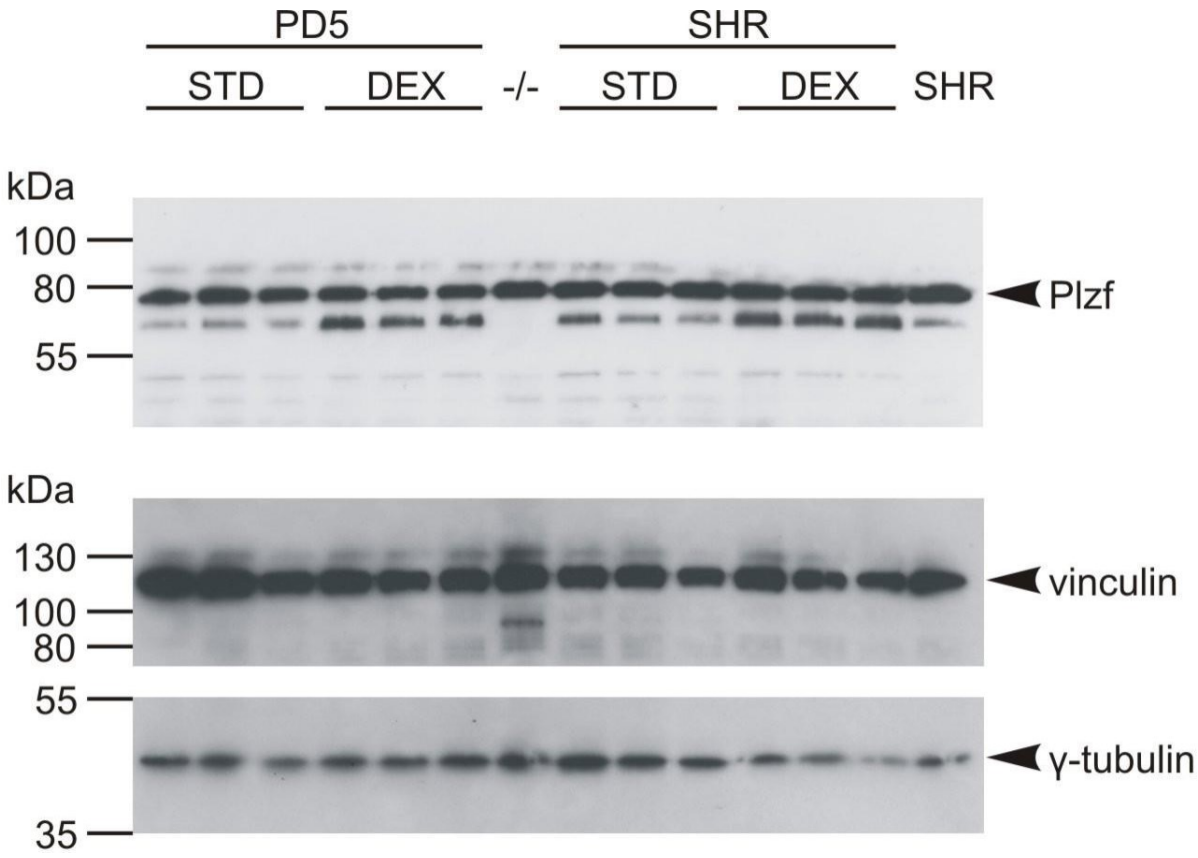

Figure 41: *Plzf* protein expression in liver tissue of PD5 strain on standard diet (PD5 STD, n=3), PD5 exposed to dexamethasone (PD5 DEX, n=3), knockout *Plzf* (PlzfKO, n=1), SHR on standard diet (SHR STD, n=3), SHR exposed to dexamethasone (SHR DEX, n=3), SHR on high fat diet (SHR HFD, n=1). PLZF Western Blot with expected molecular weight of the mature polypeptide 74 kDa and Western blots of Vinculin (116,6 kDa) and α-tubulin (50 kDa) were used as loading controls.

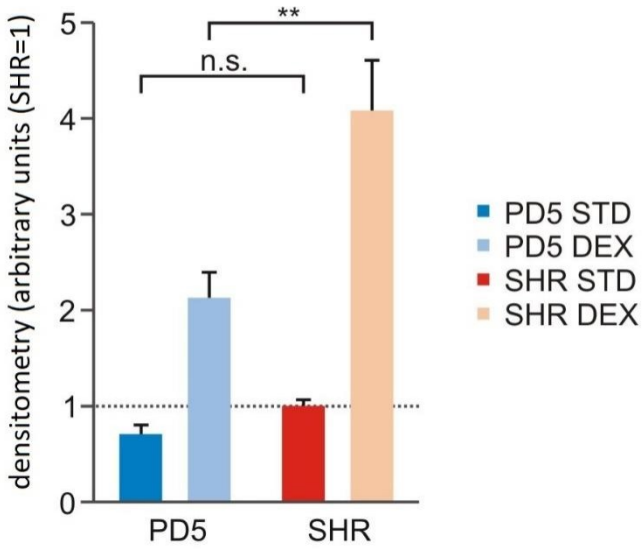

Figure 42: Densitometry of PLZF Western Blot using ImageJ, density of γ-Tubulin was used as control. PD5 on standard diet (PD5 STD, n=3), PD5 exposed to dexamethasone PD5 DEX, n=3), SHR on standard diet (SHR STD, n=3), SHR exposed to dexamethasone (SHR DEX, n=3) and knockout *Plzf* (PlzfKO, n=1). Data are presented as arithmetic means ± SEM in arbitrary units, where SHR STD mean is set to 1. Statistical significance levels for the factor strain and dexamethasone treatment of two-factor ANOVA are indicated for pairwise post hoc unequal N HSD test (honestly significant difference) as follows: * $p < 0.05$, ** $p < 0.01$, *** $p < 0.001$. (n=3 for each dexamethasone treatment*strain combination).

11.4.6. Plzf deleted segment contains a potential enhancer

Our luciferase reporter experiments were performed with two different reporter vectors pGL4.23 with intrinsic minimal promoter activity and pGL4.10 lacking a promoter. Initially we used the HEK293 cells (human embryonic kidney), which are typically used for pilot luciferase assays due to their easy transfection and transfected them with both pGL4.10 and pGL4.23 vectors carrying longer construct denoted as "full" (figure 6) spanning spanning the intronic Plzf deletion and short conserved segment adjacent to the 5′ end of the deletion. However, we did not observed a marked activation signal. On the other hand, both promoterless and minimal promoter constructs plasmids containing "out" and shorter constructs ("A, "L", "R" and "out") transfected to HepG2 cells (of liver tumor origin) did lead to significant activation of the reporter in comparison to controls, although dexamethasone treatment did not further increase the reporter gene expression. This finding suggests that the deleted region in PD5 has a promoter/enhancer activity but rules out the direct effect of dexamethasone on the intronic Plzf deletion (Figure 43-45).

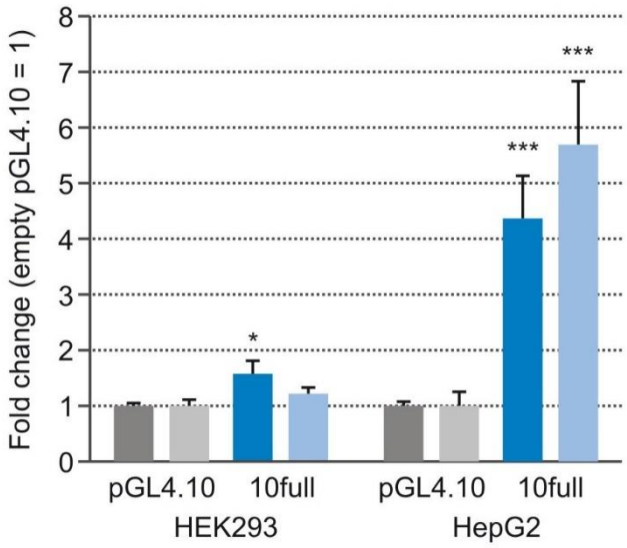

Figure 43: Luciferase reporter assay, intensities of firefly luminescence signal normalized to renilla luminescence signal were further normalized so that the mean of the empty vector = 1. Empty vector (pGl4.10) resp. full vector ((pGl4.10 with construct "full") were transfected into HepG2 or HEK293 cells with (lighter shade) / without (dark shade) dexamethasone. Data are presented as arithmetic means ± SEM. Statistical significance levels of vector with construct ("full") compared to empty vector (pGl4.10) are indicated for post hoc Student's T test as follows: * $p < 0.05$, ** $p < 0.01$, *** $p < 0.001$, n.s. – non significant. The Luminescence signal for each vector was measured 3-times.

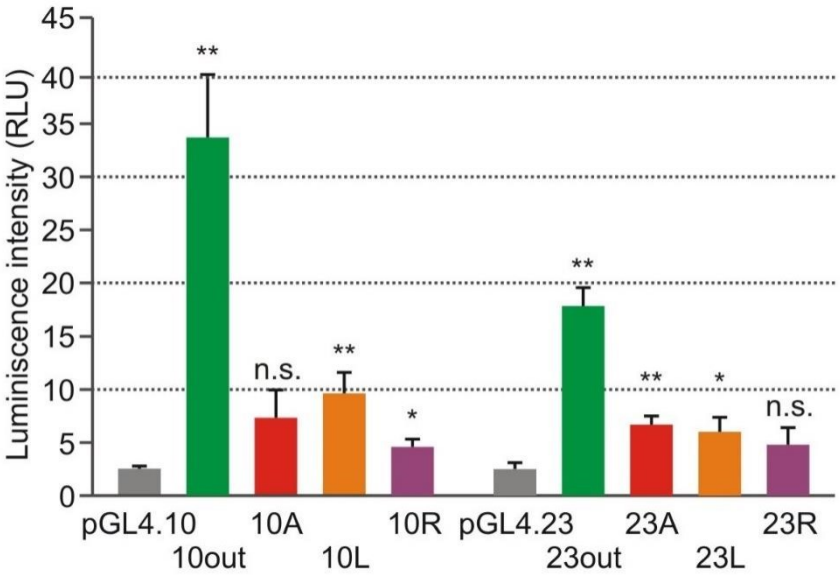

Figure 44: Luciferase reporter assay, intensities of firefly luminescence signal normalized to renilla luminescence signal. Empty vector (pGl4.10; pGl4.23) resp. full vector ((pGl4.10 resp. pGl4.23 with constructs out, A, L, R) were transfected into HepG2 cells. Data are presented as arithmetic means ± SEM. Statistical significance levels of vector with construct (out, A, L, R) compared to empty vector (pGl4.10; pGl4.23) are indicated for post hoc Student's T test as follows: * $p < 0.05$, ** $p < 0.01$, *** $p < 0.001$. The Luminescence signal for each vector was measured 3-times. RLU relative luminescence units

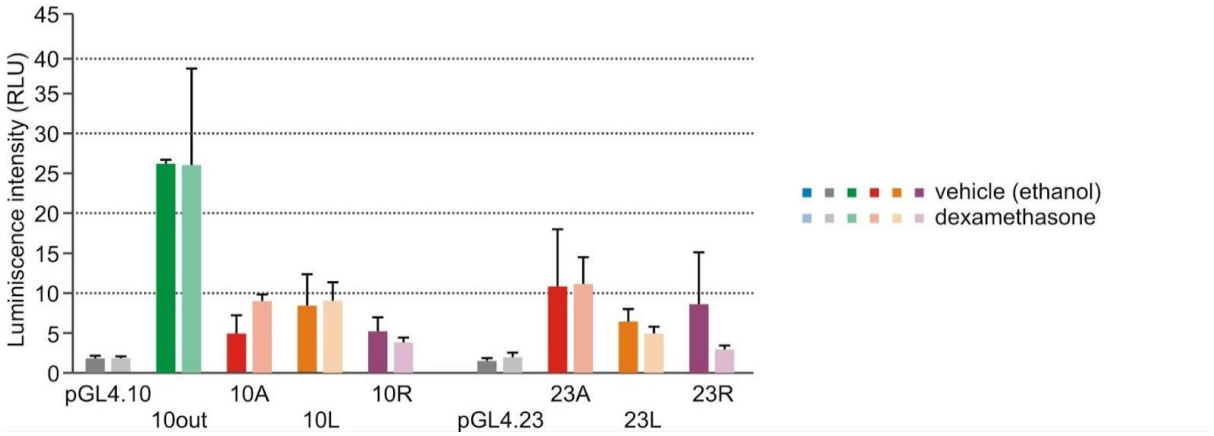

Figure 45: Luciferase reporter assay, intensities of firefly luminescence signal normalized to renilla luminescence signal. Empty vector (pGl4.10; pGl4.23) resp. full vector ((pGl4.10 resp. pGl4.23 with constructs out, A, L, R) were transfected into HepG2 cells with / without dexamethasone. Data are presented as arithmetic means ± SEM. Statistical significance levels of vector with construct (Rout, Rc, A, L, R) compared to empty vector (pGl4.10; pGl4.23) are indicated for post hoc Student's T test as follows: * $p < 0.05$, ** $p < 0.01$, *** $p < 0.001$, n.s. – non significant. The Luminescence signal for each vector was measured 3-times. RLU relative luminescence units.

11.4.7. GST pull down assay

11.4.7.1. Synthesis of GST fusion protein and GST control protein

To unravel proteins interacting with PLZF we performed a GST-pull down assay. We tested the only anti-Plzf antibody that works for the rat in Western blotting (see Methods and Fig. 41); however, the immunoprecipitate did not contain any identifiable Plzf protein. We opted for GST pull-down assay utilizing interaction between Glutathione-S-transferase and its substrate GSH. This method enabled us to bypass the need for antibodies. We managed to produce GST-tagged fusion proteins containing PLZF fragments and one containing the whole PLZF sequence, in accordance with our expectation, the latter with poor yields due to poor solubility (Figure 46-53).

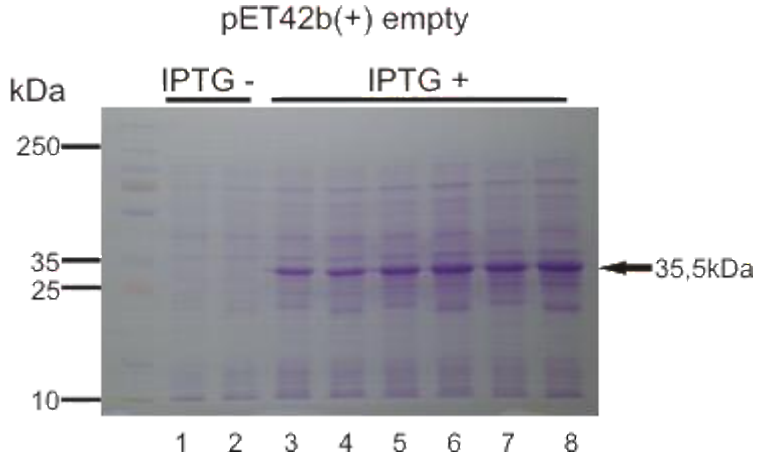

Figure 46: Production of GST control protein. Plasmid pet42b(+) without inserted construct, marked with an arrow labeled with the expected molecular weight 35,5 kDa. The samples are in the following order: 1-2) before addition of IPTG (0. hours), 3-4) 1 hour after IPTG addition, 5-6) 2 hours after IPTG addition, 7-8) 3 hours after IPTG addition.

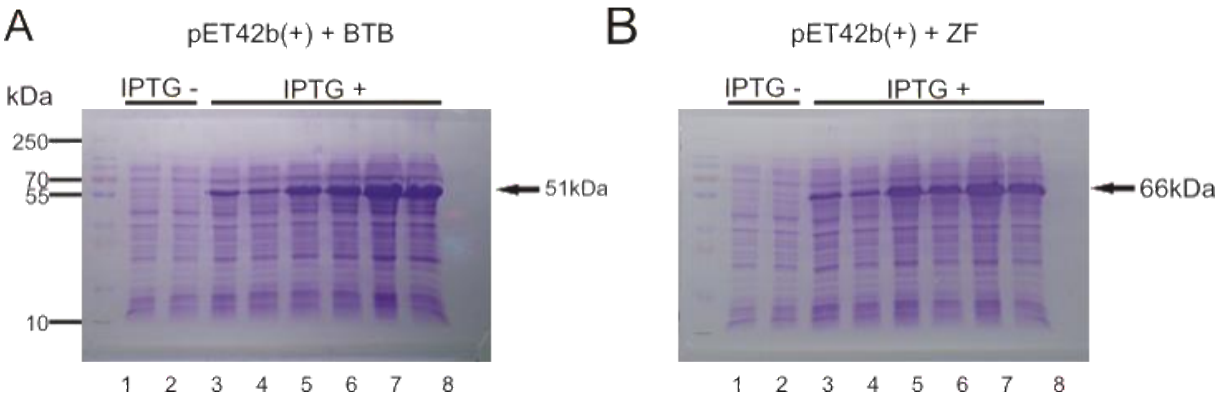

Figure 47: Production of GST fusion protein. A) plasmid pet42b(+) with inserted BTB domain (marked with an arrow labeled with the expected molecular weight 51kD. The samples are in the following order: 1-2) before addition of IPTG (0. hours), 3-4) 1 hour after IPTG addition, 5-6) 2 hours after IPTG addition, 7-8) 3 hours after IPTG addition, B) plasmid pet42b(+) with inserted ZF domain (marked with an arrow labeled with the expected molecular weight 66,6kD. The samples are in the following order: 1-2) before addition of IPTG (0. hours), 3-4) 1 hour after IPTG addition, 5-6) 2 hours after IPTG addition, 7-8) 3 hours after IPTG addition.

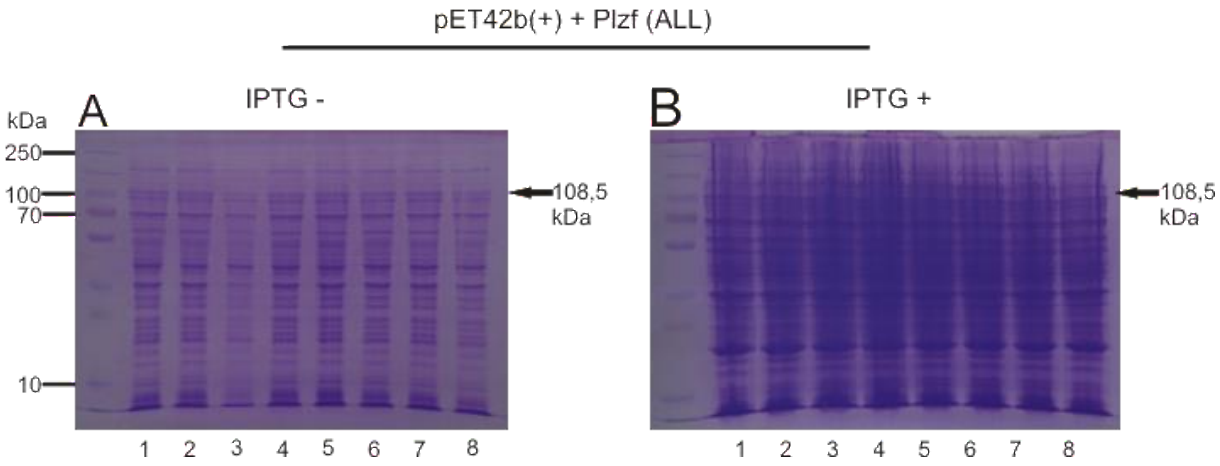

Figure 48: Production of GST fusion protein (plasmid pet42b(+) with complete *Plzf* sequence marked with an arrow labeled with the expected molecular weight 108,5 kDa). A) before addition of IPTG, B) after addition of IPTG(overnight incubation). Each gel contains 8 samples with complete *PLzf* (ALL) sequence.

11.4.7.2. Purification of fusion GST and control GST protein

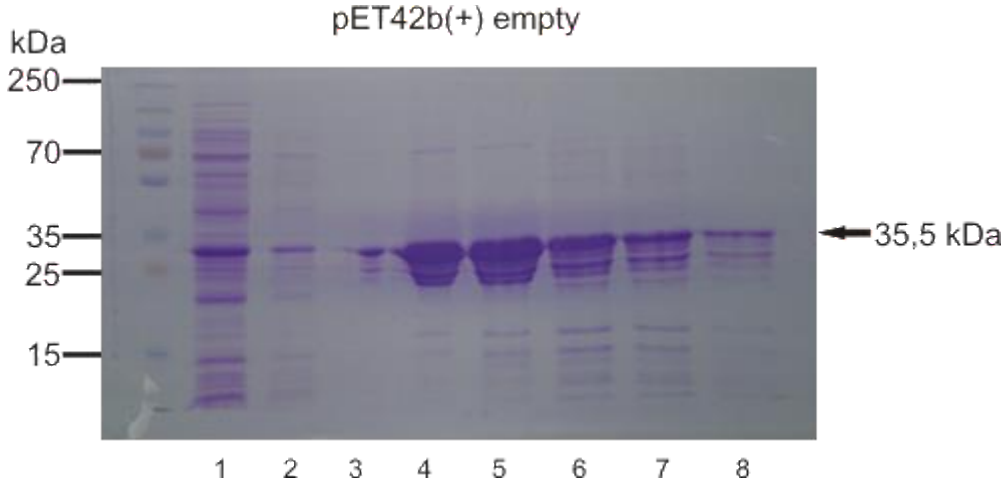

Figure 49: Purification of GST control protein (plasmid pet42b(+) without inserted construct, marked with an arrow labeled with the expected molecular weight 35,5 kDa). The samples are in the following order: 1) Eluted lysate (containing proteins not binding onto the Glutathione HiCap Matrix, 2) first wash, 3) second wash, 4-8) elution fractions 1-5.

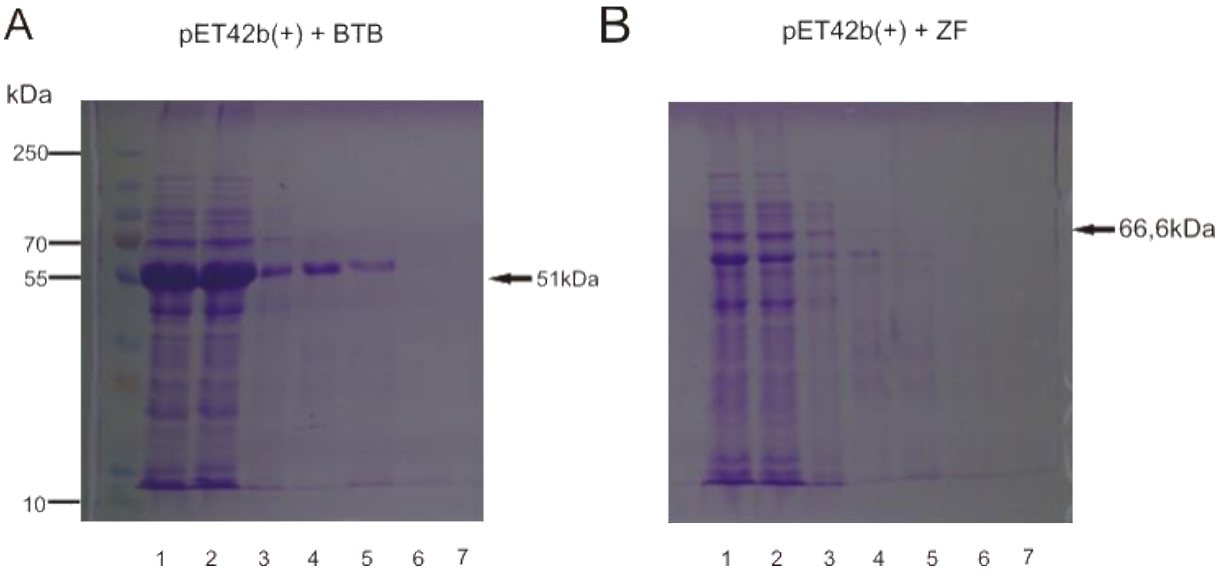

Figure 50: Purification of GST fusion protein. A) Plasmid pet42b(+) with inserted BTB domain, marked with an arrow labeled with the expected molecular weight 51 kDa. The samples are in the following order: 1) applied supernatant containing all protein, 2) flow-through - proteins not binding onto the Glutathione HiCap Matrix, 3) first wash- BTB, 4-7) elution fractions BTB, B) Plasmid pet42b(+) with inserted ZF domain, marked with an arrow labeled with the expected molecular weight 66,6 kDa. The samples are in the following order: 1) applied supernatant containing all protein, 2) flow-through - proteins not binding onto the Glutathione HiCap Matrix, 3) first wash- ZF, 4-7) elution fractions ZF.

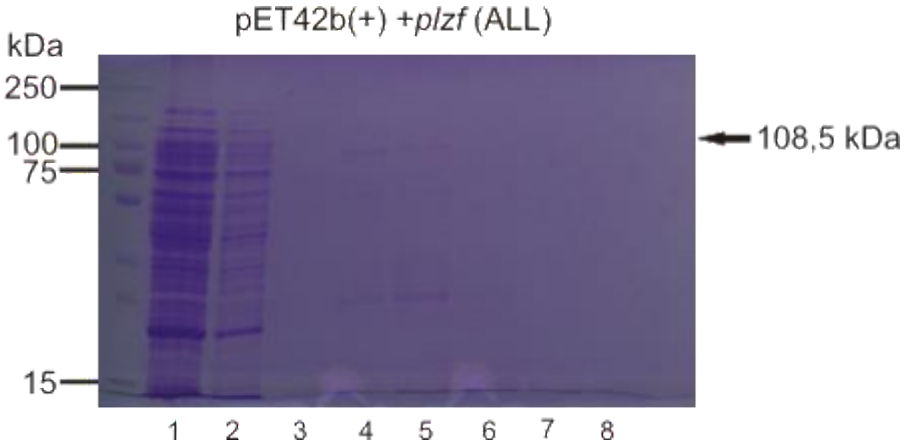

Figure 51: Purification of GST fusion protein. Plasmid pet42b(+) with inserted complete *Plzf* sequence (ALL), marked with an arrow labeled with the expected molecular weight 108,5 kDa). The samples are in the following order: 1) flow-through lysate (containing proteins not binding onto the Glutathione HiCap Matrix), 2-3) first and second wash, 4-8) elution fractions 1-5.

11.4.7.3. GST pull-down assay

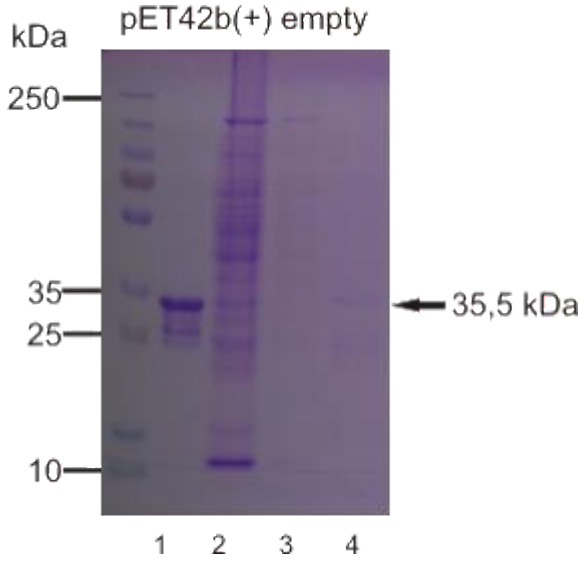

Figure 52: GST pull-down assay. GST control protein (plasmid pet42b(+) without inserted construct 35,5 kDa). The samples are in the following order: 1) Purified GST control protein, 2) Liver lysate flowthrough not containing all proteins noninteracting with GST protein, 3) First wash - BTB, 4) Eluted GST-BTB fusion protein with interacting proteins.

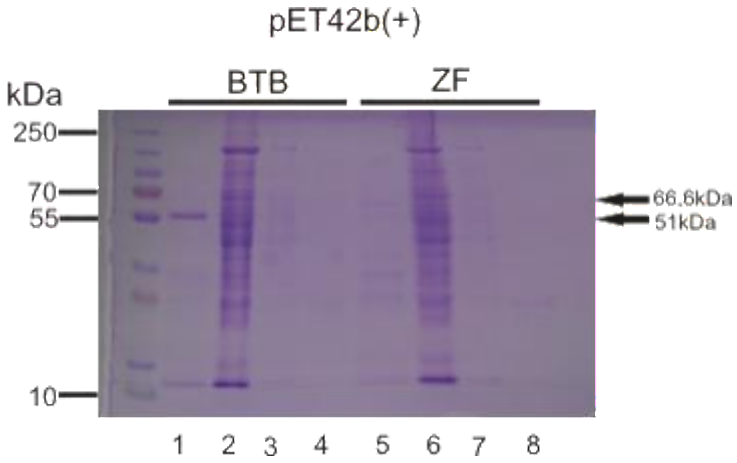

Figure 53: GST pull-down assay. A) GST fusion protein (plasmid pet42b(+) with inserted BTB domain (51 kDa) and ZF domain, (66,6 kDa). Samples are in the following order: 1) Purified GST fusion protein with BTB domain, 2) Supernatant BTB (containing all proteins not interacting with GST fusion protein), 3) first wash - BTB, 4) Eluted GST-BTB domain fusion protein with interacting proteins, 5) Purified GST-ZF fusion protein, 6) Supernatant ZF(containing all proteins not interacting with GST fusion protein), 7) First wash - ZF, 8) Eluted GST-ZF domain fusion protein with interacting proteins.

11.4.7.4. Proteomic analysis

The GST pull-down assay detected a variety of proteins that directly bind to ZF, BTB and All Plzf constructs. Analysis identified 21 proteins in total, however the subsequent proteomic analysis did not identify proteins with known Plzf interaction, which warrants further analysis (Supplementary table 17).

12. Discussion

12.1. Comparative transcriptomic analysis of myocardial tissue in SHR and its minimal congenic strain PD5

Recent research showed a pleiotropic effect of *Plzf* and highlighted its promising role as a candidate gene, which (if its function is suppressed) is deemed responsible for the attenuation of hypertension, dyslipidemia and myocardial fibrosis in PD5 strain (due to a deletion in an intronic noncoding region) and decreased cardiac fibrosis in *Plzf* knockout heterozygotes as opposed to SHR (Liška et al. 2014, 2017). In the first study we evaluated the transcriptomic landscape in PD5 and SHR cardiac myocytes with the aim to better understand the pathophysiologic changes with regard to *Plzf*. In this study *Plzf* expression was in concordance with our previous observations, however it did not reach statistical significance, probably due to multiple comparisons correction. However, some of the differentially expressed genes in this study may be regulated by *Plzf*. Another source of differential expression of cardiac genes can be reactive, as a result of the hypertension development. PD5 has been shown to have lower blood pressure compared to SHR (Liška et al. 2014), but the difference is small, and was not confirmed in *Plzf* knockout heterozygotes (Liška et al. 2017). In the cohort analyzed here, the relative heart weight in PD5 is not significantly different from controls, although the trend is in the direction previously described. This could be an advantage, since the reactive, non-primary, effects on gene expression are limited. Several of the differentially expressed genes deserve further investigation. The nuclear orphan receptors Nr4a1 and Nr4a3 are nuclear orphan receptors for which ligands have not been identified. We found *Nr4a1* upregulated in PD5 both on transcript and protein level compared to SHR (in concordance to the repressor effect of Plzf). Recent research underlined the possible role of Nr4a1 in attenuation of endometrial fibrosis (Zeng X. et al., 2018), pulmonary fibrosis and skin fibrosis (Palumbo-Zerr K. et al., 2015). Emerging data pointed out the critical importance of Nr4a1 also in the development of cardiac fibrosis (Chen J. et al., 2021) and highlighted several possible mechanisms. Nr4a1 seems to attenuate cardiac fibrosis after myocardial infarction by inhibition of Alpha-enolase (ENO1) in fibroblasts (Ji J. et al., 2022), Nr4a1 may also inhibit the endothelial to mesenchymal transition known to be substrate for cardiac fibrosis and heart failure in diabetic hearts (Qin Q. et al., 2014; Widyantoro B. et al., 2010) through negative regulation of Endothelin-1 (ET-1) or inhibitory effect on the NF-κB pathway (Chen J. et al., 2021) or

attenuatingTGF-β expression (Medzikovic L. et al., 2021) in cardiomyocytes. Furthermore *Nr4a1* mediates the transition from inflammatory monocytes to reparatory macrophages in ischemic myocardium (Marinković G. et al., 2020), suppresses apoptosis via regulation of RLN3 in ventricular myocardium (You X. et al., 2018), regulates cell differentiation, proliferation, apoptosis and inflammation (Maxwell MA. et al., 2006, Chao LC. et al., 2008). Nr4a1 influences cardiac remodeling via NPY (Medzikovic L. et al., 2018) and is integrated to the hypothalamic–pituitary–adrenal axis because Angiotensin-II induced expression of NR4a1 is concomitant with stimulation of aldosterone synthase activity (Nogueira EF. et al., 2009). Independent research groups demonstrated that NR4a1 protects against adverse effects induced by chronic β-adrenergic stimulation (Medzikovic L. et al., 2015; Yan G. et al., 2015). This mounting evidence suggests a key role of NR4a1 in myocardial hypertrophy and fibrosis. In the above mentioned experiments described by our research group, PD5 strain showed markedly attenuated myocardial fibrosis. On both transcriptomic and protein levels, we observed significant overexpression Nr4a1 in PD5 strain which is in full accordance with above mentioned findings. As evidence suggests Nr4a1 exerts pleiotropic effects on the cardiovascular system and is not confined just to myocardium. As far as hypertension is concerned, it was shown that Nr4a1 by down-regulation of β-catenin signaling in vascular smooth muscle cells (Cui M. et al., 2016) inhibits angiotensin induced phenotypic switch with enhanced proliferation, migration and matrix deposition which leads to hypertension (Vukelic S. et al., 2014). Data also indicate that NR4a1 has an essential role in regulating oxidative stress by maintaining mitochondrial homeostasis in vascular smooth muscle cells, furthermore NR4a1 knockout aggravated AngII-induced oxidative stress in vascular smooth muscle cells. (Geng N. et al., 2022) and NR4a1 deficiency promotes atherosclerosis through macrophage related inflammasome (Yuan R. et al., 2022). There might be some conflicting views on the involvement of NR4a1 in vascular calcification. Although earlier works hinted at the protective role of Nr4a1 in atherosclerosis development (Hu YW. et al., 2014), recent research indicates that NR4A1/DNA-PKcs/p53 pathway is involved in the mechanism by which lactate accelerates vascular calcification (Zhu Y. et al., 2020). Furthermore several papers dissected its role in development of cardiovascular diseases (e.g. cardiac hypertrophy, and cardiac ischemia/reperfusion injury) (Wang RH. et al., 2013, Cheng Z. et al., 2011). In our work we speculate that because we used whole tissue myocardium the *Nr4a1* overexpression may be put down to the “masking” effect of myocardial cells since they comprise the largest proportion of myocardial tissue as opposed to smooth muscle cells, where as the evidence

would suggest we expect attenuation of expression. The *Nr4a1* overexpression in PD5 may thus mirror its antifibrotic effect and well correspond to the attenuated cardiac fibrosis in PD5 strain. Regarding other aspects of metabolic syndrome, NR4a1 is also capable of reducing hepatic cholesterol based on lipid overloading, and this may be due to the decrease in LDLR and HMG-CoA reductase (HMGCR) levels (Zhang P. et al., 2012). NR4a1 influences gluconeogenic liver pathways. It enhances hepatic gluconeogenesis which consequently leads to higher blood glucose (Diaz MB. et al., 2006) and downregulation of NR4A in liver in type II diabetic db/db mice by adenoviral delivery of a dominant-negative *Nr4a1* decreased expression of gluconeogenic target genes and restored elevated glucose levels to near normal (Pei L. et al., 2006). The enriched GO-terms for Nr4a1 showed an involvement of Nr4a1 in steroid receptor signaling, regulation of type B pancreatic cell proliferation, and fat cell differentiation. These processes are important for metabolic syndrome development; however, their significance for left ventricle myocardium is unknown. Per1, downregulated in PD5 heart in comparison to SHR, is a key component of the circadian loop, displaying regulatory effects on renal epithelial sodium channel gene expression (Gumz M. et al., 2012; Gumz M. et al., 2009). Lower levels of the *Per1* mRNA were associated with attenuated sodium channel expression, increased sodium excretion, and low blood pressure (Richards J. et al., 2013). Interestingly, *Per1* knockout mice develop hypertension when given a long-lasting mineralocorticoid and a high salt diet, while wild type mice do not, suggesting that *Per1* gene expression may also be involved in sodium appetite and central control of blood pressure (Solocinski K. et al., 2017). However, apart from reports showing expression of *Per1* in the heart (Bonaconsa M. et al., 2014) its cardiac function has not been dissected, although emerging data underlined the protective role of circadian genes on radiation induced cardiotoxicity (Dakup PP. et al., 2020) . *Kcna5*, another gene downregulated in PD5 heart, encodes the Kv1.5 channel crucial for carrying the ultra-rapid potassium current (IKur) (Christophersen IE. et al., 2013). Since the importance of normal electrophysiological environment for myocardium, any alterations within the biophysical properties of IKur are associated with higher incidence of large-scale and multi-faceted electrical and structural remodeling (Workman AJ. et al., 2001, González de la Fuente M. et al., 2013), thus leading to atrial fibrillation (Christophersen IE. et al., 2013, Caballero R. et al., 2010) and other potentially life threatening dysrhythmias, increasing the risk of heart failure development and sudden cardiac arrest (Tomaselli GF. et al., 1994). There was no indication of arrhythmias during the telemetric blood pressure recording in

PD5 and SHR (Liška F. et al., 2014, unpublished data). Whether the channel upregulation in SHR can contribute to fibrosis and hypertrophy without causing arrhythmias is unknown.

To our knowledge, no direct connection among our differentially expressed genes and the genes present within the congenic segment has been reported so far, especially Plzf, which is apparently the quantitative trait gene (Liška F. et al., 2017). This may lead to the assumption that the observed differences in expression might be a secondary effect of the phenotype. However, the rats in our experiment were just two months old and the phenotypic differences in the heart weights between the groups were not yet expressed to the extent to which they normally are in older rats – therefore we suggest that the difference in expression could be a primary effect, although there is no evidence of Plzf causation. Interestingly, Plzf and NR4a1 have been shown to be part of mutual exclusive pathways responsible for T-cell maturation (O´Hagan KL. et al., 2015) or Per1 (Leigh R. et al., 2016). The relation of Plzf and metabolic syndrome was recently reviewed (Seda O. et al., 2017). In conclusion, using the microarray approach following qPCR verification we revealed several differentially expressed genes in the heart of PD5 compared to SHR. NR4a1, upregulated in PD5 in comparison to SHR both on RNA and protein level, may play a role in the differential cardiac phenotypes of PD5 and SHR, i.e. amelioration of cardiac fibrosis in PD5.

12.2. Hepatic transcriptome profiling in Polydactylous Rats with High-Fat Diet-Induced Hypertriglyceridemia and Visceral Fat Accumulation

The PD rat strain is an established rodent model for hypertriglyceridemia and insulin resistance which as our earlier studies showed is susceptible to high sucrose diet. In the second experiment we aimed to assess the extent to which a high fat diet influences metabolic and morphometric parameters compared to SHR and BN strains. SHR displays all metabolic syndrome features after a high fat diet as opposed to PD which lacks hypertension. However, as we showed here, PD is more prone to hypertriglyceridemia and insulin resistance than SHR. PD harbors the intronic Plzf deletion that was later transferred to PD5 congenic strain; however, apart from Plzf and its vicinity, PD5 has the SHR genetic background, while PD genetic background is completely different. BN serves as a “healthy” control without any metabolic syndrome features at all.

In order to eliminate excessive variability caused by the estrous cycle we opted for adult male rats. At the start of the experiment the PD strain showed a significantly higher total body weight compared to SHR and BN respectively, but there were no significant

differences in measured metabolic parameters (fasting glucose, OGTT, triacylglycerols or FFA serum levels). The high fat diet which we administered for four weeks triggered a growth spurt in all three strains but surprisingly with different dynamics. We observed continuous total body weight growth in PD strain throughout the experiment, but the SHR and BN reached the maximum body weight within the first two weeks followed by a plateau. This might be put down to the fact that the PD strain consumed the largest amount of diet. PD rats accumulated the excess caloric intake in the increased volume of fat depots (epididymal and retroperitoneal fat, which loosely correlate to perivisceral human fat depots. (Chusyd DE. et al., 2016).

The most pronounced biochemical difference was markedly elevated TAG levels in PD rats compared to both SHR and BN. Interestingly, this hypertriglyceridemia was not accompanied by hepatic steatosis. This seemingly contradictory observation might be due to increased triglyceride release from the liver of PD rats as is suggested by the nearly 10 times higher VLDL triglycerides in the plasma of PD rats when compared to SHR and BN rats (Figure 20a). As discussed elsewhere in this text, we identified intronic deletion of Plzf gene in PD strain which leads to its decreased expression in certain tissues (heart, liver and embryonal limb buds). The SHR PD5 congenic strain which harbors Plzf of PD origin shows decreased Plzf expression, and attenuation of metabolic syndrome features, which led us to the enhancer hypothesis. There are some opposing views on the function of Plzf in adipose tissue and nonalcoholic fatty liver disease (NAFLD). While some papers proved tha RNAi mediated knockdown of Plzf has an stimulating effect on adipogenesis (Mikkelsen TS. et al., 2010) , recent evidence suggest (Crosby CM. et al., 2018) an activatory role of Plzf in iNK cells and thus further progress the damage caused by the fatty liver. The liver transcriptome analysis in our experiment showed unexpectedly a statistically insignificant tendency for increased expression of *Plzf* in PD after the high fat diet; thus the role of Plzf in PD for prevention of steatosis remains inconclusive. Another mechanism to explain the lack of steatosis in PD is by upregulation of the lipogenesis genes in liver transcriptome—*Scd1*, encoding the stearoyl-CoA-desaturase 1 enzyme. Higher expression of Scd1 is possibly compensatory due to a high FAs supply and could be accompanied by higher VLDL output in PD. Alternatively, increased VLDL levels can be due to decreased lipolysis, as chylomicron levels were also excessively high. In addition, significantly higher diacylglycerol (DAG) levels were found in the liver of both PD and BN strains compared to SHR. We did not observe any differences in serum cholesterol levels after a high fat diet

among strains, we did observe a decrease in serum FFA measured after OGTT in SHR and BN, but not in PD. In normal conditions glucose intake stimulates insulin production with consequent lipolysis inhibition and decreased serum FFA. Since this fenomena was not observed in PD strain, we think that it is a symptom of insulin resistance in PD rats (Powell DJ. et al., 2003; Arrese M. et al., 2016).

Liver transcriptome pathway analysis showed significant downregulation of focal adhesion, adipogenesis, triacylglycerol synthesis, and lipid droplet metabolism pathways in PD in relation to SHR. We also found that pathways associated with chronic or acute inflammatory processes-prostaglandin synthesis, interferon signaling, and complement activation were uniquely downregulated in PD in comparison to the SHR strain. Several studies highlighted the important role of innate immune activation as a key factor in triggering and amplifying hepatic inflammation in NAFLD/NASH (Arrese M. et al., 2016). Other papers described proinflammatory fatty liver disease induced by overnutrition-triggered lipotoxicity (Farrell GC. et al., 2018). Although there was no immune activation in PD as indicated by the serum cytokine levels, the inflammatory reaction accompanying MetS features is initially organ specific and usually on subcellular levels. It is plausible that the transcriptomic pattern observed in SHR might thus reflect these initial changes, so we can only speculate whether long-term HFD feeding would not lead to more dramatic differentiation in systemic inflammation among the strains.

Another finding potentially relevant for MetS pathogenesis in PD was a significantly lower relative leptin serum level after correction to fat tissue weight. Absolute serum leptin level was highest in PD both at the start of the experiment and after high fat diet admission and there was a correlation between the serum leptin level and fat tissue amount; however, when corrected to the epididymal+retroperitoneal fat tissue amount, serum leptin level in PD was significantly lower. This suggests impairment of the leptin pathway after HFD, although it would be more appropriate to correlate the serum leptin levels to subcutaneous fat depots which were not measured. A similar finding was described previously (Ainslie DA. et al., 2000) and based on this fact, it is possible that after longer-term HFD feeding, leptin levels could become elevated, and correlate with fat reserves. However, since there could be insufficient signal provided to the hypothalamus in PD about energy reserves, it could fail to prevent higher energy intake, which we indeed observed in PD in the 4-week HFD feeding course compared to the other strains that exhibited a plateau phase, after an

initial weight increase. Leptin gene expression in epididymal fat corresponded to the fat tissue amount in all strains. The putative defect is thus more likely to arise during translation, processing, or secretion. This hypothetical dysregulation of energy intake can contribute to hypertriglyceridemia and obesity seen in PD (Iwai N. et al., 2003; Benjafield AV. et al., 2003).

PD strain displays significant downregulation of three acyl-CoA-generating enzymes (ACSM3, ACSM2A, ACSL5), which can contribute to the lower ability to utilize fatty acids and hypertriglyceridemia in this strain. ACSM3 belongs to a family of enzymes conjugating medium-chain fatty acids (C4-C14) to coenzyme A. At least some members can also contribute to excretion of xenobiotics by activating carboxylic compounds (e.g., benzoate, salicylate) before conjugation with glycine (Van der Sluis R. et al., 2016, 2018). The human genome contains seven members of the family (ACSM1, 2A, 2B, 3, 4, 5, and 6). Except ACSM4 and 6, all are localized to a ~400-kb cluster on chromosome 16 (Iwai N. et al. 2003) (hg38 chr16:20409534-20797581). In the rat, the family is contained in the syntenic region on chromosome 1, including *Acsm4* but excluding *Acsm2b* since *Acsm2* is not duplicated (rn6 chr1:189241593-189541233). The function of individual family members is far from elucidated (Van der Sluis R. et al., 2016). ACSM3 was recently proved to suppress the pathogenesis of high-grade serous ovarian carcinoma via promoting AMPK activity (Yang X. et al., 2022) and lower expression of ACSM3 conferred worsened prognosis of malignant melanoma (Zhu Z. et al., 2020), in these regards ACSM3 displays pleiotropic functions.

Interestingly, Acsm3 was proposed candidate gene for essential hypertension that was isolated by virtue of its increased expression in the kidney of spontaneously hypertensive rat compared with the kidney of normotensive Wistar-Kyoto rat (Iwai N. et al., 1991), but the association with basal or salt induced hypertension was not confirmed (St Lezin E. et al., 2000; Walsh V. et al., 2003). ACSM3 is a unique isobutyrate and butyrate preferring acyl-CoA synthetase (Fujino T. et al., 2001). Butyrate arises from the fermentation of dietary fiber by the colonic microbiota, enters mitochondria for fatty acid oxidation after activation by ACSM3 or can serve as a precursor for cholesterol synthesis or signaling molecule regulating lipid and glucose metabolism (den Besten G. et al., 2013). An increased consumption of short-chain fatty acids in diet has beneficial effects on energy metabolism as seen in short chain fatty acids (SCFA) fed mice which were protected from diet induced obesity (Yamashita H. et al., 2007), also higher butyrate concentrations can increase colonic

health and also beneficially impact other organs like liver and adipose tissue. (den Besten G. et al., 2013), on the other hand, genetically obese *ob/ob* mice and obese human subjects have increased amounts of cecal and fecal SCFAs (Turnbaugh PJ. et al., 2006), the protective effect is probably simply not strong enough to compensate for an adverse diet or genetic predisposition (den Besten G. et al., 2013) . Acsm3 deficiency can thus perform a protective role via putatively increasing butyrate levels. However, conversely, there can be a detrimental effect due to the relative butyrate increase with normal acetate and propionate levels. Notably, the *ob/ob* mouse microbiome has a higher proportion of butyrate over propionate and acetate producers (den Besten G. et al., 2013). It can be noted that the normal reaction of ACSM group transcripts in the liver after HFD seems to be upregulated, which could increase the efficiency of the liver for fat storage (Ellis JM. et al., 2015). An absence of ACSM3 in PD can thus decrease the rate of fatty acid utilization by the liver, resulting in hyperchylomicronemia. Association studies using a large cohort (4000 subjects) representing the general population in Japan found polymorphisms in the ACSM3 gene that were strongly associated with plasma triglyceride, plasma cholesterol, body mass index (BMI), waist-to-hip ratio (W/H), and blood pressure status. The effect of this genotype on blood pressure seemed to be conveyed through its effects on BMI and W/H (Iwai N. et al., 2002). Similar associations of ACSM3 gene polymorphisms with obesity were reported by Banjafield and Telgmann (Benjafield AV. et al., 2003; Telgmann R. et al., 2007). One GWAS reported an association between the ACSM cluster and dietary patterns (Guenard F. et al., 2017). Even though most of these association studies with ACSM3 as a candidate gene used less stringent statistical criteria compared to GWAS, these results are reproducible and provide compelling evidence for ACSM3 gene involvement in obesity and hypertriglyceridemia. In addition, in BXH/HXB recombinant inbred strains derived from BN and SHR progenitors (Hubner N. et al., 2005), hepatic expression of the *Acsm3* gene correlates inversely with the relative weight of epididymal fat ($r = -0.53$, $p = 0.006$) and with adipocyte volume ($r = -0.50$, $p = 0.009$) (http://www.genenetwork.org/). None of the studies, to the best of our knowledge, reported an absence of *Acsm3* expression in the liver in connection with MetS, and Acsm3-deficient mice were only studied regarding hypertension (Fujino T. et al., 2001). Potentially interesting information about the signaling and metabolic functions of ACSM3 comes from studies of hepatocellular carcinoma, where its downregulation is associated with poor prognosis. In tumor cells, ACSM3 mRNA was upregulated by HNF4α, downregulated by PPAR-γ, there was a negative feedback loop between ACSM3 and AKT, and ACSM3 expression correlated with fatty acid beta oxidation

(Gopal R. et al., 2017; Ruan HY. et al., 2017). In addition, our previous experiments in rats that were fed a normal diet also showed zero hepatic expression of the Acsm3 gene in the PD strain while the gene was expressed in SHR (Šeda O., 2021). The fact that Acsm3 is not expressed in the liver of PD rats fed both control and HFD suggests the possibility of primary genetic effects of the Acsm3 PD variant on hypertriglyceridemia, the limitation being that we do not have a complete transcriptomic profile of unchallenged PD.

Together, these results strongly suggest that Acsm3 may play a significant role in MetS development in the PD strain. The level of this significance, in a polygenic MetS model, such as PD, can be answered by transgenic rescue experiments in PD rats.

12.3. Plzf expression and transcriptomic footprint of dexamethasone- induced metabolic syndrome in SHR minimal congenic subline

Previous studies consistently showed that Plzf is associated with several components of metabolic syndrome including adipogenesis (Plaisier CL. et al., 2012), hypertension (Liška F. et al., 2014) and may be perceived as multimodal pleiotropic node in MetS (Šeda O. et al., 2017). In the present study we used dexamethasone treatment to aggravate features of MetS in an established rodent model of metabolic syndrome, the SHR rat, and its minimal congenic counterpart PD5 harboring intronic deletion in *Plzf* to explore the extent to which dexamethasone influences MetS features in relation to wild-type or decreased Plzf function.
In general, we observed mitigated effect of dexamethasone on two main MetS features namely body weight and glucose tolerance test in PD5 as opposed to SHR. Although not significant, the trend shows that dexamethasone even reduces body weight in PD5, a contradictory observation to SHR where dexamethasone boosts weight. Recently, Liška (Liška F. et al. 2017) showed that reduced expression of wild type Plzf leads to increased insulin sensitivity and reduced serum TAG and cholesterol.
In this paper, we presume that the reduced effect of dexamethasone in PD5 might be due to mutated *Plzf*. In line with this hypothesis the liver transcriptome data showed differential expression of a larger gene cohort after dexamethasone in SHR rather than in PD5. We long suspected the intronic deletion of *Plzf* to be the cause of its decreased expression, since the deletion removes a highly conserved noncoding element that presumably can work as an enhancer. Therefore we conducted a luciferase assay in order to 1) find out whether the deleted sequence has the enhancer effect and 2) whether the enhancer effect can be

modulated (increased) by dexamethasone, as suggested by the deficient increase of *Plzf* expression after dexamethasone administration in PD5. In PD5 liver tissue the PLZF expression is only insignificantly increased after dexamethasone treatment, while in SHR the expression is increased approximately 4-fold, which we confirmed by Western blot analysis. We tested two conserved noncoding elements that are in close vicinity in intron 2 of Plzf, one is in the deleted region, one is outside of it. Although the strongest enhancer activity was observed out of the deletion, the data also indicate a significant enhancer activity within the conserved region deleted in PD5 strain. However, adding dexamethasone to the luciferase assays did not change the reporter expression at all, which suggests that the PD5-deleted noncoding sequence is not directly regulated by the glucocorticoid receptor. The enhancer activity can be expected to be tissue/cell specific, indeed we did not observe any signal in HEK293 cells (derived from kidney), and the effect was significant in liver cancer derived HepG2 cells. It is possible that even HepG2 cells are not representing normal hepatocyte function as to the regulation of *Plzf* expression, therefore, a "normal" hepatocyte cell line, such as AML12 cells, may be used to confirm this data in future.

In a recent study Fu demonstrated (Fu S. et al., 2020) that PLZF and PPARγ2 synergically promote SREBP-1c transcription to increase lipid biosynthesis in iNKT cells which were found to be sensitive to lipid antigens and could show cytotoxicity against hepatocytes, thus promoting NAFLD (Crosby CM. et al., 2018). SREBP-1c has been proposed as a key intermediate in the action of insulin on genes coding for proteins involved in carbohydrate metabolism (Azzout-Marniche D. et al., 2000). Thus the observed mitigated effect of dexamethasone induced MetS in PD5 rat strain might be due to inability of the decreased PLZF response to promote PLZF SREBP-1c mediated transcriptional co-stimulation. Moreover, the primary pathogenic effect would in that case originate not from hepatocytes themselves, but from the iNKT cells which are part of the immune system.

Taken together, we showed that the intronic deletion of the Plzf gene, which is practically the sole difference between SHR and PD5 strains has an enhancer/promoter activity in the HepG2 cells, but we were not able to show that the enhancer would be regulated directly by dexamethasone.

12.4. Discussion summary

Mounting evidence indicates an indisputable role of *Plzf* in the development of metabolic syndrome as well as highlighting its importance in the pathophysiology of every metabolic syndrome feature. The experiments that we conducted in this thesis are in line with this observation, underlining the pleiotropic character of *Plzf* across two tissue types - liver and heart tissue. Previous studies from our study group identified an intronic deletion of *Plzf* gene with pleiotropic metabolic and morphologic consequences such as alleviation of systolic hypertension, together with improvement of insulin resistance and lipidogram profile.

In our first experiment we performed comparative transcriptomic profiling of myocardial tissue between SHR and PD5 strain in order to dissect the genetic background responsible for attenuated myocardial fibrosis and metabolic syndrome features in PD5 strain which harbors the above mentioned intronic *Plzf* deletion and to dissect the transcriptomic pattern in relation to the *Plzf* gene. Promisingly, we identified overexpression of nuclear receptors NR4a1 in PD5 strain on both transcriptomic and proteomic level. There is a plethora of evidence showing a positive effect of NR4a1 on myocardial fibrosis involving a wide range of molecular and physiological mechanisms. Although the mitigated myocardial fibrosis in PD5 may be secondary to lower systolic blood pressure, we speculate that because of the pleiotropic functionality of NR4a1 the transcriptional changes in NR4a1 may at least to some extent be primary. Since the *Plzf* is transcriptional repressor our findings may indicate that the NR4a1 may well be under either direct or indirect repressor effect of Plzf.

In the next project we focused on nutrigenomic analysis of PD strain. PD is an established model of insulin resistance and metabolic syndrome. We compared the morphometric and metabolic parameters among PD, SHR and BN strains after a high fat diet. The most pronounced biochemical difference was markedly elevated TAG levels in PD rats compared to both SHR and BN. Interestingly, this hypertriglyceridemia was not accompanied by hepatic steatosis. PD is more prone to hypertriglyceridemia and insulin resistance than SHR, but unlike SHR is normotensive. The transcriptomic data revealed downregulation of *Acsm3* gene encoding a short to medium chain (isobutyrate and butyrate preferring) acyl-CoA synthetase in PD strain which was confirmed on proteomic level. We may suspect that lack of *Acsm3* expression may contribute to observed elevated TAG levels and insulin resistance deterioration after a high fat diet in PD strain. PD harbors the same intronic *Plzf* deletion that is transferred to PD5 congenic strain; however, PD has a different genetic background than SHR or BN, with multiple functional genetic differences, so the resulting observed

biochemical and transcriptomic differences among strains could not be put down to direct effect of Plzf.

In our third experiment we focused on the functional characteristics of the *Plzf* intronic deletion. We observed only a mitigated effect of dexamethasone on aggravation of metabolic syndrome features in PD5 compared to its progenitor SHR. Since the PD5 harbors the "less-than-normal-functioning" *Plzf* with the intronic deletion we presumed that the deletion may be responsible for the mitigated effect of dexamethasone and it is still the most plausible hypothesis. As the luciferase assays indicated, the deleted *Plzf* segment displays intrinsic enhancer activity; however, there was no response to dexamethasone on the luciferase assays. Thus we deem that the effect of dexamethasone may be either indirect, or we were unable to uncover the effect due to the difference of the used cancer liver derived line HepG2 from the native hepatocytes. Glucocorticoid receptor is expressed in HepG2 cells (Lui WY. et al., 1993); however, the sensitivity can be lower, therefore higher dexamethasone concentration could be helpful in the future. It needs to be stated here that the concentration used was already fairly high. In order to search for the possible missing interaction partners of *Plzf* that might be necessary for its interaction with dexamethasone, we established a GST pull down assay to capture the partners. The results of the pilot experiment demonstrated that we are able to express soluble Plzf-GST fusion proteins (both fragments and full-length), and the fusion proteins are captured by the glutathione resin; however, the data is insufficient to make any conclusion about Plzf interaction partners as yet.

13. Conclusion

Plzf is a promising candidate gene in all facets of metabolic syndrome and in line with previous data we brought another evidence of its importance in development of metabolic syndrome.

The comparative transriptomic analysis in left ventricle myocardium in SHR and its minimal congenic strain PD5 harboring intronic *Plzf* deletion identified promising candidate gene Nr4a1, which we speculate has a protective role in the pathophysiology of cardiac hypertrophy and fibrosis and we managed to confirm the upregulation of this gene on proteomic level.

Next we performed two comparative transcriptomic analysis in two established rodent models of metabolic syndrome PD and PD5 after high fat diet admission and dexamethasone challenge respectively. We confirmed a higher sensitivity to glucocorticoid induced metabolic syndrome in PD5 strain and aggravation of metabolic syndrome features in PD strain after high fat diet admission. The transcriptomic data verified the polygenic etiology of metabolic syndrome and highlighted several dysregulated pathways. In order to fully elucidate the functional role of the *Plzf* intronic deletion we conducted luciferase assay experiments which identified a region with strong enhancer/promoter activity within a region in a close 5´vicinity of the deletion. The results also indicate an indirect glucocorticoid effect on the intronic deletion. For further proteomic studies we established Plzf-GST protein for further proteomic studies.

14. Publications

Publications, which form the basis for the PhD thesis:

Publication 1:

Mirchi LF, Chylíková B, Janků M, Šeda O, Liška F. Transcriptomic analysis of left ventricle myocardium in an SHR congenic line with ameliorated cardiac fibrosis. Physiol Res. 2019 Oct 25;68(5):747-755. doi: 10.33549/physiolres.934127. Epub 2019 Aug 19. PMID: 31424260.

Impact factor (2019). 1.736

Publication 2:

Junková K, **Mirchi LF**, Chylíková B, Janků M, Šilhavý J, Hüttl M, Marková I, Miklánková D, Včelák J, Malínská H, Pravenec M, Šeda O, Liška F. Hepatic Transcriptome Profiling Reveals Lack of *Acsm3* Expression in Polydactylous Rats with High-Fat Diet-Induced Hypertriglyceridemia and Visceral Fat Accumulation. Nutrients. 2021 Apr 25;13(5):1462. doi: 10.3390/nu13051462. PMID: 33923085; PMCID: PMC8147112.
Format:

Impact factor (2021): 6,706

Manuscript in preparation:

Mirchi LF, Procyková K., Chylíková B, Janků M, Vacík T., Talacko P., Šeda O., Šedová L. Pravenec M., Liška F. Plzf expression and transcriptomic footprint of dexamethasone-induced metabolic syndrome in SHR minimal congenic subline with enhanced glucose tolerance, ameliorated dyslipidemia and visceral adiposity.

15. References

AM AHMED, Basma; SEDA, Ondrej; L LAVOIE, Julie. (Pro) renin receptor as a new drug target. *Current pharmaceutical design*, 2011, 17.33: 3611-3621.

ABOU ZIKI, Maen D.; MANI, Arya. Metabolic syndrome: genetic insights into disease pathogenesis. *Current opinion in lipidology*, 2016, 27.2: 162-171.

AINSLIE, Deborah A., et al. Short-term, high-fat diets lower circulating leptin concentrations in rats. *The American journal of clinical nutrition*, 2000, 71.2: 438-442.

AITMAN, Timothy J., et al. Identification of Cd36 (Fat) as an insulin-resistance gene causing defective fatty acid and glucose metabolism in hypertensive rats. Nature genetics, 1999, 21.1: 76-83.

AKINYEMIJU, Tomi, et al. Epigenome-wide association study of metabolic syndrome in African-American adults. *Clinical epigenetics*, 2018, 10.1: 1-8.

ALBERT, R. G. M. M.; ZIMMET, P. Z. Definition, diagnosis and classification of diabetes mellitus and its complications. Part 1, Provisional report of WHO consultation. *Diabetes Med*, 1998, 15: 539-53.

ALBERTI, K. GMMF. International diabetes federation task force on epidemiology and prevention; hational heart, lung, and blood institute; American heart association; world heart federation; international atherosclerosis society; international association for the study of obesity: harmonizing the metabolic syndrome: a joint interim statement of the international diabetes federation task force on epidemiology and prevention; national heart, lung, and blood institute; American heart association; world heart federation ... *Circulation*, 2009, 120: 1640-1645.

ALONZO, Eric S.; SANT'ANGELO, Derek B. Development of PLZF-expressing innate T cells. *Current opinion in immunology*, 2011, 23.2: 220-227.

ALTSHULER, David; DALY, Mark J.; LANDER, Eric S. Epistatic interactions attenuate mutations affecting startle behaviour in Drosophila melanogaster. *Science*, 2008, 322: 881-888.

ANDERSON, J. L., et al. Intermountain Heart Collaborative (IHC) Study. Which features of the metabolic syndrome predict the prevalence and clinical outcomes of angiographic coronary artery disease. *Cardiology*, 2004, 101.4: 185-93.

ANDRONICO, G., et al. In vivo relationship between insulin and endothelin role of insulin-resistance. *Journal of human hypertension*, 1997, 11.1: 63-66.

ARMAND, Ethan J., et al. Single-cell sequencing of brain cell transcriptomes and epigenomes. *Neuron*, 2021, 109.1: 11-26.

ARONIS, Konstantinos N.; MANTZOROS, Christos S. A brief history of insulin resistance: from the first insulin radioimmunoassay to selectively targeting protein kinase C pathways. *Metabolism-Clinical and Experimental*, 2012, 61.4: 445-449.

ARRESE, Marco, et al. Innate immunity and inflammation in NAFLD/NASH. *Digestive diseases and sciences*, 2016, 61: 1294-1303.

ASHBURNER, Michael, et al. Gene ontology: tool for the unification of biology. *Nature genetics*, 2000, 25.1: 25-29.

AZZOUT-MARNICHE, Dalila, et al. Insulin effects on sterol regulatory-element-binding protein-1c (SREBP-1c) transcriptional activity in rat hepatocytes. *Biochemical Journal*, 2000, 350.2: 389-393

BALKAU, Beverley. Comment on the provisional report from the WHO consultation. European Group for the Study of Insulin Resistance (EGIR). *Diabet med*, 1999, 16: 442-443

BAUSCHARD, Michael J. *Conditional Knockdown of the Insulin Receptor in Ovarian Granulosa and Theca Cells and Female Fertility*. 2012. PhD Thesis. University of Illinois at Chicago.

BEAUFRÈRE, Hugues; GARDHOUSE, Sara; AMMERSBACH, Mélanie. Lipoprotein characterization in Quaker parrots (Myiopsitta monachus) using gel-permeation high-performance liquid chromatography. *Veterinary Clinical Pathology*, 2020, 49.3: 417-427.

BELLIA, Alfonso, et al. "The Linosa Study": epidemiological and heritability data of the metabolic syndrome in a Caucasian genetic isolate. *Nutrition, Metabolism and Cardiovascular Diseases*, 2009, 19.7: 455-461.

BEŁTOWSKI, Jerzy. Adiponectin and resistin--new hormones of white adipose tissue. *Med Sci Monit2003*, 2003, 9: 61.

BENJAFIELD, Adam V., et al. Overweight, but not hypertension, is associated with SAH polymorphisms in Caucasians with essential hypertension. *Hypertension Research*, 2003, 26.8: 591-595.

BERG, A. H.; SCHERER, P. E. The Online version of this article, along with updated information and services, is located on the World Wide Web. *Journal of the American Heart Association*, 2005, 96: 939-949.

BHATTI, Jasvinder Singh; BHATTI, Gurjit Kaur; REDDY, P. Hemachandra. Mitochondrial dysfunction and oxidative stress in metabolic disorders—A step towards mitochondria based therapeutic strategies. *Biochimica et Biophysica Acta (BBA)-Molecular Basis of Disease*, 2017, 1863.5: 1066-1077.

BILLINGHAM, R. E.; SILVERS, WILLYS K. Inbred animals and tissue transplantation immunity. *Plastic and Reconstructive Surgery*, 1959, 23.4: 399-406.

BLATON, Victor. How is the metabolic syndrome related to the dyslipidemia?. *Ejifcc*, 2007, 18.1: 15.

BLAZQUEZ, E. Velã¡ zquez, E.; Hurtado-Carneiro, V.; Ruiz-Albusac, JM Insulin in the Brain: Its Pathophysiological Implications for States Related with Central Insulin Resistance, Type 2 Diabetes and Alzheimer'sDisease. *Front. Endocrinol*, 2014, 5: 161.

BODEN, Guenther. Obesity and free fatty acids. *Endocrinology and metabolism clinics of North America*, 2008, 37.3: 635-646.

BONACONSA, Marta, et al. Differential modulation of clock gene expression in the suprachiasmatic nucleus, liver and heart of aged mice. *Experimental gerontology*, 2014, 55: 70-79.

BOYLE, Evan A.; LI, Yang I.; PRITCHARD, Jonathan K. An expanded view of complex traits: from polygenic to omnigenic. *Cell*, 2017, 169.7: 1177-1186.

BROWN, Audrey E.; WALKER, Mark. Genetics of insulin resistance and the metabolic syndrome. *Current cardiology reports*, 2016, 18: 1-8.

BURKART, Alison M., et al. Insulin resistance in human iPS cells reduces mitochondrial size and function. *Scientific reports*, 2016, 6.1: 1-12.

CABALLERO, Ricardo, et al. In humans, chronic atrial fibrillation decreases the transient outward current and ultrarapid component of the delayed rectifier current differentially on each atria and increases the slow component of the delayed rectifier current in both. *Journal of the American College of Cardiology*, 2010, 55.21: 2346-2354.

CARMELLI, Dorit; CARDON, Lon R.; FABSITZ, Richard. Clustering of hypertension, diabetes, and obesity in adult male twins: same genes or same environments?. *American journal of human genetics*, 1994, 55.3: 566.

CENTRAL, G. O., et al. The Gene Ontology knowledgebase in 2023. *Genetics*, 2023, 224.1.

CLARKE, Geraldine M., et al. Basic statistical analysis in genetic case-control studies. *Nature protocols*, 2011, 6.2: 121-133.

COHEN, B. novick D, Rubinstein M. Modulation of insulin activities by leptin. *Science*, 1996, 274: 1185-1188.

CONSIDINE, Robert V., et al. Serum immunoreactive-leptin concentrations in normal-weight and obese humans. *New England Journal of Medicine*, 1996, 334.5: 292-295.

COX, Jürgen, et al. Accurate proteome-wide label-free quantification by delayed normalization and maximal peptide ratio extraction, termed MaxLFQ. *Molecular & cellular proteomics*, 2014, 13.9: 2513-2526.

COX, Jurgen, et al. Andromeda: a peptide search engine integrated into the MaxQuant environment. *Journal of proteome research*, 2011, 10.4: 1794-1805.

COX, Roger D.; BROWN, Steve DM. Rodent models of genetic disease. *Current opinion in genetics & development*, 2003, 13.3: 278-283.

CROSBY, C. M.; KRONENBERG, M. Tissue specific functions of invariant NKT cells. *Physiol Behav*, 2018, 176.1: 139-148.

CUI, Mingli, et al. Orphan nuclear receptor Nur77 inhibits angiotensin II–induced vascular remodeling via downregulation of β-catenin. *Hypertension*, 2016, 67.1: 153-162.

DAKUP, Panshak P., et al. The circadian clock protects against ionizing radiation-induced cardiotoxicity. The FASEB Journal, 2020, 34.2: 3347-3358.

DAS, Mithun, et al. Association of DNA methylation at CPT1A locus with metabolic syndrome in the genetics of lipid lowering drugs and diet network (GOLDN) study. *PloS one*, 2016, 11.1: e0145789.

DAVID, Gregory, et al. Histone deacetylase associated with mSin3A mediates repression by the acute promyelocytic leukemia-associated PLZF protein. *Oncogene*, 1998, 16.19: 2549-2556.

DE MAGALHÃES, João Pedro; WANG, Jingwei. The fog of genetics: what is known, unknown and unknowable in the genetics of complex traits and diseases. *EMBO reports*, 2019, 20.11: e48054.

DEBOER, Mark D.; FILIPP, Stephanie L.; GURKA, Matthew J. Use of a metabolic syndrome severity Z score to track risk during treatment of prediabetes: an analysis of the diabetes prevention program. *Diabetes Care*, 2018, 41.11: 2421-2430.

DE LA MONTE, Suzanne M. Insulin resistance and neurodegeneration: progress towards the development of new therapeutics for Alzheimer's disease. *Drugs*, 2017, 77: 47-65.

DEN BESTEN, Gijs, et al. Gut-derived short-chain fatty acids are vividly assimilated into host carbohydrates and lipids. *American Journal of Physiology-Gastrointestinal and Liver Physiology*, 2013, 305.12: G900-G910.

DEN BESTEN, Gijs, et al. The role of short-chain fatty acids in the interplay between diet, gut microbiota, and host energy metabolism. *J. Lipid Res*, 2013, 54: 2325-2340.

DENNIS, Glynn, et al. DAVID: database for annotation, visualization, and integrated discovery. Genome biology, 2003, 4.9: 1-11.

DIAZ, Mauricio Berriel; LEMKE, Ulrike; HERZIG, Stephan. Discovering orphans' sweet secret: NR4A receptors and hepatic glucose production. Cell Metabolism, 2006, 4.5: 339-340.

EDGAR, Ron; DOMRACHEV, Michael; LASH, Alex E. Gene Expression Omnibus: NCBI gene expression and hybridization array data repository. Nucleic acids research, 2002, 30.1: 207-210.

ELLIS, Jessica M.; BOWMAN, Caitlyn E.; WOLFGANG, Michael J. Metabolic and tissue-specific regulation of acyl-CoA metabolism. *PloS one*, 2015, 10.3: e0116587.

FAGARD, Robert H., et al. Regression of left ventricular mass by antihypertensive treatment: a meta-analysis of randomized comparative studies. *Hypertension*, 2009, 54.5: 1084-1091.

FAHED, Gracia, et al. Metabolic syndrome: Updates on pathophysiology and management in 2021. *International Journal of Molecular Sciences*, 2022, 23.2: 786.

FANG, Jinchuan; ZHANG, Hai; JIN, Sufang. Epigenetics and cervical cancer: from pathogenesis to therapy. *Tumor Biology*, 2014, 35.6: 5083-5093.

FARRELL, Geoffrey C.; HACZEYNI, Fahrettin; CHITTURI, Shivakumar. Pathogenesis of NASH: how metabolic complications of overnutrition favour lipotoxicity and pro-inflammatory fatty liver disease. *Obesity, Fatty Liver and Liver Cancer*, 2018, 19-44.

FONSECA, Vivian. Effect of thiazolidinediones on body weight in patients with diabetes mellitus. *The American journal of medicine*, 2003, 115.8: 42-48.

FORNO, Erick, et al. Insulin resistance, metabolic syndrome, and lung function in US adolescents with and without asthma. *Journal of Allergy and Clinical Immunology*, 2015, 136.2: 304-311. E8.

FU, Sicheng, et al. Impaired lipid biosynthesis hinders anti-tumor efficacy of intratumoral iNKT cells. *Nature communications*, 2020, 11.1: 438.

FUCHS, Taíse, et al. Modelos animais na síndrome metabólica. *Revista do Colégio Brasileiro de Cirurgiões*, 2018, 45.

FUJINO, Takahiro, et al. Molecular identification and characterization of two medium-chain acyl-CoA synthetases, MACS1 and the Sa gene product. *Journal of Biological Chemistry*, 2001, 276.38: 35961-35966.

FUNKE-KAISER, Heiko, et al. Adapter proteins and promoter regulation of the angiotensin AT2 receptor—implications for cardiac pathophysiology. *Journal of the Renin-Angiotensin-Aldosterone System*, 2010, 11.1: 7-17.

Galaxy. [(accessed on 8 February 2021)]; Available online: https://usegalaxy.org

GANDA, Om P. Lipoatrophy, lipodystrophy, and insulin resistance. *Annals of Internal Medicine*, 2000, 133.4: 304-306.

GARRISON, Erik; MARTH, Gabor. Haplotype-based variant detection from short-read sequencing. *arXiv preprint arXiv:1207.3907*, 2012.

GAVRILOVA, Oksana, et al. Surgical implantation of adipose tissue reverses diabetes in lipoatrophic mice. *The Journal of clinical investigation*, 2000, 105.3: 271-278.

GENG, Na, et al. Nuclear receptor Nur77 protects against oxidative stress by maintaining mitochondrial homeostasis via regulating mitochondrial fission and mitophagy in smooth muscle cell. *Journal of Molecular and Cellular Cardiology*, 2022, 170: 22-33.

GONZÁLEZ DE LA FUENTE, Marta, et al. Chronic atrial fibrillation up-regulates β1-adrenoceptors affecting repolarizing currents and action potential duration. *Cardiovascular research*, 2013, 97.2: 379-388.

GOOSSENS, Gijs H. The metabolic phenotype in obesity: fat mass, body fat distribution, and adipose tissue function. *Obesity facts*, 2017, 10.3: 207-215.

GOOSSENS, Gijs H. The role of adipose tissue dysfunction in the pathogenesis of obesity-related insulin resistance. *Physiology & behavior*, 2008, 94.2: 206-218.

GOPAL, Ramani, et al. Integrative transcriptome analysis of liver cancer profiles identifies upstream regulators and clinical significance of ACSM3 gene expression. *Cellular oncology*, 2017, 40: 219-233.

GORTER, P. M.; OLIJHOEK, J. K.; GRAAF, Y. van der, Algra A, Rabelink TJ, Visseren FL: Prevalence of the metabolic syndrome in patients with coronary heart disease, cerebrovascular disease, peripheral arterial disease or abdominal aortic aneurysm. *Atherosclerosis*, 2004, 173: 363-369.

GRIGNANI, Francesco, et al. Fusion proteins of the retinoic acid receptor-α recruit histone deacetylase in promyelocytic leukaemia. *Nature*, 1998, 391.6669: 815-818.

GUÉNARD, Frédéric, et al. Genome-wide association study of dietary pattern scores. *Nutrients*, 2017, 9.7: 649.

GUIDEZ, F., et al. de Thé, H., Solomon, E., and Grimwade, D.(2007). RARalpha-PLZF overcomes PLZF-mediated repression of CRABPI, contributing to retinoid resistance in t (11; 17) acute promyelocytic leukemia. *Proc. Natl. Acad. Sci. USA*, 104: 18694-18699.

GUIDEZ, Fabien, et al. Histone acetyltransferase activity of p300 is required for transcriptional repression by the promyelocytic leukemia zinc finger protein. *Molecular and Cellular Biology*, 2005, 25.13: 5552-5566.

GUMZ, Michelle L., et al. Early transcriptional effects of aldosterone in a mouse inner medullary collecting duct cell line. *American Journal of Physiology-Renal Physiology*, 2003, 285.4: F664-F673.

GUMZ, Michelle L., et al. The circadian clock protein Period 1 regulates expression of the renal epithelial sodium channel in mice. *The Journal of clinical investigation*, 2009, 119.8: 2423-2434.

GUO, Christine, et al. Mineralocorticoid receptor blockade reverses obesity-related changes in expression of adiponectin, peroxisome proliferator-activated receptor-γ, and proinflammatory adipokines. *Circulation*, 2008, 117.17: 2253-2261.

HAIG, D. Coadaptation and conflict, misconception and muddle, in the evolution of genomic imprinting. *Heredity*, 2014, 113.2: 96-103.

HALL, John E., et al. Obesity-induced hypertension: interaction of neurohumoral and renal mechanisms. *Circulation research*, 2015, 116.6: 991-1006.

HALLER, H. Epidermiology and associated risk factors of hyperlipoproteinemia. *Zeitschrift fur die gesamte innere Medizin und ihre Grenzgebiete*, 1977, 32.8: 124-128.

HAMERS, Anouk AJ, et al. Bone marrow–specific deficiency of nuclear receptor Nur77 enhances atherosclerosis. *Circulation research*, 2012, 110.3: 428-438.

HARA, Ichiro; OKAZAKI, Mitsuyo. High-performance liquid chromatography of serum lipoproteins. In: *Methods in enzymology*. Academic Press, 1986. p. 57-78.

HASIN, Yehudit; SELDIN, Marcus; LUSIS, Aldons. Multi-omics approaches to disease. *Genome biology*, 2017, 18.1: 1-15.

HEGELE, Robert A. Plasma lipoproteins: genetic influences and clinical implications. *Nature Reviews Genetics*, 2009, 10.2: 109-121.

HENRIKSEN, Erik J.; PRASANNARONG, Mujalin. The role of the renin-angiotensin system in the development of insulin resistance in skeletal muscle. *Molecular and cellular endocrinology*, 2013, 378.1-2: 15-22.

HEBERT, Alexander S., et al. The one hour yeast proteome. *Molecular & Cellular Proteomics*, 2014, 13.1: 339-347.

HERNÁNDEZ-DE-DIEGO, Rafael, et al. PaintOmics 3: a web resource for the pathway analysis and visualization of multi-omics data. *Nucleic acids research*, 2018, 46.W1: W503-W509.

HOLLIDAY, Robin. Epigenetics: a historical overview. *Epigenetics*, 2006, 1.2: 76-80.

HOTAMISLIGIL, Gokhan S., et al. Increased adipose tissue expression of tumor necrosis factor-alpha in human obesity and insulin resistance. *The Journal of clinical investigation*, 1995, 95.5: 2409-2415.

HOTTA, Kikuko, et al. Plasma concentrations of a novel, adipose-specific protein, adiponectin, in type 2 diabetic patients. *Arteriosclerosis, thrombosis, and vascular biology*, 2000, 20.6: 1595-1599.

HU, Huiling, et al. Mouse promyelocytic leukemia zinc finger protein (PLZF) regulates hepatic lipid and glucose homeostasis dependent on SIRT1. *Frontiers in Pharmacology*, 2022, 4720.

HU, Yan-Wei, et al. Nur77 decreases atherosclerosis progression in apoE−/− mice fed a high-fat/high-cholesterol diet. *PloS one*, 2014, 9.1: e87313.

HUANG, P. L. A comprehensive definition for metabolic syndrome. Dis Model Mech. 2009; 2: 231–7.

HUANG, Da Wei, et al. DAVID Bioinformatics Resources: expanded annotation database and novel algorithms to better extract biology from large gene lists. *Nucleic acids research*, 2007, 35.suppl_2: W169-W175.

HUBNER, N. Wallace CA, Zimdahl H, Petretto E, Schulz H, Maciver F, Mueller M, Hummel O, Monti J, Zidek V, Musilova A, Kren V, Causton H, Game L, Born G, Schmidt S, Muller A, Cook SA, Kurtz TW, Whittaker J, Pravenec M, Aitman TJ. *Integrated transcriptional profiling and linkage analysis for identification of genes underlying disease. Nat Genet*, 2005, 37: 243-253.

HUGHES, Christopher S., et al. Single-pot, solid-phase-enhanced sample preparation for proteomics experiments. *Nature protocols*, 2019, 14.1: 68-85.

HUGHES, Christopher S., et al. Ultrasensitive proteome analysis using paramagnetic bead technology. *Molecular systems biology*, 2014, 10.10: 757.

HÜTTL, Martina, et al. Adverse effects of methylglyoxal on transcriptome and metabolic changes in visceral adipose tissue in a prediabetic rat model. *Antioxidants*, 2020, 9.9: 803.

CHAO, Lily C., et al. Inhibition of adipocyte differentiation by Nur77, Nurr1, and Nor1. *Molecular endocrinology*, 2008, 22.12: 2596-2608.

CHEN, Jiahui, et al. Nur77 deficiency exacerbates cardiac fibrosis after myocardial infarction by promoting endothelial-to-mesenchymal transition. *Journal of Cellular Physiology*, 2021, 236.1: 495-506.

CHEN, Siyu, et al. Control of hepatic gluconeogenesis by the promyelocytic leukemia zinc finger protein. *Molecular endocrinology*, 2014, 28.12: 1987-1998.

CHEN, Zhu, et al. Fusion between a novel Krüppel-like zinc finger gene and the retinoic acid receptor-alpha locus due to a variant t (11; 17) translocation associated with acute promyelocytic leukaemia. *The EMBO journal*, 1993, 12.3: 1161-1167.

CHEN, Jiahui, et al. Nur77 deficiency exacerbates cardiac fibrosis after myocardial infarction by promoting endothelial-to-mesenchymal transition. *Journal of Cellular Physiology*, 2021, 236.1: 495-506.

CHENG, Zhaokang, et al. Mitochondrial translocation of Nur77 mediates cardiomyocyte apoptosis. *European heart journal*, 2011, 32.17: 2179-2188.

CHOW, Wing-Sun, et al. Hypoadiponectinemia as a predictor for the development of hypertension: a 5-year prospective study. *Hypertension*, 2007, 49.6: 1455-1461.

CHRISTOPHERSEN, Ingrid E., et al. Genetic variation in KCNA5: impact on the atrial-specific potassium current I Kur in patients with lone atrial fibrillation. *European heart journal*, 2013, 34.20: 1517-1525.

CHUSYD, Daniella E., et al. Relationships between rodent white adipose fat pads and human white adipose fat depots. *Frontiers in nutrition*, 2016, 3: 10.

IKRAMUDDIN, S.; BUCHWALD, H. How bariatric and metabolic operations control metabolic syndrome. *Journal of British Surgery*, 2011, 98.10: 1339-1341.

IWAI, Naoharu; INAGAMI, Tadashi. Isolation of preferentially expressed genes in the kidneys of hypertensive rats. *Hypertension*, 1991, 17.2: 161-169.

IWAI, Naoharu, et al. An acyl-CoA synthetase gene family in chromosome 16p12 may contribute to multiple risk factors. *Hypertension*, 2003, 41.5: 1041-1046.

IWAI, Naoharu, et al. Association between SAH, an acyl-CoA synthetase gene, and hypertriglyceridemia, obesity, and hypertension. *Circulation*, 2002, 105.1: 41-47.

JANSEN, Joop H.; LÖWENBERG, Bob. Acute promyelocytic leukemia with a PLZF-RARα fusion protein. In: *Seminars in hematology*. WB Saunders, 2001. p. 37-41.

JI, Jing-jing, et al. Kallistatin/Serpina3c inhibits cardiac fibrosis after myocardial infarction by regulating glycolysis via Nr4a1 activation. *Biochimica et Biophysica Acta (BBA)-Molecular Basis of Disease*, 2022, 1868.9: 166441.

JIN, Yang; NENSETH, Hatice Zeynep; SAATCIOGLU, Fahri. Role of PLZF as a tumor suppressor in prostate cancer. *Oncotarget*, 2017, 8.41: 71317.

JOSLIN, Elliott P. Practical lessons for physicians and patients in diabetes. *Med. Clin. N. Am*, 1921, 22.

KAHN, C. Ronald, et al. Altered adipose tissue and adipocyte function in the pathogenesis of metabolic syndrome. *The Journal of clinical investigation*, 2019, 129.10: 3990-4000.

KANG IM, Soo, et al. Modification of promyelocytic leukemia zinc finger protein (PLZF) by SUMO-1 conjugation regulates its transcriptional repressor activity. *Journal of Biological Chemistry*, 2003, 278.51: 51479-51483.

KATSIMARDOU, Alexandra, et al. Hypertension in metabolic syndrome: novel insights. *Current Hypertension Reviews*, 2020, 16.1: 12-18.

KLEIN, Samuel, et al. Absence of an effect of liposuction on insulin action and risk factors for coronary heart disease. *New England Journal of Medicine*, 2004, 350.25: 2549-2557.

KLIBI, Jihene, et al. PLZF acetylation levels regulate NKT cell differentiation. *The Journal of Immunology*, 2021, 207.3: 809-823.

KOLOVOU, G. D.; ANAGNOSTOPOULOU, K. K.; COKKINOS, D. V. Pathophysiology of dyslipidaemia in the metabolic syndrome. *Postgraduate medical journal*, 2005, 81.956: 358-366.

KOVALOVSKY, Damian, et al. The BTB–zinc finger transcriptional regulator PLZF controls the development of invariant natural killer T cell effector functions. *Nature immunology*, 2008, 9.9: 1055-1064.

KRASSOWSKI, Michal, et al. State of the field in multi-omics research: from computational needs to data mining and sharing. *Frontiers in Genetics*, 2020, 11: 610798.

KREN, Vladimir, et al. Genetic isolation of a region of chromosome 8 that exerts major effects on blood pressure and cardiac mass in the spontaneously hypertensive rat. *The Journal of clinical investigation*, 1997, 99.4: 577-581.

KRUEGER, Felix, et al. DNA methylome analysis using short bisulfite sequencing data. *Nature methods*, 2012, 9.2: 145-151.

KRUPKOVÁ, Michaela, et al. Pharmacogenomic analysis of retinoic-acid induced dyslipidemia in congenic rat model. *Lipids in Health and Disease*, 2014, 13.1: 1-9.

KRUPKOVÁ, Michaela, et al. Single-gene congenic strain reveals the effect of Zbtb16 on Dexamethasone-induced insulin resistance. *Frontiers in Endocrinology*, 2018, 9: 185.

KYLIN, Eskil. Studien uber das Hypertoni-Hyperglyce mi-Hyperurikemi syndrom. *Zentralblatt fur innere Medizin*, 1923, 44: 105-112.

LAGRANGE, Dominique; FOURNIÉ, Gilbert J. Generation of congenic and consomic rat strains. *Rat Genomics: Methods and Protocols*, 2010, 243-266.

LEIGH, Richard, et al. An inhaled dose of budesonide induces genes involved in transcription and signaling in the human airways: enhancement of anti-and proinflammatory effector genes. *Pharmacology Research & Perspectives*, 2016, 4.4: e00243.

LEWIS, G. F. Uffelman KD, Szeto LW, Weller B, Steiner G. *Interaction between free fatty acids and insulin in the acute control of very low density lipoprotein production in humans. J Clin Invest*, 1995, 95: 158-166.

LI, Jia-Yuan, et al. Sequence-specific DNA binding and transcriptional regulation by the promyelocytic leukemia zinc finger protein. *Journal of Biological Chemistry*, 1997, 272.36: 22447-22455.

LI, Xinmin, et al. Structure-function studies of the BTB/POZ transcriptional repression domain from the promyelocytic leukemia zinc finger oncoprotein. *Cancer research*, 1999, 59.20: 5275-5282.

LIN, H.-F., et al. Heritabilities of the metabolic syndrome and its components in the Northern Manhattan Family Study. *Diabetologia*, 2005, 48: 2006-2012.

LING, Charlotte; RÖNN, Tina. Epigenetics in human obesity and type 2 diabetes. *Cell metabolism*, 2019, 29.5: 1028-1044.

LIŠKA, František, et al. Deletion of a conserved noncoding sequence in Plzf intron leads to Plzf down-regulation in limb bud and polydactyly in the rat. *Developmental Dynamics: An Official Publication of the American Association of Anatomists*, 2009, 238.3: 673-684.

LIŠKA, František, et al. Downregulation of Plzf gene ameliorates metabolic and cardiac traits in the spontaneously hypertensive rat. *Hypertension*, 2017, 69.6: 1084-1091.

LIŠKA, František, et al. Plzf as a candidate gene predisposing the spontaneously hypertensive rat to hypertension, left ventricular hypertrophy, and interstitial fibrosis. *American journal of hypertension*, 2014, 27.1: 99-106.

LIU, Tong Ming, et al. Concise review: balancing stem cell self-renewal and differentiation with PLZF. *Stem Cells*, 2016, 34.2: 277-287.

LIVAK, Kenneth J.; SCHMITTGEN, Thomas D. Analysis of relative gene expression data using real-time quantitative PCR and the 2− ΔΔCT method. *methods*, 2001, 25.4: 402-408.

LORD, Graham M., et al. Leptin modulates the T-cell immune response and reverses starvation-induced immunosuppression. *Nature*, 1998, 394.6696: 897-901.

LOWELL, Bradford B.; SHULMAN, Gerald I. Mitochondrial dysfunction and type 2 diabetes. *Science*, 2005, 307.5708: 384-387

LUI, Wing-Yiu, et al. Analysis of glucocorticoid receptors in human hepatocellular carcinoma and HepG2 cells. *Hepatology*, 1993, 18.5: 1167-1174.

MANCIA, Giuseppe, et al. The sympathetic nervous system and the metabolic syndrome. *Journal of hypertension*, 2007, 25.5: 909-920.

MARINKOVIĆ, Goran, et al. S100A9 links inflammation and repair in myocardial infarction. *Circulation research*, 2020, 127.5: 664-676.

MARUŠIĆ, Marinko, et al. NAFLD, insulin resistance, and diabetes mellitus type 2. *Canadian Journal of Gastroenterology and Hepatology*, 2021, 2021.

MASSCHELIN, Peter M., et al. The impact of oxidative stress on adipose tissue energy balance. *Frontiers in physiology*, 2020, 10: 1638.

MAXWELL, Megan A.; MUSCAT, George EO. The NR4A subgroup: immediate early response genes with pleiotropic physiological roles. *Nuclear receptor signaling*, 2006, 4.1: nrs. 04002.

MEDZIKOVIC, Lejla, et al. Nur77 protects against adverse cardiac remodelling by limiting neuropeptide Y signalling in the sympathoadrenal-cardiac axis. *Cardiovascular research*, 2018, 114.12: 1617-1628.

MEDZIKOVIC, Lejla, et al. Orphan nuclear receptor Nur77 affects cardiomyocyte calcium homeostasis and adverse cardiac remodelling. *Scientific reports*, 2015, 5.1: 1-15.

MEDZIKOVIC, Lejla, et al. Nuclear receptor nur77 controls cardiac fibrosis through distinct actions on fibroblasts and cardiomyocytes. *International Journal of Molecular Sciences*, 2021, 22.4: 1600.

MELNICK, Ari, et al. Critical residues within the BTB domain of PLZF and Bcl-6 modulate interaction with corepressors. *Molecular and cellular biology*, 2002, 22.6: 1804-1818.

MIKKELSEN, Tarjei S., et al. Comparative epigenomic analysis of murine and human adipogenesis. *Cell*, 2010, 143.1: 156-169.

MOHN, Fabio; SCHÜBELER, Dirk. Genetics and epigenetics: stability and plasticity during cellular differentiation. *Trends in Genetics*, 2009, 25.3: 129-136.

NÁRAY-FEJES-TÓTH, Anikó; BOYD, Cary; FEJES-TÓTH, Géza. Regulation of epithelial sodium transport by promyelocytic leukemia zinc finger protein. *American Journal of Physiology-Renal Physiology*, 2008, 295.1: F18-F26.

NAKATO, Ryuichiro; SAKATA, Toyonori. Methods for ChIP-seq analysis: a practical workflow and advanced applications. Methods, 2021, 187: 44-53.

NATIONAL CHOLESTEROL EDUCATION PROGRAM (US). EXPERT PANEL ON DETECTION; EVALUATION; TREATMENT OF HIGH BLOOD CHOLESTEROL IN ADULTS. *Third report of the National Cholesterol Education Program (NCEP) Expert Panel on detection, evaluation, and treatment of high blood cholesterol in adults (Adult Treatment Panel III)*. International Medical Pub, 2002

NGUYEN, Nam D.; WANG, Daifeng. Multiview learning for understanding functional multiomics. *PLoS computational biology*, 2020, 16.4: e1007677.

NICKENIG, G.; WOLF, M.; BÖHM, M. Enhanced expression and autoimmunity of Recombinant Binding Protein-jk in human dilated cardiomyopathy. In: *Circulation*. 227 EAST WASHINGTON SQ, PHILADELPHIA, PA 19106 USA: LIPPINCOTT WILLIAMS & WILKINS, 1998. p. 406-406.

NOGUEIRA, Edson F., et al. Role of angiotensin II-induced rapid response genes in the regulation of enzymes needed for aldosterone synthesis. *Journal of molecular endocrinology*, 2009, 42.4: 319.

NUOTIO, Marja-Liisa, et al. An epigenome-wide association study of metabolic syndrome and its components. *Scientific Reports*, 2020, 10.1: 1-12.

O'HAGAN, Kyle L., et al. Pak2 controls acquisition of NKT cell fate by regulating expression of the transcription factors PLZF and Egr2. *The Journal of Immunology*, 2015, 195.11: 5272-5284.

OHASHI, Koji; OUCHI, Noriyuki; MATSUZAWA, Yuji. Adiponectin and hypertension. *American journal of hypertension*, 2011, 24.3: 263-269.

OKAMOTO, Kozo; AOKI, Kyuzo. Development of a strain of spontaneously hypertensive rats. *Japanese circulation journal*, 1963, 27.3: 282-293.

OKAZAKI, Mitsuyo; YAMASHITA, Shizuya. Recent advances in analytical methods on lipoprotein subclasses: calculation of particle numbers from lipid levels by gel permeation HPLC using "spherical particle model". *Journal of oleo science*, 2016, 65.4: 265-282.

OTT, Jurg; WANG, Jing; LEAL, Suzanne M. Genetic linkage analysis in the age of whole-genome sequencing. *Nature Reviews Genetics*, 2015, 16.5: 275-284.

OUCHI, Noriyuki, et al. Adipocyte-derived plasma protein, adiponectin, suppresses lipid accumulation and class A scavenger receptor expression in human monocyte-derived macrophages. *Circulation*, 2001, 103.8: 1057-1063.

PACKARD, C. J. Triacylglycerol-rich lipoproteins and the generation of small, dense low-density lipoprotein. *Biochemical Society Transactions*, 2003, 31.5: 1066-1069.

PALUMBO-ZERR, Katrin, et al. Orphan nuclear receptor NR4A1 regulates transforming growth factor-β signaling and fibrosis. *Nature medicine*, 2015, 21.2: 150-158.

PARK, Y. W., et al. MR; HEYMSFIELD, SB. The metabolic syndrome: prevalence and associated risk factor findings in the US population from the third national health and nutrition examination survey, 1988-1994. *Arch Intern Med*, 2003, 163: 427-436.

PATEL, Sanjeev B., et al. Leptin: linking obesity, the metabolic syndrome, and cardiovascular disease. *Current hypertension reports*, 2008, 10.2: 131-137.

PEI, Liming, et al. NR4A orphan nuclear receptors are transcriptional regulators of hepatic glucose metabolism. *Nature medicine*, 2006, 12.9: 1048-1055.

PERUSSE, L. Rankinen T, Zuberi A, Chagnon YC, Weisnagel SJ, Argyropoulos G, Walts B, Snyder EE, and Bouchard C. *The human obesity gene map: the*, 2004, 381-490.

Picard. [(accessed on 8 February 2021)]; Available online: http://broadinstitute.github.io/picard

PICASCIA, Antonietta, et al. Epigenetic control of autoimmune diseases: from bench to bedside. *Clinical immunology*, 2015, 157.1: 1-15.

PLAISIER, C. L., et al. Zbtb16 has a role in brown adipocyte bioenergetics. *Nutrition & diabetes*, 2012, 2.9: e46-e46.

POLYZOS, Stergios A.; KOUNTOURAS, Jannis; ZAVOS, Christos. Nonalcoholic fatty liver disease: the pathogenetic roles of insulin resistance and adipocytokines. *Current molecular medicine*, 2009, 9.3: 299-314.

POWELL, Darren J., et al. Ceramide disables 3-phosphoinositide binding to the pleckstrin homology domain of protein kinase B (PKB)/Akt by a PKCζ-dependent mechanism. *Molecular and cellular biology*, 2003, 23.21: 7794-7808.

PRAVENEC, Michal, et al. Genetic variation in renal expression of folate receptor 1 (Folr1) gene predisposes spontaneously hypertensive rats to metabolic syndrome. *Hypertension*, 2016, 67.2: 335-341.

PRAVENEC, M., et al. HXB and BXH sets of recombinant inbred strains: strain distribution patterns of some genetic markers. In: *Transplantation proceedings*. 1990. p. 2557-2558.

PRAVENEC, Michal; KURTZ, Theodore W. Molecular genetics of experimental hypertension and the metabolic syndrome: from gene pathways to new therapies. *Hypertension*, 2007, 49.5: 941-952.

PRAVENEC, Michal; KURTZ, Theodore W. Recent advances in genetics of the spontaneously hypertensive rat. *Current hypertension reports*, 2010, 12: 5-9.

PRAVENEC, M., et al. Mutant Wars2 gene in spontaneously hypertensive rats impairs brown adipose tissue function and predisposes to visceral obesity. *Physiological research*, 2017, 66.6: 917-924.

PUCCI, Giacomo, et al. Sex-and gender-related prevalence, cardiovascular risk and therapeutic approach in metabolic syndrome: A review of the literature. *Pharmacological research*, 2017, 120: 34-42.

QIN, Qing, et al. Orphan nuclear receptor Nur77 is a novel negative regulator of endothelin-1 expression in vascular endothelial cells. *Journal of Molecular and Cellular Cardiology*, 2014, 77: 20-28.

RAPPSILBER, Juri; MANN, Matthias; ISHIHAMA, Yasushi. Protocol for micro-purification, enrichment, pre-fractionation and storage of peptides for proteomics using StageTips. *Nature protocols*, 2007, 2.8: 1896-1906.

REAVEN, Gerald M. Banting lecture 1988. Role of insulin resistance in human disease. *Diabetes*, 1988, 37.12: 1595-1607.

REES, D. A.; ALCOLADO, J. C. Animal models of diabetes mellitus. *Diabetic medicine*, 2005, 22.4: 359-370.

RICHARDS, Jacob, et al. A role for the circadian clock protein Per1 in the regulation of aldosterone levels and renal Na+ retention. *American Journal of Physiology-Renal Physiology*, 2013, 305.12: F1697-F1704.

RILEY, Leanne, et al. The World Health Organization STEPwise approach to noncommunicable disease risk-factor surveillance: methods, challenges, and opportunities. *American journal of public health*, 2016, 106.1: 74-78.

ROHART, Florian, et al. mixOmics: An R package for 'omics feature selection and multiple data integration. *PLoS computational biology*, 2017, 13.11: e1005752.

ROCHLANI, Yogita, et al. Metabolic syndrome: pathophysiology, management, and modulation by natural compounds. *Therapeutic advances in cardiovascular disease*, 2017, 11.8: 215-225.

RUAN, Hao-Yu, et al. Downregulation of ACSM3 promotes metastasis and predicts poor prognosis in hepatocellular carcinoma. *American journal of cancer research*, 2017, 7.3: 543.

RUOTOLO, Giacomo; HOWARD, Barbara V. Dyslipidemia of the metabolic syndrome. *Current cardiology reports*, 2002, 4.6: 494-500.

SADLER, Anthony J., et al. BTB-ZF transcriptional regulator PLZF modifies chromatin to restrain inflammatory signaling programs. *Proceedings of the National Academy of Sciences*, 2015, 112.5: 1535-1540.

SADLER, Anthony J., et al. The acetyltransferase HAT1 moderates the NF-κB response by regulating the transcription factor PLZF. *Nature communications*, 2015, 6.1: 6795.

SACHSE, Anja; WOLF, Gunter. Angiotensin II–induced reactive oxygen species and the kidney. *Journal of the American Society of Nephrology*, 2007, 18.9: 2439-2446.

ŠEDA, O., et al. A 14-gene region of rat chromosome 8 in SHR-derived polydactylous congenic substrain affects muscle-specific insulin resistance, dyslipidaemia and visceral adiposity. FOLIA BIOLOGICA-PRAHA-, 2005, 51.3: 53.

ŠEDA, O., et al. Metabolic characterization of insulin resistance syndrome feature loci in three brown Norway-derived congenic strains. *Folia biologica*, 2002, 48.3: 81-88.

ŠEDA, O. (Charles University, Prague, Czech Republic). Personal communication. 2021.

ŠEDA, O., et al. ZBTB16 and metabolic syndrome: a network perspective. *Physiological Research*, 2017, 66: S357-S365.

ŠEDOVÁ, L., et al. Rat Inbred PD/Cub Strain as a Model of Dyslipidemia and. *Folia Biologica (Praha)*, 2000, 46: 99-106.

SHA, Haibo, et al. The IRE1α-XBP1 pathway of the unfolded protein response is required for adipogenesis. *Cell metabolism*, 2009, 9.6: 556-564.

SHAKIBA, Ehsan; EIZENGA, Georgia C. Unraveling the secrets of rice wild species. *Rice-Germplasm, Genetics and Improvement. InTech, UK*, 2014, 1-58.

SHAMANSUROVA, Zulaykho, et al. Adipose tissue (P) RR regulates insulin sensitivity, fat mass and body weight. *Molecular metabolism*, 2016, 5.10: 959-969.

SHANIK, Michael H., et al. Insulin resistance and hyperinsulinemia: is hyperinsulinemia the cart or the horse?. *Diabetes care*, 2008, 31.Supplement_2: S262-S268.

SHINYA, Minori. Construction of the inbred strain. *Zebrafish: Methods and Protocols*, 2016, 107-118.

SCHNEIDER, Caroline A.; RASBAND, Wayne S.; ELICEIRI, Kevin W. NIH Image to ImageJ: 25 years of image analysis. *Nature methods*, 2012, 9.7: 671-675.

SCHÜTTEN, Monica TJ, et al. The link between adipose tissue renin-angiotensin-aldosterone system signaling and obesity-associated hypertension. *Physiology*, 2017, 32.3: 197-209.

SIDDLE, Kenneth. Molecular basis of signaling specificity of insulin and IGF receptors: neglected corners and recent advances. *Frontiers in endocrinology*, 2012, 3: 34.

SNIJDER, M. B., et al. Independent and opposite associations of waist and hip circumferences with diabetes, hypertension and dyslipidemia: the AusDiab Study. *International journal of obesity*, 2004, 28.3: 402-409.

SOBIESZCZUK, Dorothy F., et al. A feedback loop mediated by degradation of an inhibitor is required to initiate neuronal differentiation. *Genes & development*, 2010, 24.2: 206-218.

SOLER, Amanda, et al. Elevated 20-HETE in metabolic syndrome regulates arterial stiffness and systolic hypertension via MMP12 activation. *Journal of molecular and cellular cardiology*, 2018, 117: 88-99.

SOLOCINSKI, Kristen, et al. Desoxycorticosterone pivalate-salt treatment leads to non-dipping hypertension in Per1 knockout mice. *Acta physiologica*, 2017, 220.1: 72-82.

ST. LEZIN, Elizabeth, et al. Genetic analysis of rat chromosome 1 and the Sa gene in spontaneous hypertension. *Hypertension*, 2000, 35.1: 225-230.

STANČÁKOVÁ, Alena; LAAKSO, Markku. Genetics of metabolic syndrome. *Reviews in Endocrine and Metabolic Disorders*, 2014, 15: 243-252.

STINKENS, Rudi, et al. Targeting fatty acid metabolism to improve glucose metabolism. *Obesity Reviews*, 2015, 16.9: 715-757.

SULIMAN, Bandar Ali; XU, Dakang; WILLIAMS, Bryan Raymond George. The promyelocytic leukemia zinc finger protein: two decades of molecular oncology. *Frontiers in oncology*, 2012, 2: 74.

ŠEDA, O., et al. ZBTB16 and metabolic syndrome: a network perspective. *Physiological Research*, 2017, 66: S357-S365.

TELGMANN, Ralph, et al. SAH gene variants are associated with obesity-related hypertension in Caucasians: the PEGASE Study. *Journal of hypertension*, 2007, 25.3: 557-564.

TOMASELLI, G. F. Beuckelmann DJ, Calkins HG, Berger RD, Kessler PD, Lawrence JH, Kass D, Feldman AM, and Marban E. *Sudden cardiac death in heart failure. The role of abnormal repolarization. Circulation*, 1994, 90: 2534-2539.

TOSHIMA, Gen, et al. LipoSEARCH®; Analytical GP-HPLC method for lipoprotein profiling and its applications. *J Biol Macromol*, 2013, 13.2: 21-32.

TURNBAUGH, Peter J., et al. An obesity-associated gut microbiome with increased capacity for energy harvest. *nature*, 2006, 444.7122: 1027-1031.

TYANOVA, Stefka, et al. The Perseus computational platform for comprehensive analysis of (prote) omics data. *Nature methods*, 2016, 13.9: 731-740.

UFFELMANN, Emil; HUANG, Qin Qin; MUNUNG, Nchangwi Syntia. Jantina de Vries, Yukinori Okada, Alicia R. Martin, Hilary C. Martin, Tuuli Lappalainen, et Danielle Posthuma. 2021.«Genome-Wide Association Studies». *Nature Reviews Methods Primers*, 1.1: 1-21.

UHLÉN, Mathias, et al. A human protein atlas for normal and cancer tissues based on antibody proteomics. *Molecular & cellular proteomics*, 2005, 4.12: 1920-1932.

URNBAUGH, P. J., et al. An obesity-associated gut microbiome with increased capacity for energy harvest [J]. *Nature*, 2006, 444.7122: 1027-1031.

USUI, Shinichi, et al. Assessment of between-instrument variations in a HPLC method for serum lipoproteins and its traceability to reference methods for total cholesterol and HDL-cholesterol. *Clinical chemistry*, 2000, 46.1: 63-72.

VAGUE, Jean. The degree of masculine differentiation of obesities: a factor determining predisposition to diabetes, atherosclerosis, gout, and uric calculous disease. *The American journal of clinical nutrition*, 1956, 4.1: 20-34.

VAN DER SLUIS, Rencia. Analyses of the genetic diversity and protein expression variation of the acyl: CoA medium-chain ligases, ACSM2A and ACSM2B. *Molecular Genetics and Genomics*, 2018, 293.5: 1279-1292.

VAN DER SLUIS, Rencia; ERASMUS, Elardus. Xenobiotic/medium chain fatty acid: CoA ligase–a critical review on its role in fatty acid metabolism and the detoxification of benzoic acid and aspirin. *Expert opinion on drug metabolism & toxicology*, 2016, 12.10: 1169-1179.

VANDAMME, Thierry F. Use of rodents as models of human diseases. *Journal of pharmacy & bioallied sciences*, 2014, 6.1: 2.

VINCENT-FABERT, Christelle, et al. PLZF mutation alters mouse hematopoietic stem cell function and cell cycle progression. *Blood, The Journal of the American Society of Hematology*, 2016, 127.15: 1881-1885.

VUKELIC, Sasa; GRIENDLING, Kathy K. Angiotensin II, from vasoconstrictor to growth factor: a paradigm shift. *Circulation research*, 2014, 114.5: 754-757.

WALSH, Vanessa, et al. Analysis of the role of the SA gene in blood pressure regulation by gene targeting. *Hypertension*, 2003, 41.6: 1212-1218.

WANG, Bo, et al. Similarity network fusion for aggregating data types on a genomic scale. *Nature methods*, 2014, 11.3: 333-337.

WANG, Yun Liang; WANG, Xun. Fault Diagnosis of Wind Turbine's Converter Based on Memristive Neural Network. In: *Applied Mechanics and Materials*. Trans Tech Publications Ltd, 2015. p. 333-337.

WANG, Rong-Hao, et al. The orphan receptor TR3 participates in angiotensin II-induced cardiac hypertrophy by controlling mTOR signalling. *EMBO molecular medicine*, 2013, 5.1: 137-148.

WEISBERG, Stuart P., et al. Obesity is associated with macrophage accumulation in adipose tissue. *The Journal of clinical investigation*, 2003, 112.12: 1796-1808.

WIDYANTORO, Bambang, et al. Endothelial cell–derived endothelin-1 promotes cardiac fibrosis in diabetic hearts through stimulation of endothelial-to-mesenchymal transition. Circulation, 2010, 121.22: 2407-2418.

WONG, Sok Kuan, et al. Animal models of metabolic syndrome: a review. *Nutrition & metabolism*, 2016, 13: 1-12.

WORKMAN, Antony J.; KANE, Kathleen A.; RANKIN, Andrew C. The contribution of ionic currents to changes in refractoriness of human atrial myocytes associated with chronic atrial fibrillation. *Cardiovascular research*, 2001, 52.2: 226-235.

XIA, Xuhua; XIA, Xuhua. *What is comparative genomics?*. Springer Berlin Heidelberg, 2013.

YAMASHITA, Hiromi, et al. Improvement of obesity and glucose tolerance by acetate in Type 2 diabetic Otsuka Long-Evans Tokushima Fatty (OLETF) rats. *Bioscience, biotechnology, and biochemistry*, 2007, 71.5: 1236-1243.

YAMAUCHI, Toshimasa, et al. Globular adiponectin protected ob/ob mice from diabetes and ApoE-deficient mice from atherosclerosis. *Journal of Biological Chemistry*, 2003, 278.4: 2461-2468.

YAN, Guijun, et al. Orphan nuclear receptor Nur77 inhibits cardiac hypertrophic response to beta-adrenergic stimulation. *Molecular and cellular biology*, 2015, 35.19: 3312-3323.

YANG, Qin; VIJAYAKUMAR, Archana; KAHN, Barbara B. Metabolites as regulators of insulin sensitivity and metabolism. *Nature reviews Molecular cell biology*, 2018, 19.10: 654-672.

YANG, Xu, et al. ACSM3 suppresses the pathogenesis of high-grade serous ovarian carcinoma via promoting AMPK activity. *Cellular Oncology*, 2022, 45.1: 151-161.

YE, Jian, et al. Primer-BLAST: a tool to design target-specific primers for polymerase chain reaction. *BMC bioinformatics*, 2012, 13: 1-11.

YING, Fei, et al. Analysis of differentially expressed genes in gastrocnemius muscle between DGAT1 transgenic mice and wild-type mice. *BioMed research international*, 2017, 2017.

YOU, Xiaohua, et al. Transcriptional up-regulation of relaxin-3 by Nur77 attenuates β-adrenergic agonist–induced apoptosis in cardiomyocytes. *Journal of Biological Chemistry*, 2018, 293.36: 14001-14011.

YUAN, Ruosen, et al. Nur77 deficiency exacerbates macrophage Nlrp3 inflammasome-mediated inflammation and accelerates atherosclerosis. *Oxidative Medicine and Cellular Longevity*, 2022, 2022.

YUNG, Justin Hou Ming; GIACCA, Adria. Role of c-Jun N-terminal kinase (JNK) in obesity and type 2 diabetes. *Cells*, 2020, 9.3: 706.

YUSUF, Salim, et al. Obesity and the risk of myocardial infarction in 27 000 participants from 52 countries: a case-control study. *The Lancet*, 2005, 366.9497: 1640-1649.

ZENG, Xinliu, et al. NR4A1 is involved in fibrogenesis in ovarian endometriosis. *Cellular Physiology and Biochemistry*, 2018, 46.3: 1078-1090.

ZHANG, Hong-Xia; ZHANG, Ying; YIN, Hao. Genome editing with mRNA encoding ZFN, TALEN, and Cas9. *Molecular Therapy*, 2019, 27.4: 735-746.

ZHANG, Peng, et al. The orphan nuclear receptor Nur77 regulates hepatic cholesterol metabolism through the suppression of LDLR and HMGCR expression. *Molecular Medicine Reports*, 2012, 5.6: 1541-1547.

ZHANG, Yi, et al. Fatty acid binding protein 3 (fabp3) is associated with insulin, lipids and cardiovascular phenotypes of the metabolic syndrome through epigenetic modifications in a Northern European family population. *BMC medical genomics*, 2013, 6: 1-14.

ZHU, Yi, et al. Lactate accelerates vascular calcification through NR4A1-regulated mitochondrial fission and BNIP3-related mitophagy. *Apoptosis*, 2020, 25: 321-340.

ZHU, Zhihong, et al. Integration of summary data from GWAS and eQTL studies predicts complex trait gene targets. *Nature genetics*, 2016, 48.5: 481-487.

ZHU, Zhidong; WANG, Duoqin; SHEN, Yanyun. Loss of ACSM3 confers worsened prognosis and immune exclusion to cutaneous melanoma. *Journal of Cancer*, 2020, 11.22: 6582.

16. Supplements

Verification of SHR vs. PD5 transcriptomic data (heart)	
Primer	**Sequence (5´-3´)**
Nr4a3_e5F	CACTACAACAGGAGCCCTCG
Nr4a3_e5-6R	TGGTCGGTGGGACAGTATCT
Nr4a3_e6F	AGCTGGGCAGAAAAGATCCC
Nr4a3_e7R	TGAAGTCGGTGCAGGACAAG
Nr4a1_e3F	ATCTGCCTGGCAAACAAGGA
Nr4a1_e4R	GGCTGCTTGGGTTTTGAAGG
Nr4a1_e5-6F	CCTGGCCTACCGATCTAAGC
Nr4a1_e6R	AGGCAAAGGCAGGAACATCA
KCNA5_e1F	CACTTTCCTCTGGCCCTACG
KCNA5_e1R	CGCACGAGCAACTCAAAAGT
Per1_e17F	TTGACACCTCTTCTGTGGCG
Per1_e18R	ACACATAGCAGGGGGTTTCG

Supplementary table 1: Primers used in qPCR verification of the transcriptomic data.

Verification of SHR vs. PD vs. BN transcriptomic data (liver)	
Primer	**Sequence (5´-3´)**
Acsl5_1660F	GTACTGGACAAGGATGGCTGG
Acsl5_1795R	CAATCTTCTCTGGAGCGATGT
Acsm1_1288F	GCCATTTTACCCTTTGACATACA
Acsm1_1436R	TCAGATGTCTTCTCTGGGCTATT
Acsm2a_1712F	GCACCCTACAAGTACCCCAG
Acsm2a_1833R	GCCTGGGCTTATCCTGATGT
Acsm3_c14F	TCTCTCCCATTAAGCAGGTCT
Acsm3_c2309R	CATGGGGCAGAGATTTGGTT
Acsm3_1210F	AACCCTCTCCAAGTTTCCCAT
Acsm3_1351R	CACTTCAGGGTTGATGGGTTC
Acsm4_1218F	ATACGAGGGCTACGGACAGA
Acsm4_1367R	TCCTTGCCCGATGGTAGGAT
Acsm5_1503F	GCCATCCGCATCAAACCTAC
Acsm5_1628R	CTCGTCCATATGTGCTCGGT
Apol3_250F	GATCCCACACCAGGAAGCAAG
Apol3_393R	AGGCTTCGTCTTTGGTCAAC
Casp12_976F	GATGAGGAATGTGTGTTGAGCC
Casp12_1117R	TGGAAATGAAGAGAGAGCCAC
Cd36_1199F	TACGTCGTATGGTGTGCTGG
Cd36_1332_R	GCTCATCTTCGTTAGGATTCAAGC
Ces2e_1365F	TGGTGATGAGCTTCCTTATGTGA
Ces2e_1511R	GGTAGACCCTCACTGTTGGGA
Cyp2b1_929F	CACCACACTCCGCTATGGTT
Cyp2b1_1042R	TCATCAAGGGTTGGTAGCCG
Cyp7b1_1146F	AATTGGACAGCTTGGTCTGC
Cyp7b1_1237R	ATCCTCTTGCACTTCACGGA
Lep_102F	TGTTCAAGCTGTGCCTATCCA
Lep_244R	GCCCGGGAATGAAGTCCAAA
Ppia_c59F	TGTTCTTCGACATCACGGCT
Ppia_c178R	ATCCTTTCTCCCCAGTGCTC
Rgs16_302F	AGAAGATCCGATCAGCCACC
Rgs16_422R	GTCTTGGTCAGTTCTCGGGT
Rpl41_55F	TCTTAGCGCCATCTTCCTTG
Rpl41_170R	ATGGTTTACTTGGACCTCTGCC
Scd1_867F	CCCCTACGACAAGAACATTCAA
Scd1_950R	TGATGGTAGTTGTGGAAGCCC
Sirt3_413F	TGCGGCTCTACACACAGAAC
Sirt3_560R	TCACGTCAGCCCGTATGTCT
Ugt2a3_915F	AGTGTTTTCGCTGGGGTCAA
Ugt2a3_1034R	GCTGGCTTCTTGCCTGAGTA

Supplementary table 2: Primers used in qPCR verification of the transcriptomic data.

Verification of SHR vs. PD5 transcriptomic data (liver)	
Primer	**Sequence (5´-3´)**
Aox1_e19F	GGATTCTGAGACACGGGCAA
Aox1_e20R	ACACTCCAGCTTCCGTTCTG
Aox1_e32-33F	ATAGGCCAGGTTGAAGGTGC
Aox1_e33R	TTTGAGTGTTCGGATGGGGG
Doc2a_e3-4F	CCTGCAAGGCCAATAAGCTAAA
Doc2a_e5R	GCACTCGGATCTCCCCAATA
Gca_e5-6F	ATCGCGCTCATGGGTTACAG
Gca_e7R	GCAAGTGGTCTCTTCGCCTA
Ifih1_e11-12R	TGTTCAGTCTGAGTCATGGGC
Ifih1_e11F	TTCACAAAAACGCGGCAGAG
Ifih1_e5F	AGAAGAAGCAGGCGTGTGAA
Ifih1_e6R	GGGTATCGCCGCTTAATCCA
Ingig1_e1-2F	CCGCTGTTGTCGGCTTATTG
Ingig1_e2-3R	CTAATTTGGCACTGGCATGGT
Ingig1_e3F	GGACGTTTGATCGATCCCGA
Ingig1e_4R	CAAGGGAGCCAAGAACGGAT
Lmod2_e2-3F	AGCTACGGAGGGTGGAAGTT
Lmod2_e3R	GACTAGTGTCTGAAGCTGGGAG
Nox4_e7-8R	TCAACAAGCCACCCGAAACA
Nox4_e7F	GTGTCTGCATGGTGGTGGTA
Ppia_59F	TGTTCTTCGACATCACGGCT
Ppia_178R	ATCCTTTCTCCCCAGTGCTC
RGD1559600_e1-2F	GGGCTACTCAAGATGCAGGT
RGD1559600_e2R	TACCAATGCGATCTGAGGCT
Slc17a2_e1F	GACCTCCGTTTGGGAATGGT
Slc17a2_e2R	TTCCCTCTGCCCCAAATCAC
Slc17a2_e5-6F	AGGCTCAGGAGCAGCATTTG
Slc17a2_e7R	TCGTGAACCACAGGACACAG
Tenm3_e17F	TCACCAAACCTGGCCTACAC
Tenm3_e18R	CAGGTCCAAGCACGACTCAT
Tenm3_e25-26F	AAAGCTCAGGGTCAACGGAC
Tenm3_e26R	CCGCCATCAGCTTGCTACTA

Supplementary table 3: Primers used in qPCR verification of the transcriptomic data.

Acsm3 sequencing	
Primer	**Sequence (5´-3´)**
Acsm3_prome1F	ccaattttctaaaggggacca
Acsm3_prome1R	ctggacttgctgggttttgt
Acsm3_e2aF	tgaaaagcagtaggccaggt
Acsm3_e2aR	gatccacttgggcacttgtc
Acsm3_e2F	gcccaaagtaaagccattca
Acsm3_e2R	aagcttcccacgattttcct
Acsm3_e3F	cttagctgcattgggggtct
Acsm3_e3R	tgtagccactgctgactaccc
Acsm3_e4F	cctgacctctgagttttctgc
Acsm3_e4R	aaatgctgccaaaacacact
Acsm3_e5F	caaacagatttctcccctggt
Acsm3_e5R	ttgttgagctcactgagttgg
Acsm3_e6F	agaaaaggcccaaagcagat
Acsm3_e6R	CCAGCCAGAACctggaatac
Acsm3_e7F	ccgtgcctacagtacacaacc
Acsm3_e7R	cctcccaatctccgtgttta
Acsm3_e8F	aaagcccacaaagacaggaa
Acsm3_e8R	ctggacacagcagccatcta
Acsm3_e9F	atctgcatatggcctccagt
Acsm3_e9R	ccatacctttagtatccctcca
Acsm3_e10F	tagacacacccagccatgtg
Acsm3_e10R	ctcacccaattctcctttgg
Acsm3_e11F	tttgtgcaatgataacttgggta
Acsm3_e11R	tttgtggcctttctgcttct
Acsm3_e12F	aaatgactggacaaaagagtcaca
Acsm3_e13R	tgcatgtaacacacaggactga
Acsm3_e14F	gattcccaccacaatggttc
Acsm3_e14R	aggggcgtcactttaacctc
Acsm3_e15F	gggtaactggcatgacctga
Acsm3_e15R	TTTAAGGCATCACGGCATCT
Acsm3_e15bF	TGAAATCATATAATCACTGAATCCTT
Acsm3_e15bR	agatgagcatttgggtagtca

Supplementary table 4: Primers used for *Acsm3* sequencing.

GST pull-down	
Primer	**Sequence (5´-3´)**
BTB domain	
Plzf_c-1F_EcoRI	caaa**GAATTC**cATGGATCTGACAAAGATGGGT
Plzf_c454R_HindIII	caaa**AAGCTT**agATCGAGCCTTACGGTCCTCT
ZF domain	
Plzf_c1142F_EcoRI	caaa**GAATTC**tgAGAGGGAGCTGTTCAGCAAG
Plzf_c1997R_HindIII	caaa**AAGCTT**gGTCTTCTCTATCCTCCAGTCAGG
ALL (*Plzf* complete sequence)	
Plzf_c-1F_EcoRI	caaa**GAATTC**cATGGATCTGACAAAGATGGGT
Plzf_c2021R_SalI	caaa**GTCGAC**gCACACATAACACAGGTAGAGGTATGTC

Supplementary table 5: Primers for construct preparation for GST pull-down assay. Restriction sites for EcoRI, HindIII and SalI are marked in bold letters.

Construct name	Primer	Sequence (5´-3´)
full	Plzf_XSreg_rn_F	CAAgtcgacATGTCATTCAACCCCTGCTT
	Plzf_Sreg_rn_R	CAAgtcgacAGCACACACAAGATGTGATCG
out	Plzf_outreg_rn_F	caaGTCGACacagtggcgtctgacctcat
	Plzf_outreg_rn_R	caaGTCGACgccttctcaccccaagtgta
A	Plzf_i2_rc2F_Acc65I	caaaGGTACCtcagccatttggtagccatt
	Plzf_corereg_rn_R	caaGTCGAcctccaggctcagaaagagtt
R	Plzf_i2_rc1bF_Acc65I	caaaGGTACCgaaggcccctccttaatcc
	Plzf_corereg_rn_R	caaGTCGAcctccaggctcagaaagagtt
L	Plzf_i2_rc2F_Acc65I	caaaGGTACCtcagccatttggtagccatt
	Plzf_i2_rc2R_XhoI	caaaCTCGAgcccagaagaggatgacaag

Supplementary table 6: Primers for construct preparation for luciferase assay. For cloning, restriction enzymes XhoI (restriction site CTCGAG) and Acc65I (restriction site GGTACC) were used.

Crude nutrients	%
Dry matter	95.1
Crude protein (Nx6,25)	20.8
Crude fat	30.2
Crude fibre	5.0
Crude ash	5.6
N free extracts	33.4
Starch	22.1
Sugar	13.0

Fatty acids	%
C 4:0	0.12
C 6:0	0.11
C 8:0	0.50
C 10:0	0.45
C 12:0	2.81
C 14:0	1.77
C 16:0	8.57
C 16:1	0.4
C 17:0	0.13
C 18:0	2.63
C 18:1	8.83
C 18:2	1.60
C 18:3	0.12
C 20:0	0.07
C 20:1	0.01
C 20:4	0.02
Cholesterol (mg/kg)	171

Supplementary table 7: The individual components of the high fat diet.

			PD	SHR	BN
Class	Sub-Class	Total Cholesterol of all factions [mg/dL]	52.15 ± 4.19	34.96 ± 1.47	45.84 ± 2.02
CM (>80nm)		G01 fraction cholesterol [mg/dL]	4.33 ± 0.91	0.05 ± 0.01	0.31 ± 0.13
		G02 fraction cholesterol [mg/dL]	1.77 ± 0.27	0.02 ± 0.01	0.17 ± 0.08
VLDL (30-80nm)	large VLDL	G03 fraction cholesterol [mg/dL]	3.00 ± 0.28	0.07 ± 0.02	0.42 ± 0.17
		G04 fraction cholesterol [mg/dL]	3.46 ± 0.22	0.18 ± 0.06	0.81 ± 0.21
		G05 fraction cholesterol [mg/dL]	3.02 ± 0.15	0.36 ± 0.09	1.43 ± 0.18
	medium VLDL	G06 fraction cholesterol [mg/dL]	1.32 ± 0.10	0.30 ± 0.04	1.23 ± 0.07
	small VLDL	G07 fraction cholesterol [mg/dL]	0.36 ± 0.04	0.08 ± 0.01	0.59 ± 0.07
LDL (16-30nm)	large LDL	G08 fraction cholesterol [mg/dL]	0.65 ± 0.07	0.28 ± 0.03	1.33 ± 0.15
	medium LDL	G09 fraction cholesterol [mg/dL]	0.97 ± 0.12	1.04 ± 0.08	2.84 ± 0.13
	small LDL	G10 fraction cholesterol [mg/dL]	1.94 ± 0.25	2.18 ± 0.13	2.62 ± 0.18
	very small LDL	G11 fraction cholesterol [mg/dL]	0.96 ± 0.16	0.08 ± 0.03	0.59 ± 0.12
		G12 fraction cholesterol [mg/dL]	2.29 ± 0.60	2.99 ± 0.11	1.38 ± 0.30
		G13 fraction cholesterol [mg/dL]	1.49 ± 0.43	2.31 ± 0.09	1.29 ± 0.23
HDL (8-16nm)	very large HDL	G14 fraction cholesterol [mg/dL]	1.46 ± 0.44	2.65 ± 0.13	1.59 ± 0.23
		G15 fraction cholesterol [mg/dL]	3.34 ± 0.78	3.65 ± 0.20	3.98 ± 0.42
	large HDL	G16 fraction cholesterol [mg/dL]	12.62 ± 1.11	9.73 ± .61	13.65 ± 0.91
	medium HDL	G17 fraction cholesterol [mg/dL]	6.17 ± 0.32	5.02 ± 0.30	6.95 ± 0.42
	small HDL	G18 fraction cholesterol [mg/dL]	1.74 ± 0.11	2.15 ± 0.10	2.49 ± 0.09
	very small HDL	G19 fraction cholesterol [mg/dL]	0.73 ± 0.04	0.99 ± 0.04	1.26 ± 0.03
		G20 fraction cholesterol [mg/dL]	0.53 ± 0.05	0.86 ± 0.02	0.90 ± 0.03

Supplementary table 8: Serum levels of lipoprotein particles in PD, SHR and BN rat strains. CM chylomicrons, VLDL very low density lipoproteins, LDL low density lipoproteins, HDL high density lipoproteins. Data are expressed as aritmetic mean ± SEM.

	PD		SHR		BN	
	before HFD	after HFD	before HFD	after HFD	before HFD	after HFD
MCP-1 (pg/ml)	1393.23 ± 67.96	1329.75 ± 97.29	1523.29 ± 114.08	1255.53 ± 82.87	1685.23 ± 81.22	1543.65 ± 59.30
IL-1a (pg/ml)	1008.78 ± 16.40	894.33 ± 62.47	842.58 ± 84.58	874.05 ± 37.53	832.18 ± 92.09	947.68 ± 48.82
IL-1b (pg/ml)	336.80 ± 13.03	265.78 ± 20.30	300.61 ± 26.98	260.04 ± 16.72	429.16 ± 11.86	422.00 ± 33.15
IL-2 (pg/ml)	8620.72 ± 238.68	7510.59 ± 573.11	6572.68 ± 1014.59	7474.38 ± 395.77	6384.21 ± 530.29	7332.76 ± 285.40
IL-4 (pg/ml)	534.67 ± 15.88	447.08 ± 39.38	441.98 ± 50.47	436.83 ± 21.64	390.92 ± 11.72	441.93 ± 7.49
IL-5 (pg/ml)	1201.16 ± 17.56	1140.29 ± 34.31	1091.19 ± 78.88	1110.75 ± 21.12	1074.01 ± 39.13	1089.06 ± 12.02
IL-6 (pg/ml)	1406.31 ± 87.79	1236.42 ± 152.73	1088.86 ± 174.99	1318.95 ± 138.50	1216.76 ± 160.18	1519.78 ± 53.86
IL-7 (pg/ml)	297.92 ± 8.83	245.09 ± 14.77	266.28 ± 30.68	234.74 ± 15.01	362.93 ± 30.50	376.42 ± 30.04
IL-10 (pg/ml)	301.85 ± 3.71	259.49 ± 18.16	256.42 ± 23.74	251.43 ± 11.09	242.57 ± 18.52	242.84 ± 4.38
IL-12(p70) (pg/ml)	1886.65 ± 86.96	1471.49 ± 144.58	1703.01 ± 155.78	1519.70 ± 111.68	1434.92 ± 191.49	1458.04 ± 27.45
IL-13 (pg/ml)	620.76 ± 42.16	612.38 ± 53.06	358.18 ± 113.99	493.57 ± 69.41	392.96 ± 74.20	604.58 ± 39.89
IL-17 (pg/ml)	124.50 ± 2.81	108.84 ± 7.66	93.86 ± 16.06	100.05 ± 3.68	94.93 ± 9.52	103.51 ± 1.81
IL-18 (pg/ml)	7941.55 ± 668.54	10624.25 ± 3463.23	6000.48 ± 444.75	6090.49 ± 212.29	6752.79 ± 1066.55	5875.92 ± 84.23
G-CSF (pg/ml)	35.15 ± 3.40	30.39 ± 5.19	23.16 ± 5.46	32.16 ± 3.60	28.11 ± 2.69	34.89 ± 2.26
GM-CSF (pg/ml)	265.49 ± 9.30	225.43 ± 14.73	244.21 ± 25.46	218.71 ± 11.16	366.36 ± 22.47	370.96 ± 28.16
GRO/KC (pg/ml)	327.39 ± 12.18	333.06 ± 39.43	364.91 ± 25.62	287.98 ± 17.57	401.15 ± 28.78	418.37 ± 26.86
IFN-g (pg/ml)	852.52 ± 27.98	741.64 ± 74.58	690.52 ± 92.76	738.01 ± 46.00	727.35 ± 68.16	862.10 ± 22.10
M-CSF (pg/ml)	162.56 ± 9.33	137.79 ± 17.20	130.36 ± 20.69	146.88 ± 8.42	132.07 ± 20.04	147.86 ± 5.05
MIP-1a (pg/ml)	80.56 ± 1.27	62.45 ± 1.96	97.80 ± 4.25	71.62 ± 4.92	104.76 ± 6.04	104.65 ± 6.59
MIP-3a (pg/ml)	74.79 ± 6.58	72.67 ± 12.78	38.30 ± 4.55	46.03 ± 3.40	37.04 ± 4.59	44.20 ± 1.21
RANTES (pg/ml)	1403.23 ± 145.83	1368.75 ±182.06	1664.14 ± 284.34	1065.89 ± 116.06	857.33 ± 60.55	592.81 ± 51.27
TNF-a (pg/ml)	1970.42 ± 115.57	1712.45 ± 193.45	1476.37 ± 325.72	1657.04 ± 175.62	1284.17 ± 162.68	1632.29 ± 111.98
VEGF (pg/ml)	301.27 ± 7.11	227.19 ± 22.91	241.02 ± 39.87	213.14 ± 12.03	323.71 ± 59.18	331.62 ± 22.99

Supplementary table 9: Serum cytokine levels in PD, SHR and BN strain before and after HFD. Data are expressed as aritmetic mean ± SEM.

	PD		SHR		BN	
	before HFD	after HFD	before HFD	after HFD	before HFD	after HFD
Adiponectin (ug/ml)	0.40 ± 0.09	0.46 ± 0.04	0.42 ± 0.02	0.54 ± 0.15	0.48 ± 0.07	0.33 ± 0.03
C-Peptide (pg/ml)	642.72 ± 22.57	899.16 ± 133.65	554.20 ± 82.29	610.21 ± 91.62	539.77 ± 63.48	805.05 ± 113.48
GIP (pg/ml)	57.38 ± 7.13	39.98 ± 7.12	16.72 ± 3.61	30.95 ± 9.51	20.99 ± 4.05	21.62 ± 9.66
GLP-1 (pg/ml)	312.41 ± 25.59	268.45 ± 44.27	234.83 ± 58.82	214.96 ± 28.47	205.76 ± 21.67	198.20 ± 36.52
Glucagon (pg/ml)	58.67 ± 6.22	36.69 ± 7.14	50.75 ± 15.70	35.98 ± 3.81	46.99 ± 11.80	38.69 ± 6.66
PP (pg/ml)	66.60 ± 4.17	48.97 ± 11.11	57.07 ± 1.60	44.41 ± 6.42	58.13 ± 11.32	56.47 ± 8.52

Supplementary table 10: Serum levels of Adiponectin, C-Peptide, GIP (gastric inhibitory peptide), GLP-1 (glucagon like peptide 1) and PP (pancreatic polypeptide) in PD, SHR and BN strain before and after HFD. Data are expressed as aritmetic mean ± SEM.

SHR vs. BN pathway enrichment analysis	Genes total	Upregulated in BN	Downregulated in BN	-log(p value)
GPCRs, Class A Rhodopsin-like	4	0	Ptger4,Ednra,Ntsr1,Ednrb	5,10
Oxidative Stress	9	Maoa,Gpx1,Ugt1a6,Xdh	Nfix,Gpx3,Txnrd1,Sod3,Mapk10	3,37
Tryptophan metabolism	12	Ddc,Echs1,Gcdh,Cyp7b1,Cyp2a1,Cyp2a2,Aldh1a1,Aldh9a1	Cyp2j4,Ogdh,Aox1,Cyp2f4	3,02
TNF-alpha NF-kB Signaling Pathway	29	Psmd12,Psmd1,Rpl30,Kpna3,Papola,Kpna6,Chuk,Cul1,Mtif2, Rpl4,Rps6kb1	Rela,Tradd,Tifa,Cdc37,Stat1,Pml,Gsk3b,Ywhag,Tnip1,Src,Csnk2b,Btrc, Nkiras2,Polr1a,LOC681193,Dap,Bag4,Traf4	2,86
Glucuronidation	7	Pgm1,Ugt1a5,Ugt2a3,Ugt1a6,Ugt1a3,Ugt1a1,Ugt1a2	0	2,73
Complement Activation, Classical Pathway	6	0	C1qa,C1qb,C1qc,C1r,C6,C7	2,70
Fatty Acid Omega Oxidation	5	Adh6,Adh1,Adh4,Aldh1a1,Adh7	0	2,37
Retinol metabolism	9	Cd36,Aldh1a1,Adh4,Adh1	Scarb1,Rxra,Abcg5,Lrat,Rbp1	2,22
Cytoplasmic Ribosomal Proteins	16	Rpl3,Rpl7,Rpl4,Rpl14,Rpl19,RGD1562923,Rpl32,Rpl35a, Rpl39,Rps4x,Rps8,Rps25,Rps6kb1,Rpl30	Rpl34,Fau	2,12
ErbB signaling pathway	10	Egf,Nrg4,Nck1,Rps6kb1	Nrg1,Plcg1,Src,Araf,Gsk3b,Eif4ebp1	2,07
TCA Cycle	7	Idh3B,Sdhb,Idh2,Pdhx,Pdhb	Pc,Ogdh	1,96
Fatty Acid Biosynthesis	6	Echs1,Acsl5	Ech1,Acaa2,Pc,Echdc2	1,93
Selenium metabolism Selenoproteins	9	Gpx1,Selenbp1,Rpl30	Dio1,Txnrd1,Gpx3,Seli,Fabp1,Rela	1,93
Folic Acid Network	7	Xdh,Kmo,Gpx1	Mthfr,Fads2,Gpx3,Txnrd1	1,88
Steroid Biosynthesis	4	Hsd3b5,F13b,Cyp17a1,Hsd17b7	0	1,88
Nucleotide Metabolism	5	Adss	Dhfr,Polg,Srm,Oaz1	1,71
Selenium Micronutrient Network	7	Xdh,Kmo,Gpx1	Mthfr,Fads1,Fads2,Gpx3	1,65
Endochondral Ossification	11	Bmpr1a,Vegfa,Serpinh1	Igf1,Ghr,Tgfb1,Fgfr3,Stat1,Plat,Plau,Mgp	1,63
Eukaryotic Transcription Initiation	8	Gtf2b,Polr2b,Mnat1	Ilk,Gtf2h4,Polr2e,Polr1a,Polr2j	1,59
Metapathway biotransformation	21	Fmo5,Ugt1a1,Ugt1a2,Ugt1a5,Ugt1a3,Ugt1a6,Tpmt,Cyp7b1, Cyp17a1,Cyp27a1,Akr1d1,Mgst2,Chst9	Ephx1,Gstt1,Cyp2u1,Cyp4b1,Ephx2,Gpx3,Gstk1,Gsto1	1,58
Urea cycle and metabolism of amino groups	5	Arg1,Otc,Oat,Cps1	Srm	1,52
Glycogen Metabolism	7	Agl,Pgm1,Ppp2r5a,Ppp2r3a	Gsk3b,Ppp2r1a,Ppp2r4	1,51
Type II interferon signaling (IFNG)	7	0	Stat1,Stat2,Irf9,Oas1a,Cxcl10,Icam1,Irf2	1,51
Estrogen metabolism	4	Ugt1a1,Ugt1a3,Ugt1a2	Sts	1,49

Focal Adhesion	26	Egf,Hgf,Cav2,Met,Map2k6,Rock1,Vegfa,Farp2,Pik3r4, Ppp1r12a,Mylk	Igf1,Pelo,Itgb2,Src,Ilk,Actn1,Pdgfra,Araf,Pxn,Capn1,Gsk3b,Itga9,Itga2b, Tln1,Parvb	1,38
MAPK Cascade	6	Map2k6	Mapk10,Mbp,Sipa1,Rras,Araf	1,37
EGFR1 Signaling Pathway	24	Egf,Gja1,Eppk1,Ptpn12,Plscr1,Appl2,Pkn2,Cav2,Nck1	Stat1,Stat2,Ap2a1,Epn1,Tnip1,Pxn,Araf,Plcg1,Ptpn6,Src,Ptk2b,Git1,Rgs16, Inppl1,Arf4	1,33
Integrin-mediated cell adhesion	15	Rock1,Cav2,Capn2,Map2k6	Araf,Src,Capn5,Capn9,Tln1,Capn1,Itga9,Itgb2,Mapk10,Pxn,Ilk	1,31

Supplementary table 11: Differentially expressed genes in the liver after HFD. Pathway enrichment analysis using Transcriptomic analysis console software. Pathway enrichment analysis SHR vs. BN comparison. Significantly pathways were selected based on a p-value < 0.05.

SHR vs. PD pathway enrichment analysis	Genes total	Upregulated in PD	Downregulated in PD	-log(p value)
Tryptophan metabolism	11	Ddc,Acat1,Echs1,Cyp2a1,Cyp2a2,Aldh1a1	Cyp2j4,Ogdh,Acmsd,Cyp7b1,Inmt	5,15
Beta Oxidation Meta Pathway	8	Echs1,Acat1,Lipc,Acsl5	Lpl,Tpi1,Crat,Cpt1a	4,20
Fatty Acid Beta Oxidation	8	Echs1,Acsl5,Lipc,Acat1	Crat,Cpt1a,Gk,Lpl	4,00
Fatty Acid Beta Oxidation	7	Echs1,Acsl5,Lipc	Lpl,Cpt1a,Crat,Tpi1	3,85
Retinol metabolism	8	Rxra,Aldh1a1,Adh1,Retsat	Cd36,Lpl,Lrat,Aldh1a3	3,64
Fatty Acid Biosynthesis	6	Echs1,Acsl5,Scd1,Acaa2,Acaca	Echdc1	3,50
Prostaglandin Synthesis and Regulation	7	0	Ptgs1,Anxa3,Hsd11b1,Ednrb,Ednra,Tbxas1,Ptger3	3,44
Selenium Micronutrient Network	7	Kmo,Sod1,Gpx1	Mthfr,Fads1,Fads2,Tbxas1	3,35
Complement Activation, Classical Pathway	5	0	C1qa,C1qb,C1qc,C1r,C1s	3,29
Triacylglyceride Synthesis	6	Lipc	Gk,Agpat2,Lpl,Agpat5,Agpat3	2,98
Fatty Acid Omega Oxidation	4	Adh1,Aldh1a1,Adh7	Cyp3a2	2,69
Type II interferon signaling (IFNG)	6	Icam1	Stat1,Irf9,Cybb,Ifit2,Cxcl9	2,44
TCA Cycle	5	Sdha,Idh3B,Pdhb	Idh2,Ogdh	2,13
Folic Acid Network	5	Sod1,Kmo,Gpx1	Mthfr,Fads2	2,06
Urea cycle and metabolism of amino groups	4	Gamt,Otc	Asl,Arg1	1,96
Adipogenesis	12	Rxra,Scd1,Fzd1,Nampt	Lpl,Rbl2,Stat1,Stat6,Il6st,Hif1a,Irs1,Agpat2	1,79
Cholesterol metabolism	4	Lipc	Hmgcs1,Dhcr7,Lpl	1,75
Lipid Droplet Metabolism	4	0	Gk,Agpat3,Agpat2,Agpat5	1,62
Nuclear Receptors	5	Rorc,Rxra,Esr1	Nr2f2,Nr1i3	1,58
Aflatoxin B1 metabolism	2	Akr7a3,Ephx1	0	1,58
Oxidative Stress	4	Gpx1,Junb,Sod1	Mapk10	1,51
Focal Adhesion	15	Fn1,Vegfa,Farp2	Pelo,Ilk,Actn1,Met,Pdgfra,Pxn,Capn1,Rac1,Itgb5,Itga2b,Tln1,Parvb	1,49
Glucocorticoid Metabolism	2	0	Cyp17a1,Hsd11b1	1,44
Fatty Acid Beta Oxidation 3	2	Echs1,Acat1	0	1,33

Supplementary table 12: Differentially expressed genes in the liver after HFD. Pathway enrichment analysis using Transcriptomic analysis console software. Pathway enrichment analysis SHR vs. PD comparison. Significantly pathways were selected based on a p-value < 0.05.

BN vs. PD pathway enrichment analysis	Genes total	Upregulated in BN	Downregulated in BN	-log(p value)
GPCRs, Class A Rhodopsin-like	7	P2ry2,Avpr1a,Ednrb	Adra2c,Cckbr,Galr3,Gpr27	6,00
Proteasome Degradation	15	Psma2,Psmd12,Psmb4,Psma3,Psmd13,Psmd6,Psmd5,Nedd4,Psmc6, Psmc4,Psma4,Psmd1,Psmd2	Psmd9,Psmb8	2,94
Fatty Acid Biosynthesis	8	Acsl5,Echdc1	Scd1,Acaa2,Pc,Acly,Acaca,Echdc2	2,41
Cytoplasmic Ribosomal Proteins	20	Rpl3,Rpl7,Rpl4,Rpl19,RGD1562923,Rpl22,Rpl24,Rpl35a,Rpl37, Rpl39,Rps23,Rps11,Rps4x,Rps8,Rps21,Rps25,Rps6kb1,Rpl10	Rpl13,Rpl30	2,06
Glucuronidation	7	Ugt1a5,Ugt2a3,Ugt1a6,Ugt1a3,Ugt1a1,Ugt1a2	Ugt2b17	1,94
Fatty Acid Omega Oxidation	5	Cyp2e1,Cyp3a2,Adh6,Adh1,Adh4	0	1,77
Nucleotide Metabolism	6	Prps2,Adss	Dhfr,Polg,Srm,Oaz1	1,72
Cholesterol metabolism	7	Hmgcs1,Idi1,Fdft1,Lss,Nsdhl	Scarb1,Lipc	1,71
GPCRs, Other	3	Alg6	Cckbr,Gpr183	1,66
G1 to S cell cycle control	15	Cdk7,Cdk2,Creb3,Orc3,Mnat1,E2f6,Orc2,Creb1,Atm,Orc4,Prim1	Cdkn1a,Tp53,Ccnb1,Creb3l1	1,64
TGF-beta Receptor Signaling Pathway	28	Arrb2,Ap2b1,Fnta,Cav1,Pard3,Cul1,Anapc1,Anapc4,Cdc16,Anapc5, Ctcf,Cops5,Map2k6,Smurf2,Snx2,Cdk2,Rbl2,Rock1,Xpo1,Pias1	Gipc1,Esr1,Tp53,Atf3,Junb,Trap1,Cdkn1a,Nfyb	1,63
Estrogen metabolism	5	Comt,Ugt1a1,Ugt1a3,Ugt1a2	Sts	1,63
Aflatoxin B1 metabolism	3	0	Akr7a3,Gstt1,Ephx1	1,53
EGFR1 Signaling Pathway	32	Egf,Raf1,Shoc2,Sos1,Pik3cb,Gja1,Eppk1,Plscr1,Cblb,Eps15,Sh3bgrl ,Reps2,Appl2,Mta2,Asap1,Pkn2,Creb1,Hat1,Itch,Cav1,Cav2,Nck1, Rasa1	Stat3,Stat2,Map2k2,Ap2a1,Araf,Ptpn6,Rgs16,Inppl1,Ptpn11	1,53
Cholesterol Biosynthesis	5	Idi1,Hmgcs1,Fdft1,Lss,Nsdhl	0	1,50
Signaling of Hepatocyte Growth Factor Receptor	9	Itga1,Rasa1,Sos1,Raf1,Met,Hgf	Ptpn11,Stat3,Map2k2	1,49
EPO Receptor Signaling	7	Ptprc,Raf1,Sos1,Rasa1	Map2k2,Stat3,Ptpru	1,43

Supplementary table 13: Differentially expressed genes in the liver after HFD. Pathway enrichment analysis using Transcriptomic analysis console software. Pathway enrichment analysis BN vs. PD comparison. Significantly pathways were selected based on a p-value < 0.05.

Pathway enrichment analysis dexamethasone admission	Total	Upregulated after dexamethasone	Downregulated after dexamethasone	-log(p value)
Glutathione metabolism	12	Gpx3	Anpep,Idh1,Gsr,Gclc,Gstm3,Gsta5,Gsta2,Gstm2,Gstt1,Gstt2,Gclm	7,00
Tryptophan metabolism	18	Ddc,Acmsd,Kynu,Tdo2,Cyp2f4,Aldh9a1	Cyp2j4,Mdm2,Acat1,Gcdh,Cat,Cyp7b1,Aox1,Inmt,Cyp1a2,Cyp2a2,Aldh1a1,Aldh2	7,00
Complement and Coagulation Cascades	19	Cd59	C1s,C2,C9,Masp1,Cfi,C3ar1,F10,Plg,Kng1,C7,C8b,C1qa,C1r,C4a,Mbl1,F13b,Klkb1,Serpinc1	7,00
Oxidative Stress	12	Gpx3	Nfkb1,Hmox1,Nqo1,Cat,Txnrd1,Gclc,Gsr,Cyba,Junb,Sod1,Sod3	7,00
Complement Activation, Classical Pathway	9	0	C1qa,C1qc,C1r,C1s,C2,C5,C7,C8b,C9	6,00
Type II interferon signaling (IFNG)	13	Socs1	Ifngr2,Jak1,Socs3,Stat1,Prkcd,Psmb9,Tap1,Cybb,Il1b,Icam1,Cxcl9,Irf8	6,00
Spinal Cord Injury	22	Zfp36,Mbp,Arg1,Vim	Plxna2,Cd47,Il1b,Tgfb1,Rtn4,C5,Cxcl1,Ccng1,Ntn1,Ccr2,Pla2g2a,Icam1,Cdk4,Ccnd1,Casp3, Rhoc,Lilrb3,Nox4	4,96
Fatty Acid Beta Oxidation	11	Pnpla2,Cpt2,Crat	Gcdh,Acsl5,Acsl1,Decr1,Lipc,Cpt1a,Gk,Acat1	4,46
IL-5 Signaling Pathway	16	Nfkbia,Pik3r1,Socs1,Foxo3,Cdkn1b	Prkcb,Nfkb1,Mapk9,Pla2g4a,Hcls1,Prkcd,Icam1,Itgb2,Itgam,Jak1,Stat1	4,26
Apoptosis	17	Nfkbia,Cflar,Pik3r1	Mdm2,Nfkb1,Fas,Casp4,Casp3,Tnfrsf1a,Tnfrsf1b,Bid,Casp7,Irf7,Nfkbie,Xiap,Tnfsf10,Casp6	3,96
Fatty Acid Biosynthesis	8	Scd1,Acly,Acaca	Acsl5,Acsl1,Decr1,Mecr,Echdc2	3,78
IL-2 Signaling Pathway	16	Pik3r1,Foxo3,Sos1,Socs1,Crk,Prkcz	Jak1,Socs3,Cd53,Icam1,Nmi,Itm2b,Hsp90aa1,Nfkb1,Mapk9,Stat1	3,72
Apoptosis Modulation by HSP70	7	0	Map3k1,Casp3,Bid,Casp6,Casp7,Nfkb1,Tnfrsf1a	3,58
Aflatoxin B1 metabolism	4	0	Cyp1a2,Akr7a3,Gstt1,Ephx1	3,30
Beta Oxidation Meta Pathway	9	Crat,Cpt2,Pnpla2	Acsl1,Cpt1a,Acat1,Gcdh,Lipc,Acsl5	3,23
Nuclear receptors in lipid metabolism and toxicity	9	Ppard,Nr1h4,Nr1i2,Cyp26a1	Abca1,Abcb1a,Cyp8b1,Cyp2b2,Cyp1a2	3,23
MAPK Signaling Pathway	34	Crk,Dusp1,Ntrk1,Map2k6,Map3k6,Atf4,Sos1,Rasgrp3, Map3k5,Cacnb4	Mapk9,Arrb2,Stk4,Casp3,Flna,Tnfrsf1a,Hspb1,Tgfb1,Cdc25b,Rac2,Prkcd,Il1b,Map3k8,Fgfr2, Rras2,Nfkb1,Ntf3,Tgfbr2,Fas,Pla2g4a,Nras,Cacnb2,Fgf1,Pak1	3,02

Hexoses metabolism in proximal tubules	12	Slc2a5,Pgk1,Gpi,Pdhb,Pklr,Aldob,Pdk1,Acly,Pfkl,Tkfc, Mdh1	Sord	3,02
IL-3 Signaling Pathway	18	Tec,Pik3r1,Sos1,Crk,Ppp2ca,Foxo1	Jak1,Stat1,Stat6,Prkcb,Src,Socs3,Rac2,Pak1,Nfkb1,Hspb1,Tnfrsf1b,Mapk9	2,97
Folic Acid Network	8	Cbs,Gpx3	Cat,Sod1,Fads2,Kmo,Gsr,Txnrd1	2,87
Adipogenesis	21	Ppard,Cyp26a1,Mef2d,Scd1,Agt,Cdkn1a,Gadd45b,Bmp1, Foxo1,Socs1,Il6st,Rora,Agpat2,Lpin1	Fas,Tgfb1,Cfd,Stat1,Stat6,Socs3,Mbnl1	2,84
FAS pathway and Stress induction of HSP regulation	9	Cflar	Fas,Hspb1,Casp3,Casp7,Pak1,Casp6,Lmnb1,Map3k1	2,74
Fructose Metabolism in Proximal Tubules	6	Gpi,Tkfc,Pfkl,Aldob,Slc2a5	Sord	2,73
Retinol metabolism	9	Sult1a1,Cyp26a1	Scarb1,Aldh1a1,Adh1,Lrat,Rbp1,Rdh5,Retsat	2,65
Fatty Acid Omega Oxidation	5	0	Adh1,Cyp3a2,Cyp1a2,Aldh1a1,Aldh2	2,65
Keap1-Nrf2	5	0	Nqo1,Nfe2l2,Gclc,Gclm,Hmox1	2,65
Metapathway biotransformation	22	Fmo1,Fmo2,Fmo3,Sult1a1,Cyp26a1,Cyp27a1,Gpx3	Cyp1a2,Akr7a3,Ephx1,Gstt1,Comt,Tpmt,Cyp7b1,Cyp8b1,Cyp17a1,Akr1d1,Gstm3,Gsto1,Gstt2, Mgst2,Gsr	2,63
Toll-like receptor signaling pathway	16	Pik3r1,Nfkbia,Map2k6	Irak4,Nfkb1,Map3k8,Irf7,Cxcl9,Tlr7,Mapk9,Il1b,Ccl5,Stat1,Cd80,Tlr3,Lbp	2,63
Lipid Droplet Metabolism	7	Plin2,Pnpla2,Dgat2,Agpat2,Lpin1	Acsl1,Gk	2,61
IL-4 Signaling Pathway	12	Pik3r1,Prkcz,Pawr,Sos1,Socs1	Jak1,Stat6,Nfkb1,Socs3,Stat1,Src,Prkcd	2,55
EPO Receptor Signaling	7	Pdk1,Socs1,Ptpru,Sos1	Src,Stat1,Ptprc	2,50
Nuclear factor, erythroid-derived 2, like 2 signaling pathway	40	Map3k5,Map2k6,Prkcz,Pik3r1,Atf4,Bach1,G6pd,Dnajb9,Herpud1,Fmo1,Cdkn1a,Slc35b1	Nras,Rras2,Nfe2l2,Map3k1,Mapk9,Prkcd,Prkcb,Mdm2,Hmox1,Gclm,Gsta2,Gclc,Gsta3,Gstm2, Gstm3,Gsto1,Gstt1,Gstt2,Mgst2,Nqo1,Sod1,Sod3,Aox1,Txnrd1,Akr7a3,Ephx1,Scarb1,Gsr	2,47
Fatty Acid Beta Oxidation 1	7	Crat,Cpt2,Pnpla2	Cpt1a,Acsl5,Lipc,Acsl1	2,40
Triacylglyceride Synthesis	7	Dgat2,Lpin1,Agpat2,Pnpla2	Gk,Acsl1,Lipc	2,40
One Carbon Metabolism	7	Ftcd,Ahcy,Ahcyl2,Mat1a	Shmt1,Dhfr,Tyms	2,40
Insulin Signaling	23	Pik3r1,Map3k5,Crk,Foxo1,Sos1,Map2k6,Pfkl,Prkcz,Prkaa2, Socs1,Mapk4,Foxo3,Map3k6	Socs3,Prkcd,Prkcb,Rac2,Enpp1,Map3k8,Sgk1,Mapk9,Flot1,Sgk2	2,39

TNF-alpha NF-kB Signaling Pathway	25	Trpc4ap,Prkcz,Ppp2ca,Nfkbia,Cflar,Fkbp5,Usp2	Flna,Nfkb1,Hspb1,Tnfrsf1b,Tnfrsf1a,Casp7,Stat1,Bcl3,Unc5cl,Src,Casp3,Nfkbie,Hsp90aa1,Map3k1,Map3k8,Nsmaf,Akap8,Dap	2,38
B Cell Receptor Signaling Pathway	22	Sos1,Pik3r1,Tec,Crk,Foxo1,Nfkbia,Mapk4,Rasgrp3,Itpr1	Hcls1,Actr2,Arpc2,Pik3ap1,Nedd9,Casp7,Sh3bp2,Lcp2,Prkcd,Cdk4,Prkcb,Ptprc,Stat1	2,20
IL-6 Signaling Pathway	16	Il st,Tec,Sos1,Pik r1,Pp 2ca,Map2k6 6 3 p	Jak1,Tyk2,Stat1,Nfkb1,Prkcd,Socs3,Erbb3,Casp3,Fgr,Hspb1	2,13
T Cell Receptor Signaling Pathway	19	Pik3r1,Crk,Sos1,Itpr1	Fyb,Map3k1,Stat1,Pak1,Src,Cd4,Sh3bp2,Rac2,Nfam1,Lcp2,Nedd9,Evl,Ptprc,Cd2ap,Dock2	2,13
PI3K-AKT-NFKB pathway	14	Nfkbia,Pik3r1,Ppp a 2c	Fas,Cfb,Irak4,Mdm2,Nfkbie,Abca1,Igfbp2,Nfkb1,Psmb9,Sod1,Tap1	2,12
PKC-SCP2	17	Ahcy,St8sia1,Slc6a9,G6pd,Prkcz	Amacr,Pdzk1,Slc10a1,Rtn4,Gne,Nqo1,Pla2g4a,Sod1,Sod3,Prkcb,Prkcd,Nox4	2,10
Senescence and Autophagy	16	Cdkn1a,I 6st,Map1lc3b,Cdkn1b,Ulk1	Col3a1,Cdc25b,Mdm2,Tgfb1,Cdk4,Src,Igfbp7,Rnasel,Lamp1,Il1b,Irf7	2,07
GPCRs, Class A Rhodopsin-like		l P2ry1,Avpr1b	Cmklr1,Ptger3,Gpr81,Adra2b,C3ar1,Ccr5	2,03
Selenium Micronutrient Network	8	Gpx3	Gsr,Cat,Kmo,Sod1,Fads1,Fads2	1,98
Cytokines and Inflammatory Response (BioCarta)	7		Cxcl1,Il1b,Tgfb1,Csf1,Cd4,RT1-Db1	1,79
Estrogen metabolism	6	Sult1a1	Cyp1a2,Comt,Nqo1	1,70
Integrin-mediated cell adhesion	4	Mapk4,Sos1,Map k6,Crk,Tns1 2	Rac2,Cav2,Src,Capn5,Itga4,Itgal,Itgam,Itgb2,Pak1	1,63
p53 signal pathway	14		Mdm2,Fas,Cdk4,Bid,Casp3,Ei24	1,57
Methylation	6	Mat1a	Comt,Tpmt	1,55
ErbB signaling pathway	3	Nrg4,Crk,Sos1,Cdkn1b,Cdkn1a	Nrg1,Erbb3,Src	1,55
Myometrial Relaxation and Contraction Pathways	8		Prkcb,Igfbp2,Arrb2,Gsto1,Rgs10,Rgs18,Il1b,Adcy9,Prkcd,Dgkz,Nfkb1	1,52
Mitochondrial LC-Fatty Acid Beta-Oxidation	19	It r3,Pde4d,Pr cz,Grk5 Itpr1 Atp2a2,Atf ,Ywhaq p k , , 4	Ehhadh,Cpt1a,Acsl1	1,50
Kit Receptor Signaling Pathway	4	Cpt2	Src,Stat1,Fgr,Prkcb	1,41
Glycolysis and Gluconeogenesis	1 0	Pik3r1,Crk,Ptpru,Tec,Socs1,Sos1	0	1,37
p38 MAPK Signaling Pathway	7	Pfk ,Aldob,Pklr,Gp Pgk1,Pdh ,Mdh1 l i, b	Hspb1,Stat1,Pla2g4a	1,33
	6	Map2k6,Mef2d,Map3 5 k		

Nucleotide Metabolism	4	Polg	Dhfr,Adss,Rrm2b	1,32
EGFR1 Signaling Pathway	21	Pik3r1,Sos1,Prkcz,Pkn2,Foxo1,Crk,Socs1,Dusp1	Nras,Jak1,Stat1,Map3k1,Prkcb,Plscr1,Pld1,Sh3bgrl,Asap1,Pak1,Src,Cav2,Socs3	1,32
Steroid Biosynthesis	3	0	Hsd17b2,F13b,Cyp17a1	1,31

Supplementary table 14: Differentially expressed genes in the liver after HFD. Pathway enrichment analysis using Transcriptomic analysis console software. Pathway enrichment analysis BN vs. PD comparison. Significantly pathways were selected based on a p-value < 0.05.

Strain - Pathway enrichment analysis	Genes total	Upregulated in PD5	Downregulated in PD5	-log(p value)
Oxidative Stress	3	Txnrd2,Gclc,Sod1	0	4,14
Keap1-Nrf2	2	Gclc,Gclm	0	3,17
Glutathione metabolism	2	Gclc,Gclm	0	2,75
Lipid Droplet Metabolism	2	Acsl1,Dgat2	0	2,59
Triacylglyceride Synthesis	2	Dgat2,Acsl1	0	2,53
Folic Acid Network	2	Sod1,Txnrd2	0	2,47
Tryptophan metabolism	2	Aox1	Dhcr24	2,04
IL-2 Signaling Pathway	2	Hsp90aa1	Icam1	1,67
Spinal Cord Injury	2	Nox4	Icam1	1,42
The effect of Glucocorticoids on target gene expression	1	Hsp90aa1	0	1,36
Mitochondrial LC-Fatty Acid Beta-Oxidation	1	Acsl1	0	1,33

Supplementary table 15: Differentially expressed genes in the liver after. Pathway enrichment analysis using Transcriptomic analysis console software. Pathway enrichment analysis SHR vs. PD5, comparison for the factor strain. Significantly pathways were selected based on a p-value < 0.05.

Interaction - pathway enrichement analysis	Upregulated in SHR + DEX	Downregulated in SHR + DEX	-log(p value)
Insulin induced PI3K-Akt and MAPK in hepatocytes	0	Pfkfb2	1,47
PI3K-AKT-NFKB pathway	0	Pfkfb2	1,09
Regulation of Actin Cytoskeleton	0	Baiap2	0,87
PKC-SCP2	0	St3gal5	0,00

Supplementary table 16: Differentially expressed genes in the liver. Pathway enrichment analysis using Transcriptomic analysis console software. Pathway enrichment analysis SHR vs. PD5, comparison for the factor interaction (strain x diet). None of the enriched pathways reached significance level of $p<0.05$.

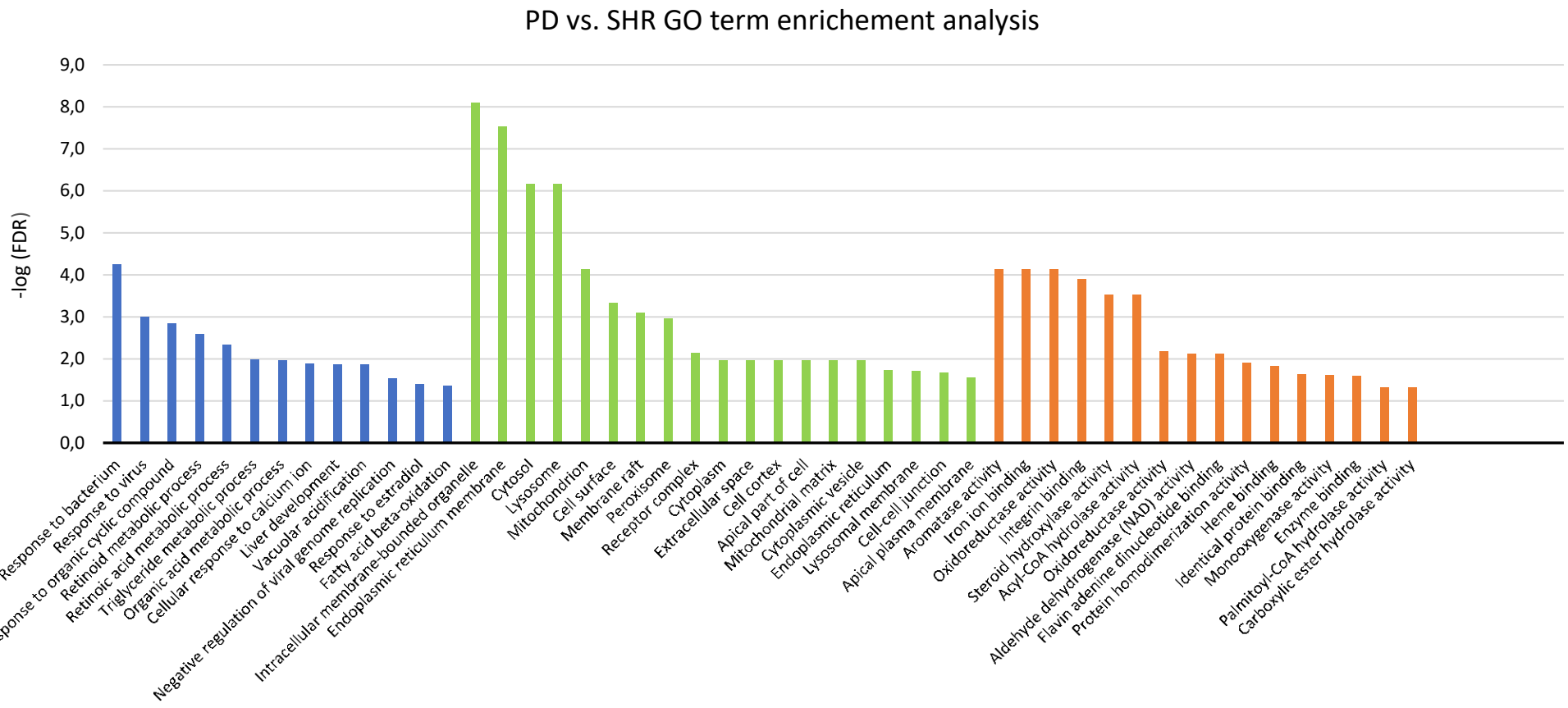

Supplementary figure 1: PD vs. SHR. Gene Ontology (GO) term enrichment analysis. Significantly enriched GO terms were selected based on a FDR < 0.05. GO terms of the categories of Biological Processes, Cellular Components, and Molecular Functions are depicted in blue, green, and orange, respectively.

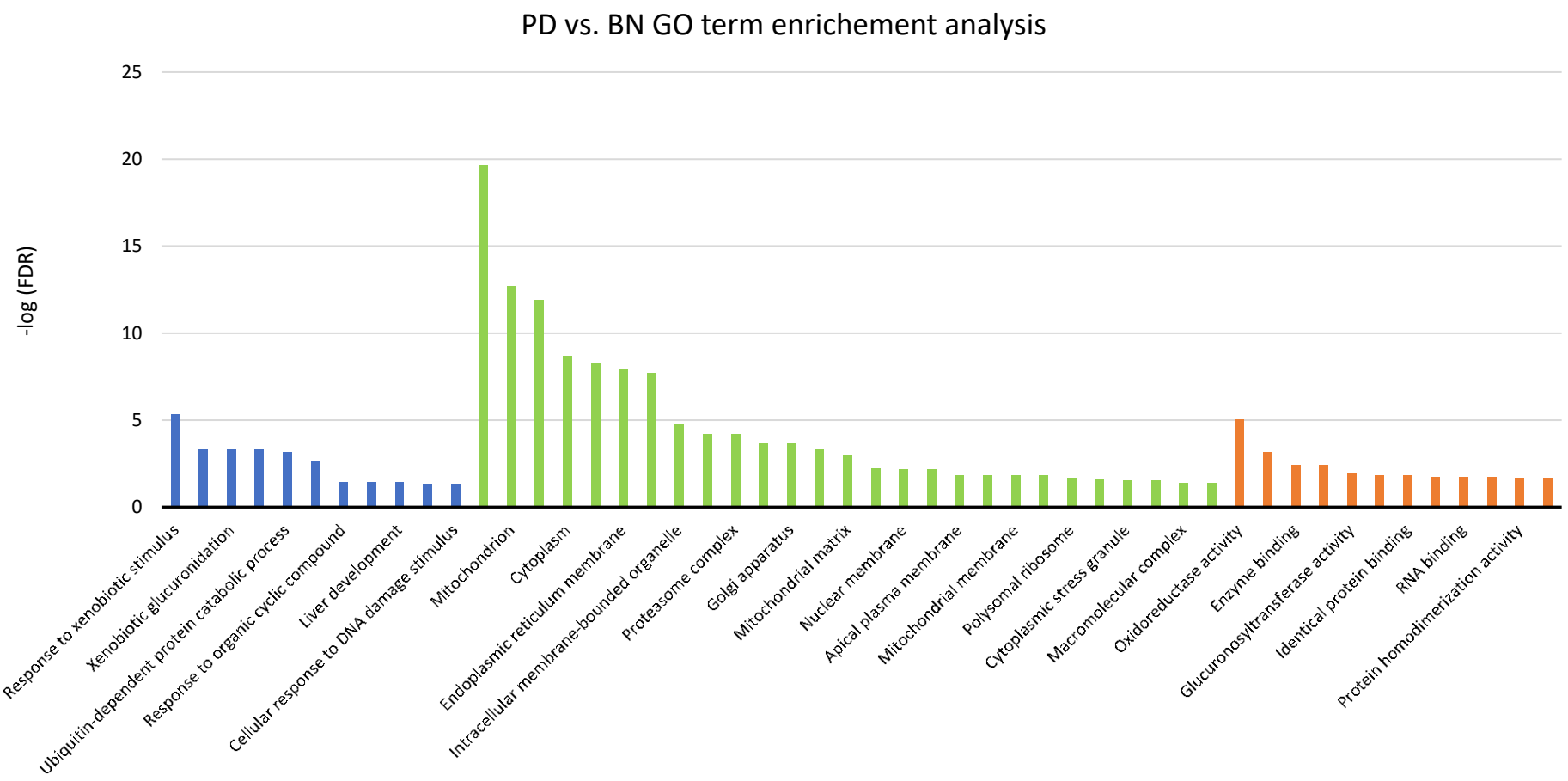

Supplementary figure 2: PD vs. BN. Gene Ontology (GO) term enrichment analysis. Significantly enriched GO terms were selected based on a FDR < 0.05. GO terms of the categories of Biological Processes, Cellular Components, and Molecular Functions are depicted in blue, green, and orange, respectively.

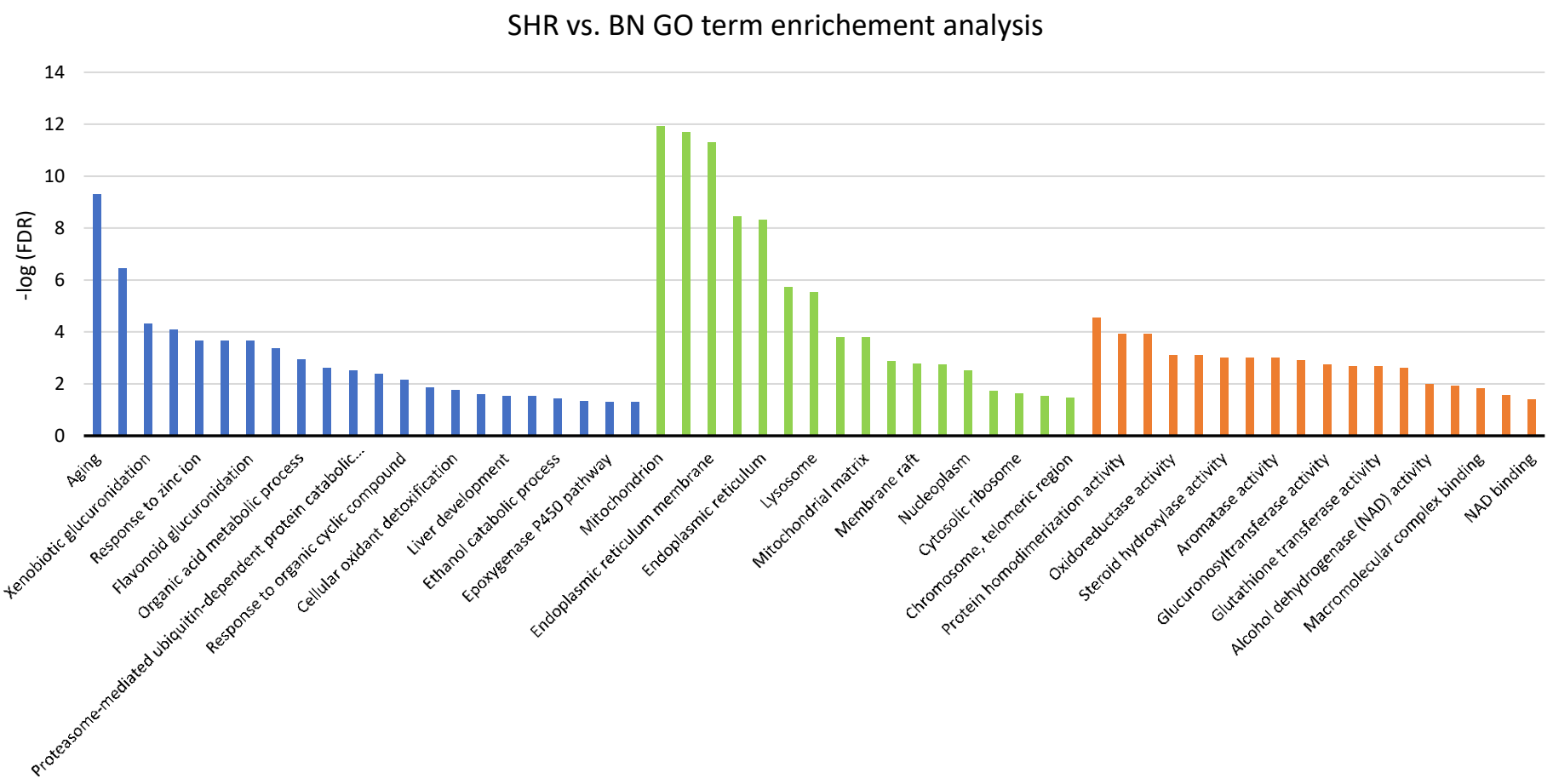

Supplementary figure 3: SHR vs. BN Gene Ontology (GO) term enrichment analysis. Significantly enriched GO terms were selected based on a FDR < 0.05. GO terms of the categories of Biological Processes, Cellular Components, and Molecular Functions are depicted in blue, green, and orange, respectively.

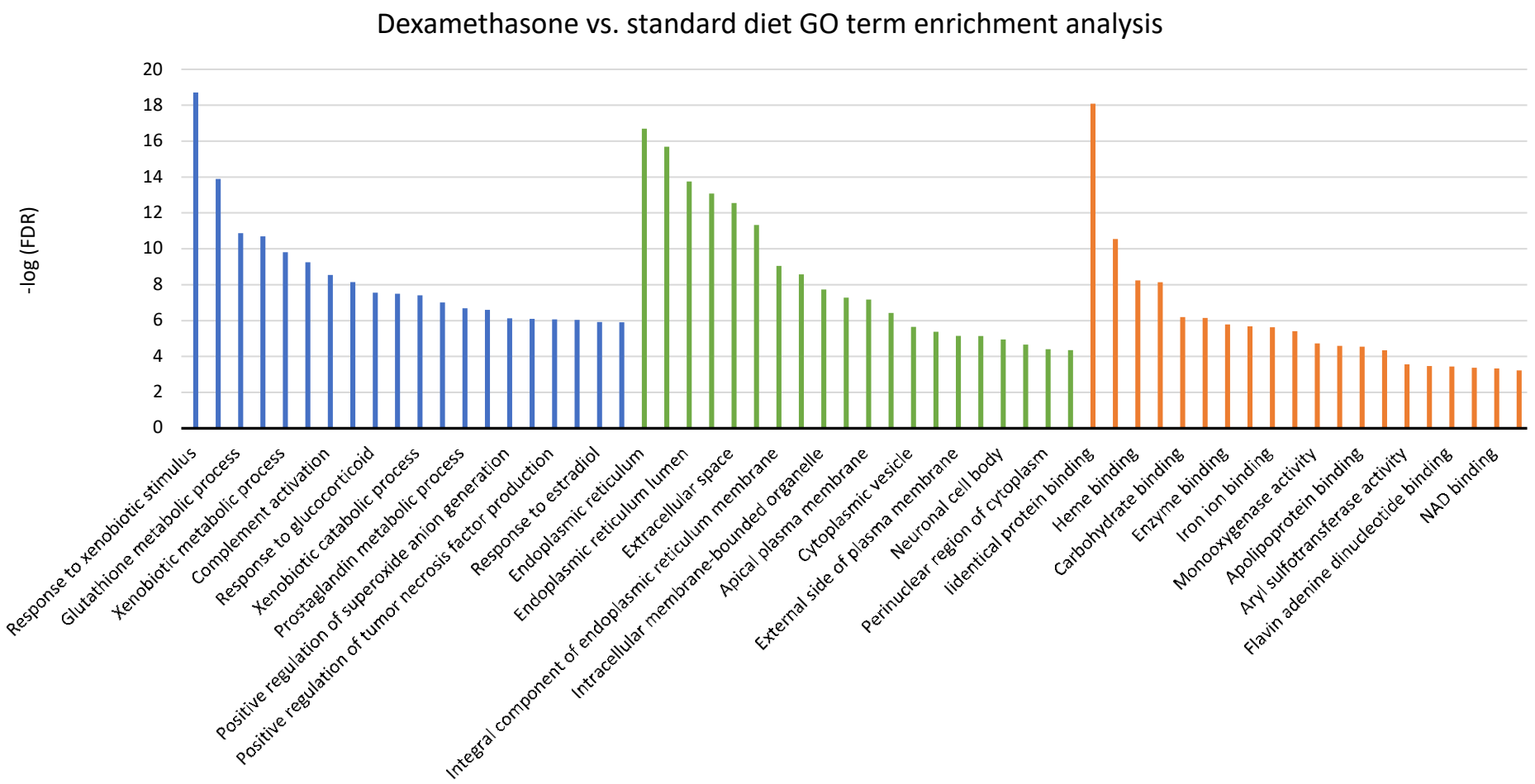

Supplementary figure 4: SHR vs. PD5 (Dexamethasone vs. standard diet. Gene Ontology (GO) term enrichment analysis. Top 20 significantly enriched GO terms for each category were selected based on a FDR < 0.05. GO terms of the categories of Biological Processes, Cellular Components, and Molecular Functions are depicted in blue, green, and orange, respectively.

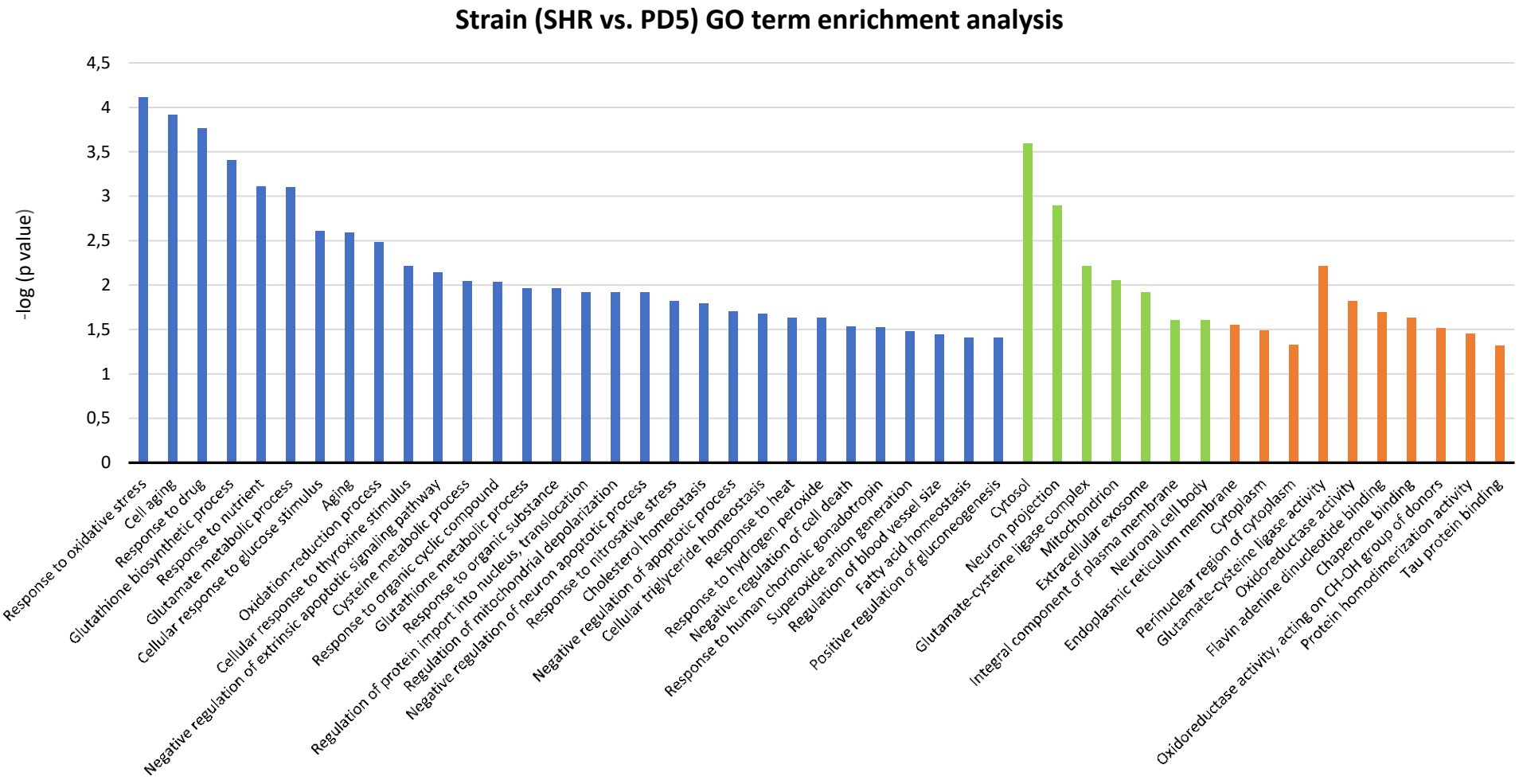

Supplementary figure 5: SHR vs. PD5 (strain). Gene Ontology (GO) term enrichment analysis. Significantly enriched GO terms were selected based on a $p < 0.05$ since none of the enriched pathways reached FDR treshold of <0.05. GO terms of the categories of Biological Processes, Cellular Components, and Molecular Functions are depicted in blue, green, and orange, respectively.

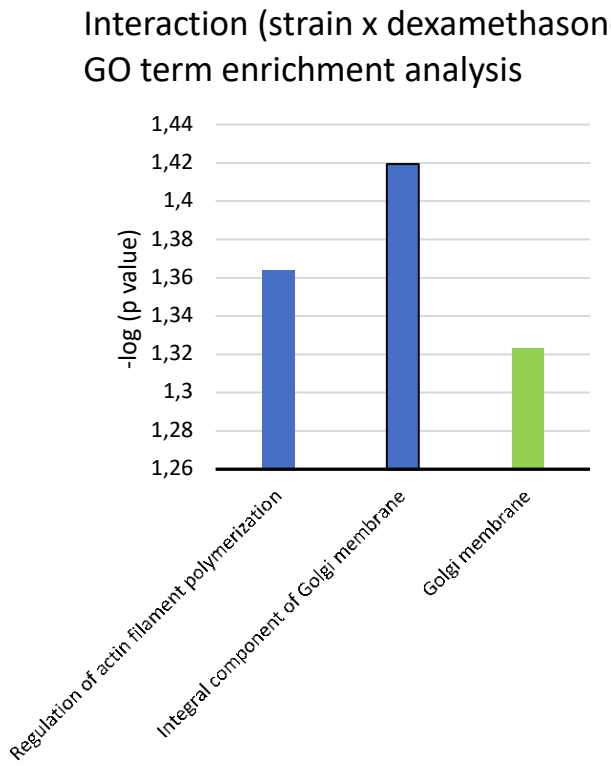

Supplementary figure 6: SHR vs. PD5 (interaction dxeamethasone x strain). Gene Ontology (GO) term enrichment analysis. None of the Significantly enriched GO terms reached a significance treshold of $p < 0$. GO terms of the categories of Biological Processes, Cellular Components are depicted in blue, green, respectively. No genes were enriched in the Molecular function category.

Majority protein IDs	Gene names	Razor + unique peptides	Unique peptides	Sequence coverage [%]	Q-value	Score	Intensity
Q9WVK3	Pecr	12	12	12	32,433	0	323,31
Q60587	Hadhb	28	28	28	51,414	0	323,31
Q6AXY0	Gsta6	9	7	7	25,808	0	207,82
Q9WUL0	Top1	20	20	20	90,759	0	161,03
P04176	Pah	26	26	26	51,821	0	323,31
P04905	Gstm1	26	24	21	25,914	0	323,31
P62630;M0R757;F1M6C2	Eef1a1;LOC100360413;LOC100360150	18	18	18	50,113	0	225,81
P14942;A0A8I6AQP1	Gsta4	12	10	10	25,51	0	227,92
P08010	Gstm2	31	31	17	25,702	0	323,31
Q10758	Krt8	38	30	28	54,018	0	323,31
O09171	Bhmt	22	22	19	44,976	0	323,31
P22791	Hmgcs2	26	26	25	56,885	0	323,31
P19112	Fbp1	19	19	19	39,609	0	323,31
P04762	Cat	25	25	25	59,756	0	323,31
A0A8I6AUI8;Q64119	Myl6	7	7	7	20,554	0	88,102
P63018;M0RCB1;A0A8I6AQL9	Hspa8;LOC102549957	29	27	27	70,87	0	323,31
Q02253	Aldh6a1	23	23	23	57,807	0	323,31
Q03336	Rgn	14	14	14	33,389	0	252,74
P02770	Alb	23	23	23	68,73	0	323,31
P10860	Glud1	28	28	28	61,415	0	323,31
Q5XIC0	Eci2	10	10	10	43,021	0	323,31

Supplementary table 17: PLZF-ALL GST pull-down assay. Significant proteins were selected based on FDR<1%intesity >23. Peptides with larger intensities in GST control group than in PLZF-ALL sample were not further considered